



**Politecnico
di Torino**

Politecnico di Torino

Master of Science in Energy and Nuclear Engineering

Academic Year 2022/2023

Graduation Session March 2023

Analysis of the energy production of a photovoltaic system integrated with a transport system derived from cableways

Supervisor:

Prof. Spertino Filippo

Candidate:

Bonsignorio Laura

Co-supervisor:

Dott.Ing. Bazzolo Stefano

Summary

Abstract	5
1. Introduction	6
1.1. European energy policy framework.....	8
1.2. The Italian energy situation	18
2. Integrated photovoltaics	28
2.1. Photovoltaic and transport infrastructures.....	29
2.1.1. PV and railways.....	30
2.1.2. PV and highways	33
2.1.3. Photovoltaic and noise barriers.....	35
2.2. Agrivoltaic.....	38
2.3. Floating PV	40
3. CableSmart: general system	42
3.1. Traditional cableway	42
3.2. Hybrid cable-self-propelled system.....	43
4. The study procedure	47
5. Energy load profile	51
5.1. Acceleration phase.....	51
5.2. Elevation.....	52
5.3. Frictions.....	53
5.4. The capacity and the final energy load.....	55
6. Energy Simulation	57
6.1. PV sizing	57
6.1.1. Avalanche barriers.....	58
6.1.2. Roofs and walls	60
6.2. Electric grid	62
6.3. Storage system.....	62
7. Economic Analysis	65
7.1. Fundamental quantities.....	65
7.1.1. Initial investment	65
7.1.2. Costs	65
7.1.3. Incomes.....	65
7.2. The procedure	66
8. CASE STUDY	67
8.1. Energy load profile	68
8.2. Energy simulation.....	75

8.2.1.	First scenario: avalanche barriers integrated PV	75
8.2.2.	Second scenario: cableway integrated PV	85
8.3.	Sensitivity analysis	91
8.3.1.	The distance L	91
8.3.2.	The tilt angle β	97
8.3.3.	Line length l	101
8.3.4.	Number of rollers n_{roll}	103
8.4.	First scenario with storage.....	105
8.5.	Economic analysis	116
8.5.1.	First scenario.....	116
8.5.2.	Second scenario	118
8.5.3.	First scenario with storage.....	121
9.	CableSmart and traditional cableway	126
10.	Conclusion.....	131
	Bibliography	135

Abstract

The climate crisis has sped up the energy transition, which is nowadays a global problem. The energy transition is already begun by carrying out effective energy policies. The case study presented in this work is consistent with the objectives that have been prearranged for Europe and Italy in terms of energy sustainability. One of the main challenges will be the inclusion of renewable energy systems in the current scenario.

The goal of this thesis is to conduct an analysis of the energy production of photovoltaic panels integrated with a cableway to feed part of its energy request. The cableway under investigation will be built in the Italian region Aosta Valley by adopting an innovative transport system named CableSmart.

The energy load profile of the cableway and the production profile of the PV plant installed are deduced, the latter by means of software as PVGIS, *Solarlog* and *Helioscope*. The data have been extrapolated on hourly basis with time horizon of one year and inserted in the implemented Excel file to carry out the energy simulation. This procedure has been done considering two scenarios which provide two different sizes of the PV plant: in the first one, the photovoltaic modules are supposed to be integrated with avalanche barriers erected in the mountains next to the infrastructure; in the second one PV modules are supposed to be integrated also on the roofs and the walls of cabins and stations. The results of energy simulations take into account that both configurations are connected with the electric grid. A *sensitivity analysis* of the first scenario has been carried out to examine the results dependence on the main components that characterize the transport system or the photovoltaic panels. A further interesting energy simulation of the first scenario has been done by introducing in the model the presence of a storage system, in this case batteries. The economic analysis of all the presented scenarios is reported.

To conclude, a slight pause on the adopted CableSmart transport system is proposed: the greater efficiency and the lower energy impact of this system with respect to a traditional cableway is demonstrated by reporting computations.

This case study puts into evidence the good luck of renewable energy technologies integration on existing infrastructures and faces important themes as the one related to innovation and sustainability into the transport sector: all points of interest of the actual Italian energy policy and consistent with investments and measures to be realized by Italy in the next decade.

1. Introduction

The impact of human activities on the planet requires a rapid ecological transition. There is the urgency of a radical transformation of current economic, industrial and social structures to face the climate crisis already in place.

Today, the world population is estimated at 7.7 billion and it is expected to grow exponentially leading to an increase of the world energy demand and that's exactly the energy sector the responsible for more greenhouse gas emissions, as shown in *Figure 1* [1], [2].

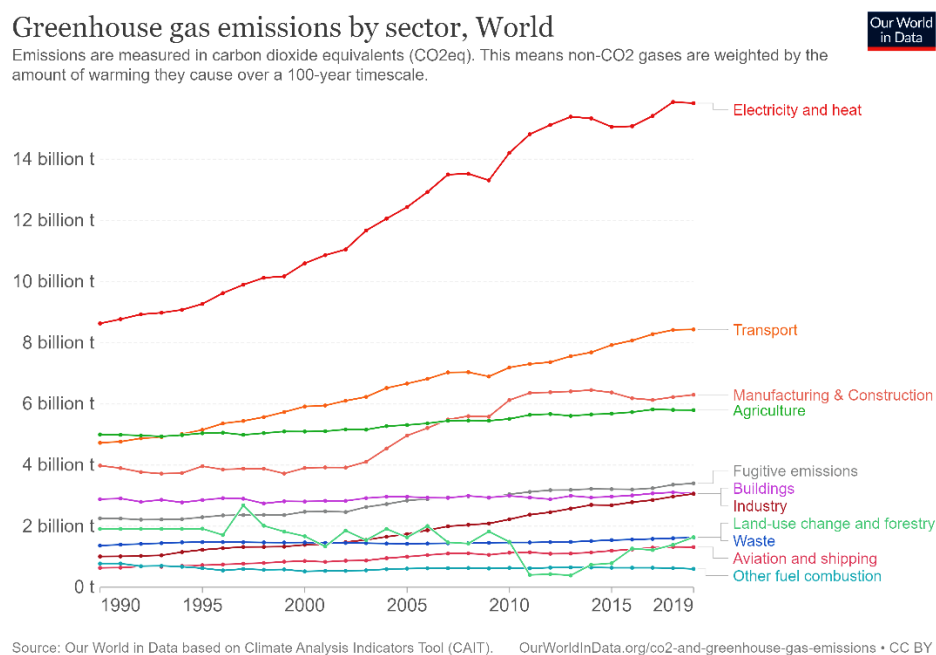


Figure 1 - World greenhouse gas emissions by sector [3].

According to the latest report of IEA (International Energy Agency), global energy-related CO₂ emissions grew to a record level of 36.3 gigatonnes (Gt) reached in 2021, 6% more than the previous year [4]. This increment was in line with the jump in global economic output of 5.9%: this marks the strongest coupling of CO₂ emissions with Gross Domestic Product (GDP) growth [4]. Historically, CO₂ emissions have been strongly correlated with the economic growth of a country: a GDP growth causes an increase in energy consumption and, consequently, in CO₂ emissions. This is the trend at World level, but many countries have managed to achieve economic growth while reducing emissions introducing low-carbon technologies, which produce more energy without the emissions that used to come with it [3].

Among the most evident effects of the CO₂ concentration increment in the atmosphere, there is the global warming. Indeed, in 2021 the global surface temperature has risen about 0.8 °C compared to the 1961-1990 average temperature (*Figure 2*).

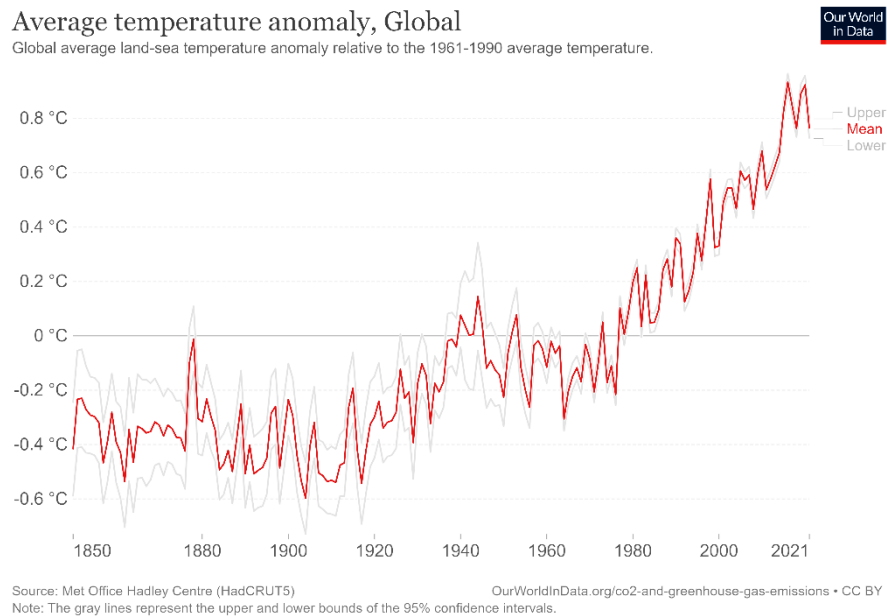


Figure 2 - World average temperature anomaly [3].

Therefore, population, CO₂ emissions and temperature anomaly present the same trend and their time series are reported in the following graph.

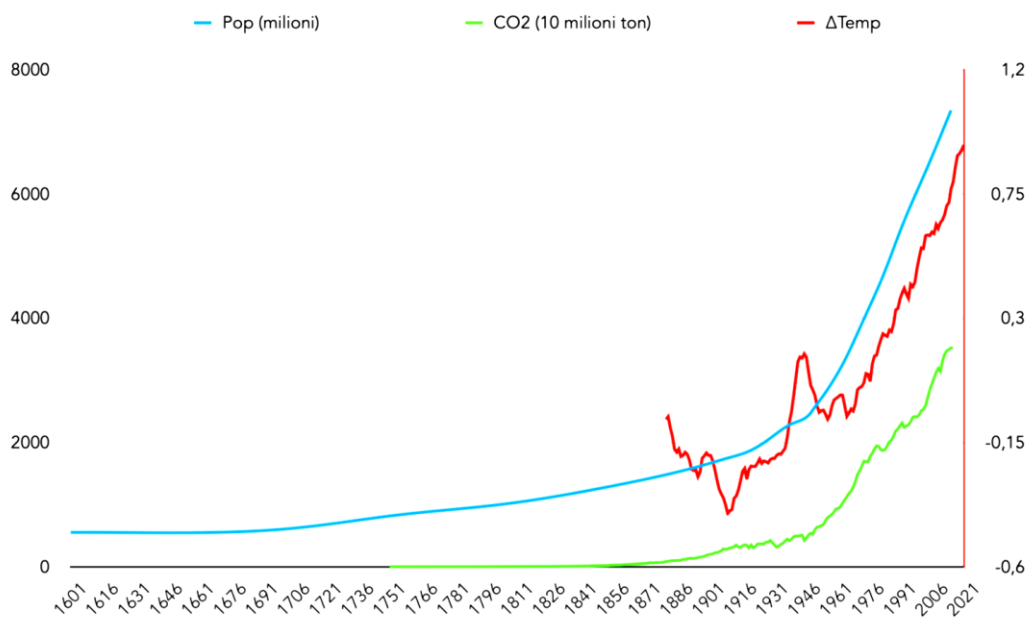


Figure 3 - Time series of population, CO₂ emissions and temperature [1].

A transition implies the initiation of long-term changes which cover several fields: economy, agriculture, industry, production and distribution and consumption of goods and services, and energy [1].

In the past, policy measures have been taken at global and local level to reverse the course of this climate situation and further commitments have to be respected in the future. From this perspective, the next few years will be decisive in ensuring that irreversible and catastrophic climate change is avoided.

In the following paragraphs, the European energy policy framework is presented and then a focus on the role of Italy in this context is pointed out. This because climate change cannot be countered or resolved by unilateral commitments but requires global cooperation which involves a fair division of efforts to be accepted and put into practice [1].

1.1. European energy policy framework

The first international environmental agreement concerning the global warming issue was signed in 1994: it was the *United Nations Framework Convention on Climate Change* (UNFCCC). Since that time, the member countries have met annually in the *Conference of the Parties (COP)* to analyse progresses in tackling the phenomenon of climate change.

Last decade, one of the most important *Conference of the Parties* was held: on 12 December 2015, the *Paris Agreement*, also called *COP21*, ended with an agreement aimed at the containment of the temperature increase well below 2°C with respect to the pre-industrial levels [5]. The participating Member States have to fix and reach their national contributions *INDC*, *Intended Nationally Determined Contribution*. The *Paris Agreement* became effective in 2016 and it is applied from 2021 [5]. It is part of a wider project defined by the *2030 Agenda for Sustainable Development*: a global action program to eradicate poverty, protect the planet and ensure prosperity and peace [6]. The program has been adopted in 2015 by 193 United Nations Member States and it contains 17 *Sustainable Development Goals (SDGs)* and 169 *Targets* associated with them [6], [7].



Figure 4 - 17 SDGs from 2030 Agenda for Sustainable Development [2].



Figure 5 - Conceptual structuring of the SDGs [2].

Figure 5 shows the three balanced pillars which often summarize the concept of sustainable development: environmental protection, economic growth, and social equality. The bottom “biosphere” can be seen as representing the ecological pillar (4 SDGs), while “society” and “economy” represent the social (8 SDGs) and economic (4SDGs) pillars. The “top” SDG 17 is not to be seen as the top of a pyramid, but as transcending the structure [2].

Several goals are directly or indirectly related with the theme of energy. It is the case of Goal 7 and Goal 13 reported below.

Goal 7 Ensure access to affordable, reliable, sustainable and modern energy for all

7 AFFORDABLE AND CLEAN ENERGY



- 3 targets and 2 resources.
- Become more energy-efficient and invest in clean energy sources to provide cheap energy to more people and protect the environment.
- By 2030, ensure universal access to affordable, reliable and modern energy services, increase substantially the share of renewable energy in the global energy mix, and double the global rate of improvement in energy efficiency.

Figure 6 - Goal 7 of SDGs [2].

Goal 13. Take urgent action to combat climate change and its impacts

13 CLIMATE ACTION



- 3 targets and 2 resources.
- It is still possible, with the political will and technological measures, to limit the increase in global mean temperature to two degrees Celsius above pre-industrial levels, and thus avoid the worst effects of climate change.
- It is necessary to strengthen resilience and adaptive capacity to climate-related hazards, integrate climate change measures into policies and improve education.

Figure 7 - Goal 13 of SDGs [2].

To save energy and raw materials, to produce minimum wastes, to recycle, to reuse, to repair materials and goods as much as possible and to protect the environment by not emitting pollutants are the main actions to be implemented to safeguard the planet by means of effective policies.

The *Paris Agreement* fits with *Goal 13* of the *2030 Agenda* concerning the *Climate Actions* and in particular with *Target 2* which requests the willingness to “*integrate climate change measures into national policies, strategies and planning*” [5], [8].

In 2016, the European Union and all its Member States have signed and ratified the *Paris Agreement* and they are strongly determined to implement it. Following these commitments, the European Union has defined all the *INDC* objectives for the period from 2021 to 2030. The main purpose is the greenhouse gas emissions reduction by 40% with respect to the level recorded in 1990 [5].

Between the end of 2018 and the beginning of 2019, the EU overhauled its energy policy framework to move away from fossil fuels towards cleaner energy by approving the *Clean Energy Package* [5]. It includes measures on energy efficiency, on renewable energies and on electricity markets. It is composed by the following legislative acts that set the new EU goals for 2030 [2], [5], [9]:

- *Regulation on the Governance of the Energy Union and Climate Action 2018/1999/EU* [9] to fundamentally transform Europe’s energy system. Under this strategy, each EU country is required to establish integrated 10-year *National Energy and Climate Plans* (NECPs) for period 2021-2030.
- *Regulation 2018/842/EU* [9] sets the target of emissions reduction of EU by at least 40% with respect to the level of greenhouse gas emissions of 1990. It also establishes the corresponding target for each Member State.
- *Directive on Energy Efficiency 2018/2002/EU* [9] sets the binding target of decreasing of primary energy consumption by at least 32.5% with respect to the scenario of 2007.
- *Renewable Energy Directive 2018/2001/EU (RED II)* [9] sets the binding target of 32% for renewable energy sources in the EU’s final gross energy consumption and the target of 14% in final consumption in transport sector by 2030.
- *Energy Performance of Buildings Directive 2018/844/EU (EPBD)* [5], [9] outlines specific measures for the building sector to tackle the climate crisis. Indeed, buildings result to be responsible for around 40% of energy consumption and 36% of CO₂ emissions in EU.
- *Regulation 2019/943/EU* [5], [9] for internal market for electricity.
- *Directive 2019/944/EU* [5], [9] for common rules for the internal market for electricity.
- *Regulation 2019/941/EU* [5], [9] for risk-preparedness in the electricity sector.

- Regulation 2019/942/EU [5], [9] establishes the *Agency for the Cooperation of Energy Regulators* (ACER).

The approach adopted by the NECPs requires a coordination of purpose across all government departments. Each Plan is a fundamental tool to change the energy and environmental policy of countries towards decarbonisation. The areas covered by NECPs are [2]:

- Decarbonization
- Energy Efficiency
- Energy Security
- Internal Market
- Research, Innovation and Competitiveness

As regards the Directive RED II, it is divided into the following articles [2], [10]:

- Financial support for electricity from renewable sources.
- Self-consumption of the electricity from renewable sources.
- RES energy use in the heating and cooling sectors and in the transport sector.
- The cooperation between Member States and between Member States and third countries on projects for the RES electricity production.
- Guarantees of energy origin from RES, administrative procedures, information and training on RES.

The Directive also lays down criteria for sustainability and reduction of greenhouse gas emissions for biofuels, bioliquids and biomass fuels [10].

The *Clean Energy Package* was then changed: a general revision of targets in emissions reduction, energy efficiency and renewable energies was done. Indeed, in 2019 the European Commission has published the *European Green Deal*. The document has reformulated new basis to face problems related to the climate and the environment, in line with the goals of the *Paris Agreement*. Moreover, in the successive year, the European Commission added the EU objective of 55% emissions reduction by 2030 leading to the increase of the share of renewable energy up to 38-40% [5]. The main objectives of the *Green Deal* are presented in *Figure 8*.



Figure 8 - European Green Deal objectives [11].

The European Green Deal embraces 8 policy areas [1], [11]:

- 1) Increasing the EU's Climate ambition for 2030 and 2050. With the aim to reach climate neutrality by 2050, the intermediate objective of 55% emissions reduction by 2030 has been set updating the energy policies ongoing.
- 2) Supply clean, affordable and secure energy. The progressive substitution of fossil fuels with renewable energy sources is planned.
- 3) Mobilising industry for a clean and circular economy. The industrial sector must face the green transition and the digitalization adopting a sustainable product policy.
- 4) Building and renovating in an energy and resource efficient way. This objective involves a policy focused on the promotion of restructuring operations.
- 5) Accelerating the shift to sustainable and smart mobility. The shift will occur enhancing electrification, digitalization, the utilization of alternative fuels and new forms of mobility.
- 6) From "Farm to Fork": a fair, healthy and environmentally friendly food system. It lays down a new approach to ensure a sustainable food chain in agriculture, fisheries and aquaculture sectors. Moreover, strategies that push consumers to choose sustainable food will be developed.
- 7) Preserving and restoring ecosystems and biodiversity. It is a long-term plan for protecting nature and reversing the degradation of ecosystems and this plan sets out new ways to

implement existing legislation more effectively, new commitments, measures, targets and governance mechanisms.

- 8) *A zero-pollution ambition for a toxic-free environment.* The decarbonization is supported by specific targets to battle air, water and soil pollutions as well as waste generation.

A further update of the package of legislative acts are introduced including [5]:

- ETS (*Emission Trading Scheme*) [5], ESR (*Effort Sharing Regulation*) [5] and LULUCF (*Land use, land use change and forestry*) [5].
- Revision of RED II, EPBD and Directive on Energy Efficiency.
- Revision of the rules for the internal gas market, the Energy Taxation Directive [5] and the Alternative Fuels Infrastructure Directive [5].

In detail, the successive revision of Energy Taxation Directive is part of the section “*Achieving Climate Neutrality*”, the revision of RED II and the Directive on Energy Efficiency is inserted in “*Clean, Reliable and Affordable energy*” and the review of Alternative Fuels Infrastructure Directive is found in “*Sustainable Transport*” section included in the *European Green Deal* text [2]. Some strategies are then presented to accelerate energy transition towards the net zero emission by 2050: strategies for energy system integration mainly with infrastructures, strategies for hydrogen storage and integration into the transport sector, strategies for building renovations and for offshore renewable energies that allow to move towards decarbonization and finally rules on *EU Trans-European Networks for Energy* (TEN-E) [5], [2].

In 2020, the COVID-19 pandemic crisis, and the consequent economic crisis, has made necessary the launch of the *Next Generation EU* (NGEU) program. NGEU is an additional temporary tool to stimulate recovery after the pandemic, with the aim to use this particular period to encourage the development of a more ecological, digital and resilient Europe [7]. This program includes mainly two support tools for the Member States: REACT-EU to initially boost the economy in 2021-2023 and RRF (*Recovery and Resilience Facility*) which concerns the period 2021-2026 [5]. To access the NGEU funds, each Member State had to prepare a *National Recovery and Resilience Plan* (NRRP). The NGEU marks an epochal change for the EU and the writing of the Plan outlines a future update of the *National Energy and Climate Plans*. The resources deployed to boost growth, investments and reforms amount to EUR 750 billion [12]. The subdivision of the available resources is the one represented in *Figure 9*.

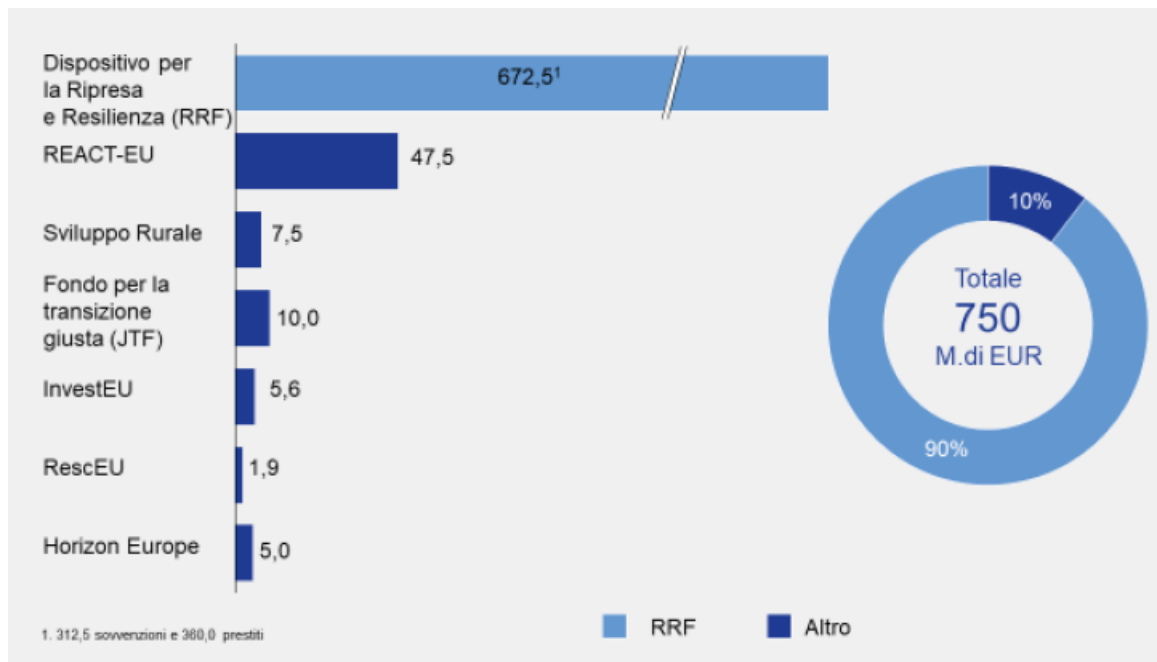


Figure 9 - NRRP resources in EUR billion [12].

The allocation mechanism between Member States reflects not only structural variables such as the population, but also variables such as loss of Gross Domestic Product due to the COVID-19 pandemic [12].

The Plan is broken down into 6 *Missions*, which represent the structural thematic areas of intervention [13]:

1. Digitalization, Innovation, Competitiveness, Culture and Tourism
2. Green Revolution and Ecological Transition
3. Infrastructure for Sustainable Mobility
4. Education and Research
5. Inclusion and Cohesion
6. Health

Between these components figures the *Green Revolution and Ecological Transition* that directly derives from the *Green Deal*. The NGEU guidelines provide at least 37% of the total investment for the climatic objectives [5], [12].

A central role is assumed by the theme related to the development of renewable energy sources. In this regard, in September 2021 the European Commission launches the seven *Flagship programmes*, intermediate goals of the NRRP to reach in 2025 [5], [7], [12]:

- “*Power up*” aims to increase by 200 GW the production of renewable energy by 2025 and to the installation of 6 GW capacity of electrolyser for hydrogen production.
- “*Renovate*” aims to enhance the performance of buildings in terms of energy efficiency by doubling the restructuring rate.
- “*Recharge and refuel*” aims to the construction of 1 million charging stations and 500 hydrogen stations.
- “*Connect*” aims to spread ultra-broad band connections, also using 5G radio technologies available.
- “*Modernise*” aims to enhance the digitalization of some important public services such as identification, authentication, justice and health.
- “*Scale up*” aims to double the production of advanced semiconductors in Europe.
- “*Reskill and upskill*” aims to improve digital and professional skills, that are now necessary, through investments in education and training.

In the same year, the European Commission has presented the so called “*Fit for 55%*” to revise the EU legislation in different sectors in order to reach the climatic goals for 2030. The essential points are presented in *Figure 10*.

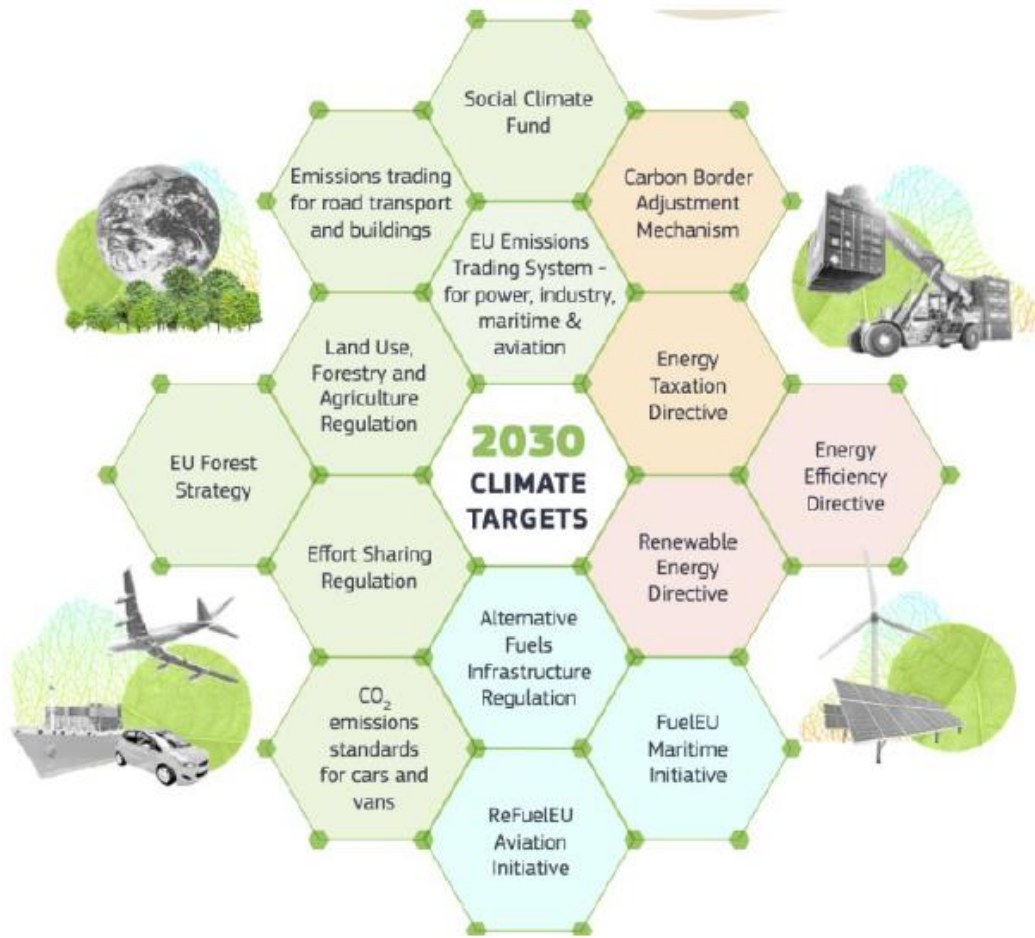


Figure 10 – “Fit for 55%” package of proposals [1].

In addition to revisions, further proposals have been introduced [14]:

- The *Carbon Border Adjustment Mechanism* (CBMA) [14] to ensure that the price of goods imported from third countries takes account of their carbon content, that is the amount of emissions released during their production.
- The *ReFuel Aviation* [14] and *ReFuel Maritime* [14] to promote the use of sustainable fuels for planes and ships.
- The realization of infrastructures for alternative fuels.
- The foundation of a *Social Climate Fund* to manage the social and economic impact of the new Emission Trading Scheme (ETS) in construction and transport sectors.

The case study analysed in this work is perfectly consistent with the actual energy policies and meets more than one of the objectives abovementioned. Obviously, being the thesis focused on the integration of photovoltaic panels, it is totally compliant with all the interventions to launch green

transition and power up the production of energy from renewable sources which is a topic largely covered in the *2030 Agenda for Sustainable Development*, with a dedicated goal (*Goal 7*), and then recalled by the *European Green Deal*. Moreover, it is part of the NRRP investments programme to speed up the ecological revolution.

The proposed photovoltaic installation is integrated with a cable-based infrastructure, which is one of the transport systems with lower energy impact. Such a system fits well with the themes related to high efficiency systems and sustainability in transport sector debated by *2030 Agenda for Sustainable Development* and then recalled by the “*Fit for 55%*” package. In the NRRP also, investments are provided for the mass transport infrastructure empowerment, included cableways.

1.2. The Italian energy situation

During 2020, renewable energy sources (RES) have been confirming their central role in the Italian energy scenario by producing energy in electric sector, in thermal sector for heating and cooling and also in transport sector. At the end of 2020, the Italian renewable plants count for a power installed of 56.6 GW (+2,0% with respect to 2019) [15]. This is mainly due to new photovoltaic and wind installations, +785 MW and +192 MW respectively.

Totally, in 2020 the gross final energy consumption from renewable sources was 21.90 Mtep/year corresponding to 254.7 TWh/year. Compared to 2019, there is a modest growth in total energy consumption from Renewable Energy Sources - RES (+0.1%). This dynamic is the result of the growth of the electricity sector (+2.5%) and biofuels (+2.2%), on one hand, and from the contraction observed in thermal sector (-2.4%), on the other hand [15].

Mtep	2015	2016	2017	2018	2019	2020	Variazione % 2020/2019
Settore Elettrico	9,43	9,50	9,73	9,68	9,93	10,18	2,5%
Idraulica (dato normalizzato) (*)	3,95	3,97	3,96	4,02	4,05	4,13	2,0%
Eolica (dato normalizzato) (*)	1,32	1,42	1,48	1,54	1,65	1,71	3,6%
Solare	1,97	1,90	2,10	1,95	2,04	2,14	5,3%
Geotermica	0,53	0,54	0,53	0,52	0,52	0,52	-0,8%
Bioenergie (**)	1,67	1,67	1,66	1,64	1,68	1,68	0,3%
Settore Termico	10,69	10,54	11,21	10,67	10,63	10,38	-2,4%
Geotermica	0,13	0,14	0,15	0,15	0,15	0,14	-7,3%
Solare termica	0,19	0,20	0,21	0,22	0,23	0,24	3,6%
Bioenergie (**)	7,78	7,59	8,20	7,71	7,76	7,53	-3,0%
Energia rinnovabile da pompe di calore (***)	2,58	2,61	2,65	2,60	2,50	2,48	-0,9%
Settore Trasporti (biocarburanti sostenibili)	1,16	1,04	1,06	1,25	1,32	1,35	2,2%
TOTALE	21,29	21,08	22,00	21,61	21,88	21,90	0,1%

Table 1 - Italian gross final consumption from RES in Mtep [15].

Looking at the electric sector in *Table 1*, the gross energy production from RES results equal to 118.4 TWh/year (10.18 Mtep/year), that is around 42% of the national electricity production (280.5 TWh/year) [15].

In detail, the recorded variations in production compared to 2019 are [15]:

- + 5.3% from PV
- +2.0% from hydroelectric
- +0.3% from bio energies
- +3.6% from wind energy
- -0.8% from geothermal energy

The main contribution to production is given by hydroelectric energy (40.7% of the energy by RES) followed by solar energy (21.3%) [15].

Almost one fifth (19.9%) of energy consumptions in thermal sector is satisfied by RES. The majority of these are classified as direct consumptions from the sources like energy from solar panels, heat pumps and plants that exploit the geothermal heat. The remaining part regards the heat derived consumptions as the case of the district heating system fed by biomass. Compared to 2019, there is a decrease by 2.4% in total thermal consumption from RES [15].

The amount of biofuels produced in Italy in 2020 reaches 1.5 million tons, for an energy content of 1.35 Mtep (+2.2% with respect to the previous year) [15].

In 2020, the total gross final consumptions of energy in Italy were about 107.6 Mtep corresponding to 1251.4 TWh. Hence, the share of RES in gross final energy consumption recorded in 2020 is 20.4% that is already greater than the *overall target* imposed to Italy by European Directive 2009/28/EU (RED I) for this year. Indeed, RED I fixed the objective of 17% share of RES on final consumption. The previous year this percentage was 18.2%.

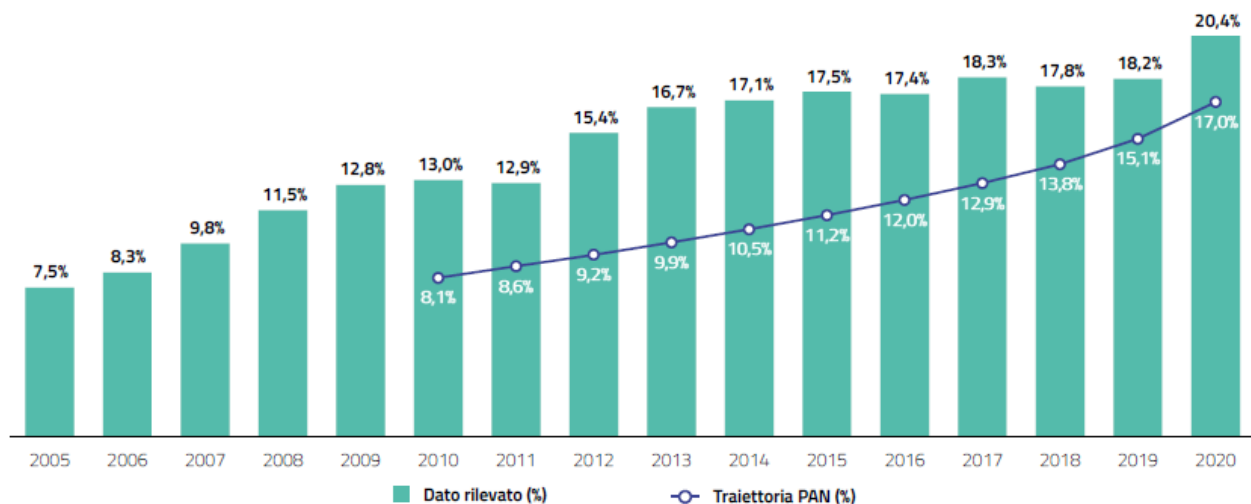


Figure 11 - Share of gross final consumption of energy covered by RES [15].

The share of RES in transport sector recorded in 2020 is 10.7% higher than the *overall target* imposed by RED I for this year that was fixed at 10%. The percentage increase is notable compared to 9% observed in 2019 [15]. This is an evident effect of the COVID-19 crisis: global energy consumptions of the Nation have significantly decreased, in particular in transport sector, whereas the energy consumption from RES is stable.

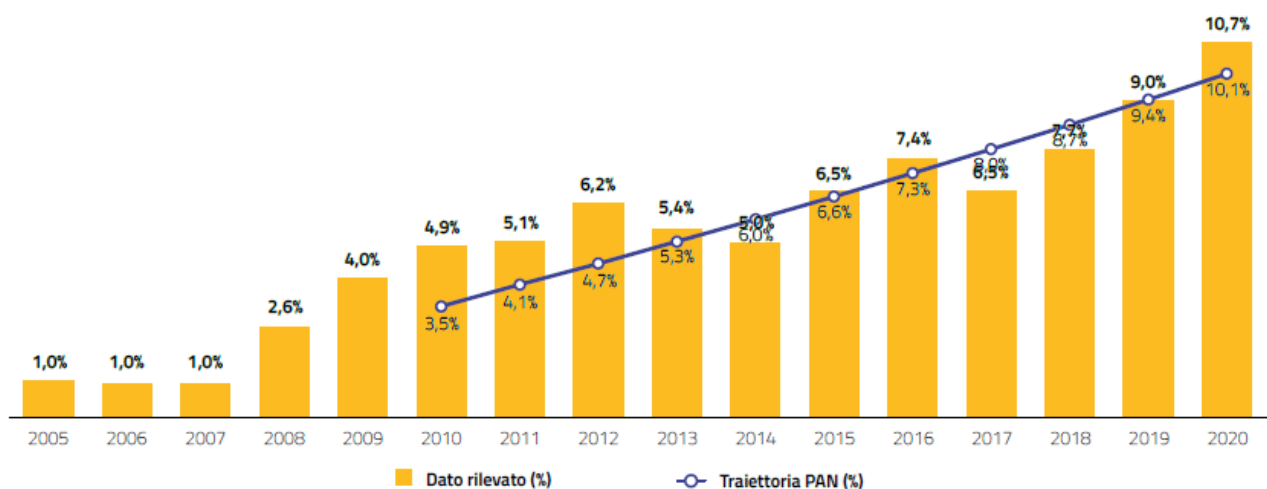


Figure 12 - Share of gross final energy consumption in the transport sector covered by RES [15].

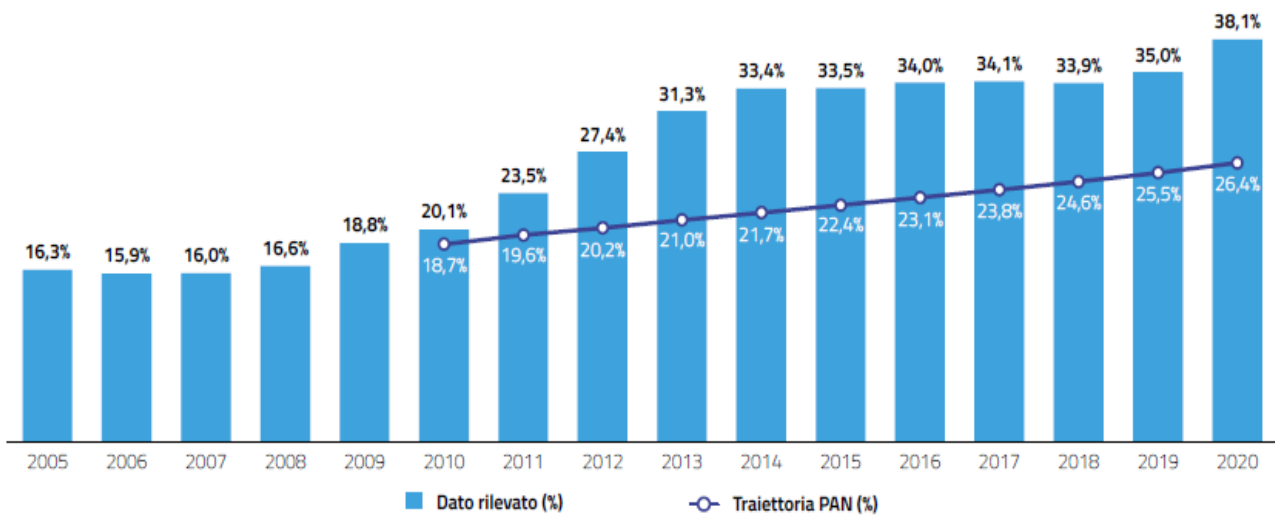


Figure 13 - Share of gross final energy consumption in the electricity sector covered by RES [15].

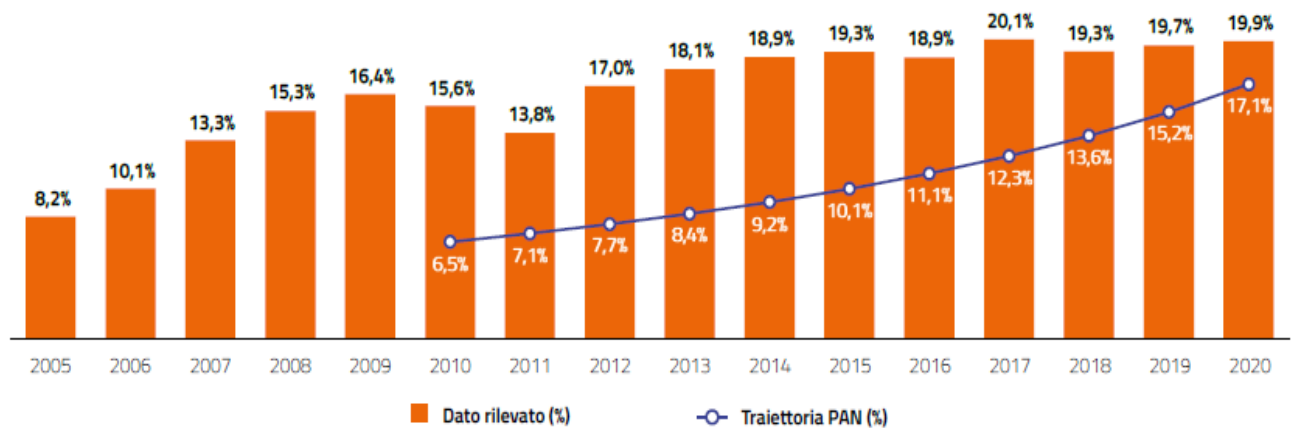


Figure 14 - Share of gross final energy consumption in the thermal sector covered by RES [15].

Data related to final consumptions are monitored over time to obtain the percentages shown in the previous figures to guarantee the realization of objectives fixed by PAN (*Piano d'Azione Nazionale*), the Italian plan strictly bound to Directive 2009/28/EU (RED I). In particular, the graphs in *Figure 12*, *Figure 13* and *Figure 14* compare the predicted trajectories with the detected consumption data.

Since the present thesis is based on the integration of photovoltaic systems, the actual Italian situation in the field of solar photovoltaics is presented below.

The evolution of the historical series of the number of the PV plants and the installed PV power in Italy, is shown in *Figure 15*.

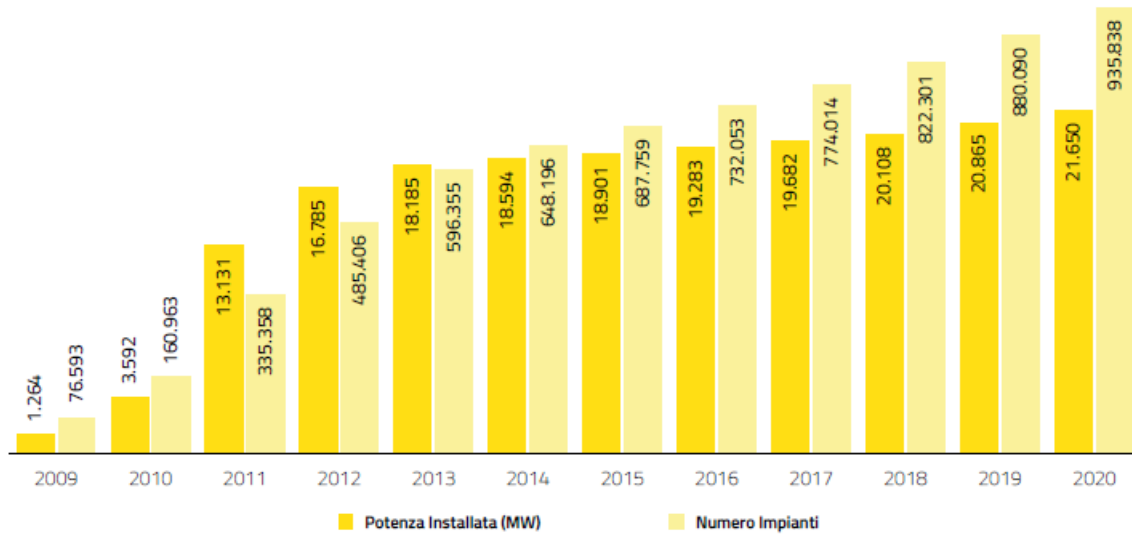


Figure 15 - Number and installed power of PV in Italy over time [15].

From 2013 the growth rates are slowed due to the end of the incentive mechanism called *Conto Energia*. Overall, in 2020 the increase of the number of PV plants and the installed PV power results to be +6.3% and +3.8% respectively, which is more contained than in previous years [15]. At the end of 2020 the photovoltaic plants installed in Italy result to be 935,838 for a total nominal power slightly lower than 22 GW, as reported in *Table 2*.

Classi di potenza	Numero	Potenza (MW)	Produzione (GWh)
$P \leq 3$	312.196	839	916
$3 < P \leq 20$	552.571	3.912	4.183
$20 < P \leq 200$	58.542	4.585	4.752
$200 < P \leq 1.000$	11.361	7.652	9.078
$P > 1000$	1.168	4.662	6.013
Totale	935.838	21.650	24.942

Table 2 - PV plants data updated to the end of 2020 [15]. Values in “classi di potenza” column are expressed in kWp.

It is evident that the higher number of installations is registered for plants with nominal power lower than 20 kW, indeed they represent 92% of the total existing plants. Overall, power from PV accounts for 38% of the entire national renewable power [15]. The annual energy production is almost 25 TWh that is 21% of the total renewable energy production of the Nation. Moreover, 61% of this electricity is produced by PV plants of size greater than 200 kW [15].

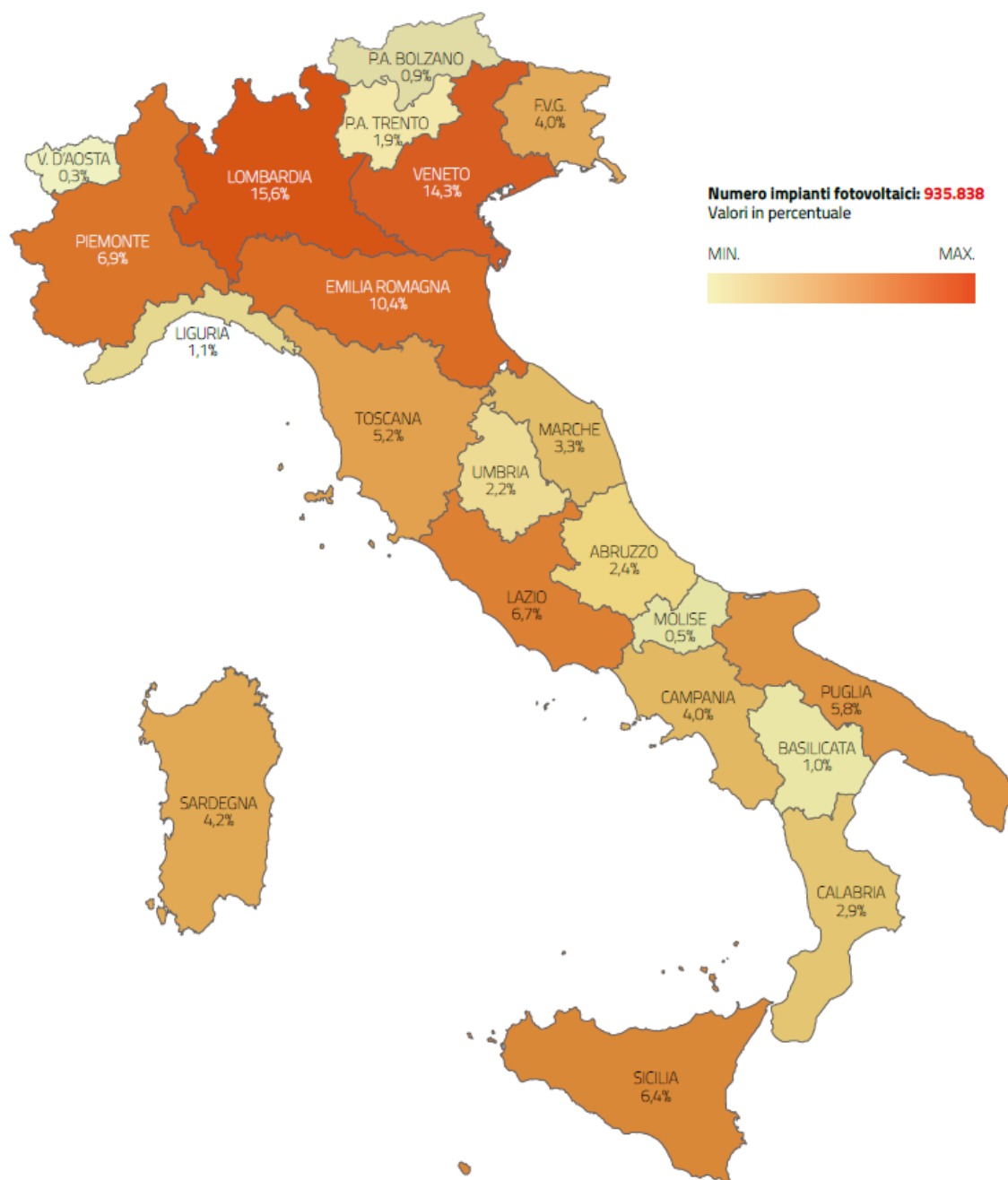


Figure 16 - Regional distribution of the number of photovoltaic systems at the end of 2020 [15].

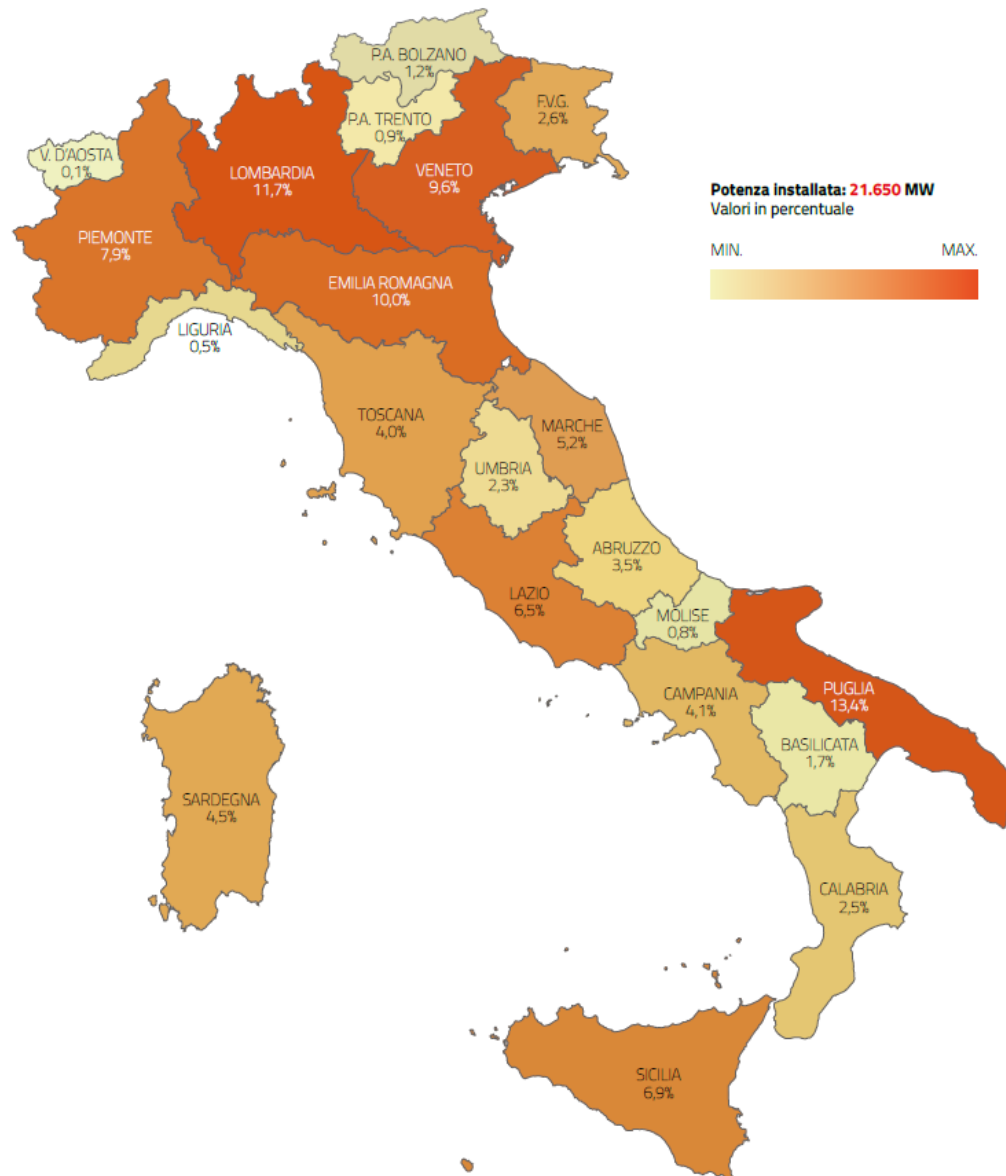


Figure 17 - Regional distribution of the PV power installed at the end of 2020 [15].

Looking at *Figure 16*, 55.4% of PV plants are in North Italy with Lombardy as first region for number of plants, whereas Puglia contributes most to the amount of power installed (*Figure 17*) [15].

Up to year 2020, the Italian energy strategies are dictated in compliance with Directive RED I. At the present time, the energy policy follows the directives reported in the previous paragraph, which are effective for the decade 2021-2030, looking at more ambitious goals for 2050. The targets and the regulatory backdrops provided by the Directive RED II, the Italian NECP and then the NRRP are implementing.

According to Directive RED II, the Italian NECP indicates the contribution of Italy to the EU's *overall target* aiming at 30% as share of RES energy of the gross final consumption by 2030. Concerning the transport sector, the NECP sets the share of RES for Italy at 22%, higher than the *overall target* 14% defined by RED II [5]. This target will be reached by pushing towards low-carbon emitting technologies while increasing biofuel usage rate, and by encouraging the penetration of e-mobility. One of the objective declared in 2011 by the “*White book on transport*”, a document which articulates strategies to achieve a sustainable transport system, moves in this direction: it aims to helve the use of “conventionally fuelled” cars in urban cities by 2030 and to accelerate the development and deployment of clean vehicles [16]. This last challenge meets the necessity to develop renewables in the electric sector: indeed, the Italian goal in this field is 55% provided mainly by photovoltaic, with at least 52 GW of solar power installed, and by wind power, with 19 GW of power installed (*Table 3*) [5]. To reach these objectives, the Plan provides for incentives, promotion of energy communities and *self-consumption* and also simplification of authorization procedures. In thermal field, the target attended is 33.9% thanks to heat pumps and biomass plants [5].

Fonte	2016	2017	2025	2030
Idrica	18.641	18.863	19.140	19.200
Geotermica	815	813	920	950
Eolica	9.410	9.766	15.950	19.300
di cui off shore	0	0	300	900
Bioenergie	4.124	4.135	3.570	3.760
Solare	19.269	19.682	28.550	52.000
di cui CSP	0	0	250	880
Totale	52.258	53.259	68.130	95.210

Table 3 - Italian 2030 targets in RES power (MW) [5].

The implementation of Directive RED II is an integral part of projects and reforms contained in *National Recovery and Resilience Plan*. Concerning the NRRP, the total sum allocated to Italy is equal to EUR 222.1 billion [1]. As mentioned in *Chapter 1.1*, the NRRP is made up of *16 Components*, which are grouped into *6 Missions*, listed in *Figure 18*.







 M1. DIGITALIZZAZIONE, INNOVAZIONE, COMPETITIVITÀ, CULTURA E TURISMO	PNRR (a)	React EU (b)	Fondo complementare (c)	Totale (d)=(a)+(b)+(c)
M1C1 - DIGITALIZZAZIONE, INNOVAZIONE E SICUREZZA NELLA PA	9,75	0,00	1,40	11,15
M1C2 - DIGITALIZZAZIONE, INNOVAZIONE E COMPETITIVITÀ NEL SISTEMA PRODUTTIVO	23,89	0,80	5,88	30,57
M1C3 - TURISMO E CULTURA 4.0	6,68	0,00	1,46	8,13
Totale Missione 1	40,32	0,80	8,74	49,86
 M2. RIVOLUZIONE VERDE E TRANSIZIONE ECOLOGICA	PNRR (a)	React EU (b)	Fondo complementare (c)	Totale (d)=(a)+(b)+(c)
M2C1 - AGRICOLTURA SOSTENIBILE ED ECONOMIA CIRCOLARE	5,27	0,50	1,20	6,97
M2C2 - TRANSIZIONE ENERGETICA E MOBILITÀ SOSTENIBILE	23,78	0,18	1,40	25,36
M2C3 - EFFICIENZA ENERGETICA E RIQUALIFICAZIONE DEGLI EDIFICI	15,36	0,32	6,56	22,24
M2C4 - TUTELA DEL TERRITORIO E DELLA RISORSA IDRICA	15,06	0,31	0,00	15,37
Totale Missione 2	59,47	1,31	9,16	69,94
 M3. INFRASTRUTTURE PER UNA MOBILITÀ SOSTENIBILE	PNRR (a)	React EU (b)	Fondo complementare (c)	Totale (d)=(a)+(b)+(c)
M3C1 - RETE FERROVIARIA AD ALTA VELOCITÀ/CAPACITÀ E STRADE SICURE	24,77	0,00	3,20	27,97
M3C2 - INTERMODALITÀ E LOGISTICA INTEGRATA	0,63	0,00	2,86	3,49
Totale Missione 3	25,40	0,00	6,06	31,46
 M4. ISTRUZIONE E RICERCA	PNRR (a)	React EU (b)	Fondo complementare (c)	Totale (d)=(a)+(b)+(c)
M4C1 - POTENZIAMENTO DELL'OFFERTA DEI SERVIZI DI ISTRUZIONE: DAGLI ASILI NIDO ALLE UNIVERSITÀ	19,44	1,45	0,00	20,89
M4C2 - DALLA RICERCA ALL'IMPRESA	11,44	0,48	1,00	12,92
Totale Missione 4	30,88	1,93	1,00	33,81
 M5. INCLUSIONE E COESIONE	PNRR (a)	React EU (b)	Fondo complementare (c)	Totale (d)=(a)+(b)+(c)
M5C1 - POLITICHE PER IL LAVORO	6,66	5,97	0,00	12,63
M5C2 - INFRASTRUTTURE SOCIALI, FAMIGLIE, COMUNITÀ E TERZO SETTORE	11,17	1,28	0,34	12,79
M5C3 - INTERVENTI SPECIALI PER LA COESIONE TERRITORIALE	1,98	0,00	2,43	4,41
Totale Missione 5	19,81	7,25	2,77	29,83
 M6. SALUTE	PNRR (a)	React EU (b)	Fondo complementare (c)	Totale (d)=(a)+(b)+(c)
M6C1 - RETI DI PROSSIMITÀ, STRUTTURE E TELEMEDICINA PER L'ASSISTENZA SANITARIA TERRITORIALE	7,00	1,50	0,50	9,00
M6C2 - INNOVAZIONE, RICERCA E DIGITALIZZAZIONE DEL SERVIZIO SANITARIO NAZIONALE	8,63	0,21	2,39	11,23
Totale Missione 6	15,63	1,71	2,89	20,23

Figure 18 - NRRP breakdown by Mission and by Component (EUR million) [17].

The investments in the field of energy transition and RES are present mainly in *Mission 2*.

The *Component 1 “Circular economy and sustainable agriculture”* has resolved to improve on one hand, the waste management and the circular economy system and, on the other hand, to develop smart and sustainable agricultural and food chains. These last includes investments on agri-voltaic (id est PV plants serving farms and installed in integrated and synergic to agricultural fields) projects up to 0.43 GW of PV installations without land consumption and encouraging the emergence of *Green communities*, especially in rural and mountain areas [1], [12].

The *Component 2 “Energy transition and sustainable mobility”* provides the increment of renewable energy penetration and of grid resilience. For instance, concerning the photovoltaic, the Italian objective is to reach at least 52 GW of PV installations by 2030 [12]. Overall, the target for the share of RES on final consumption is fixed at 30% by 2030 [12]. Moreover, this component gives prominence to the development of Italian *supply chains* of innovative technologies such as photovoltaic panels and batteries, markets in which Chinese manufacturers dominate [1]. Moreover, a focus is present on the decarbonization of industrial and transport sectors with solutions based on the use of hydrogen, biofuels, PV and batteries.

The *Component 3 “Energy efficiency and renovation of buildings”* aims to reduce emissions enhancing the energy performance of public and private buildings. Interventions provides the enlargement the district heating networks [12].

The *Component 4 “Protection of land and water resources”* deals with the fight against climate change by means of interventions for the protection of land, the safeguard of biodiversity and for the removal of pollution of land and water [12].

The case study of the present thesis is consistent with the themes of *Component 2* in NRRP, in particular with the concept of integrated photovoltaics that is examined in depth in *Chapter 2*.

2. Integrated photovoltaics

In accordance with the increasing global energy demand and the actual policy efforts toward sustainable development, new solutions on inclusion of renewable energy systems in current world scenario have been considered. Among them, the photovoltaic is the most mature and accessible technology due to the flexible installations of PV panels. One of the main challenges will be the integration of photovoltaic with existing structures as buildings, power stations, railways, rooftops and others, which leads to many advantages. Firstly, the available construction is exploited as a support of the PV modules and this brings a double benefit: the manufacturing costs may decrease, and the new power system is installed without soil consumption, which is an important feature nowadays. It is also convenient to use the electricity from photovoltaic to satisfy, as much as possible, the energy demand of the structure where panels are located: the proximity of power generators and loads minimizes the power losses. Moreover, from the point of view of the electricity network, the energy demand of the structure integrated with PV is lower. Nevertheless, the incorporation of solar panels and existing structures exhibits one big limitation. Generally, solar panels are installed taking into account all the fundamental parameters that maximize the power production: depending on the geographical coordinates of the location, the optimal tilt angle, orientation and layout of modules are calculated and adopted in order to increase the power production and the efficiency of the installation itself. This is not always possible in case of PV integration because of the physical constraints related to the construction: so, the disposition of the panels is not the optimal one, as well as the power production is not the maximum possible.

Pros and cons of PV integration with existing infrastructures are summarized in *Table 4*.

PROS	CONS
Lower PV manufacturing costs	No optimal tilt angle
No soil consumption	No optimal azimuth angle
Contribution to satisfy the energy demand of the interested structure	No maximum power production
Lower power losses	
Lower energy from the grid	

Table 4 - Pros and cons of photovoltaic integration with existing infrastructure.

In recent years, many theoretical research and pilot projects dealing with photovoltaic integration have been investigated in different sectors. Some of these applications are reported in the following paragraphs.

2.1. Photovoltaic and transport infrastructures

The transport sector is a major contributor to air pollution, being responsible for almost one-quarter of the global carbon dioxide emissions from fuel combustion [18]. Electrification with renewable energy is emerging as a key solution for reducing greenhouse gases by means of PV generation integrated into road and rail transportation taking full advantage of the existing infrastructures. Therefore, a good PV integration aims at rationally exploiting the areas that are suitable for laying PV panels.



Figure 19 - Examples of PV integration in roads and rails. (a) Covered land. (b) Tunnel median. (c) Station rooftop. (d) Trackside land [1].

From a sustainable point of view, solar energy-powered road and rail transportation will play a vital role in the evolution of the sustainable transportation; from a techno-economic point of view, it promotes the further evolution of both the energy and transport sectors toward a low-carbon, green and sustainable future, which brings about more positive benefits, including the technical progress, the industrial upgrading, and the economic growth [18].

2.1.1. PV and railways

Railway is one of the lower emissions-intensive mode of passenger transport with a global average of GHG intensity equal to $19 \text{ gCO}_{2,\text{eq}}/(\text{passenger} \cdot \text{km})$ and emissions from electrified passenger rail could be even lower, particularly when powered through renewable energy [19]. The expansion of railway electricity networks will be important for achieving emission reductions: for this reason, investments in rail transport are planning, especially in Europe [19]. The presence of electrified track systems and their ongoing development turns out to be a considerable advantage for the inclusion of a renewable electricity source like photovoltaic.

All over the world, there are solar installations in railways which demonstrate the feasibility and convenience of this kind of integration. In 2011, the East Japan Railway Company introduced PV modules on the shed of Tokyo Station and the generated electricity is used for lighting, air conditioning, and other loads. The annual energy produced by the PV system is around 340 MWh, which is equivalent to 0.3% of the total electric energy used in Tokyo Station [20]. In Belgium, 16,000 solar panels are installed on the roof of a 3.6 km rail tunnel supplying 3,300 MWh of electricity annually. The produced electricity supplies lightings, signals, stations and powers the electric trains in the Belgian rail network. This solution reduces carbon emission by 2,400 tons per year [18]. In Australia, Byron Bay Railway Company launched an on-board solar energy-powered electric train. Special curved solar panels were fitted to the train roof, generating up to 6.5 kW of power to charge the train's battery bank. In addition, there is another large array of solar panels on the station rooftops capable of producing up to 30 kW [18], [21].



Figure 20 - Byron Bay Solar Train [3].

Solar energy can find wide application in the railways sector in tropical countries. This is the case of the Indian Railways which is also one of the largest railway networks in the world and one of the largest consumers of diesel in the country, with annual consumption of 2.7 billion litre [22]. The “Solar Rail Coach” experiment was carried out to quantify the reduction in diesel consumption of the End-on Generation system that powers the electrical load in the new generation coaches (LHB coaches). One of these coaches is retrofitted with two mono-crystalline flexible SPV modules, each of 190 W_p. This is done for three high speed trains and the performances of the panels are investigated in DT (Dynamic Trials) and ST (Static Trials), where the static case is considered as the ideal performance of the PV system. It comes up a daily average module efficiency equal to 16.9% during ST and 15 % during DT, with a Performance Ratio (PR) of 79.5% and 71.6%, respectively. The annual diesel saving estimated is around 1,708-1,863 litre per coach with annual reduction of 4.5-4.9 tonne of CO₂ emission, supposing the available rooftop area of a typical LHB coach in operation on all days, the Indian annual average daily GHI equal to 5.5 kWh/m² and an average of 300 sunny days in a year. Considering the number of coaches that are operational in the country, the saving of diesel would be significantly large [22].

The perspective of solar energy-powered rail transportation has been deeply explored in China because of its actual rapid development. Indeed, by 2030, the scale of the national railway network is expected to reach 200,000 km and, as a consequence, the energy demand in rails is dramatically increasing [18], [20]. China has abundant solar energy resources, but the solar radiation is not uniformly distributed across the country. Hence, based on annual irradiation, China is divided into four Zones [18].

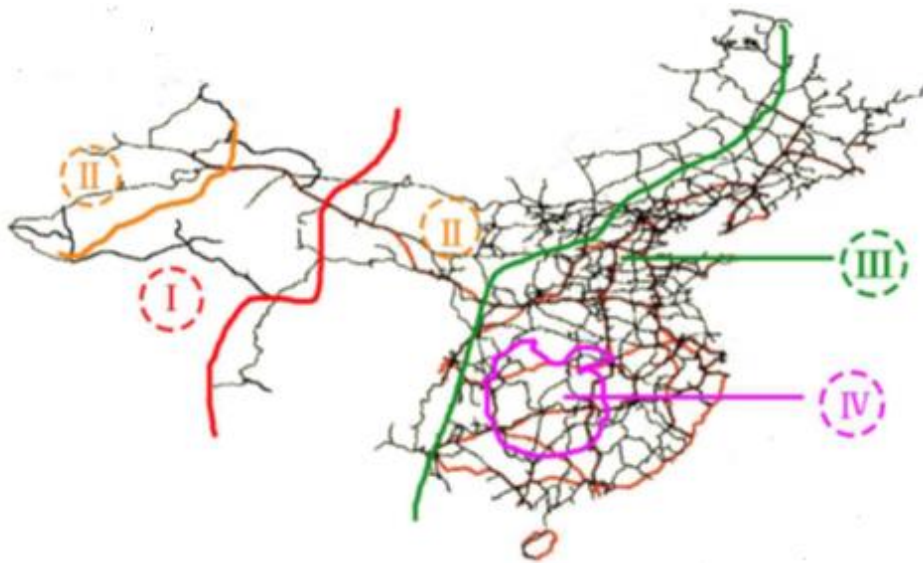


Figure 21 - Distribution of railway networks and solar energy resources in China [20].

Figure 21 shows the division in Zones of the country: the average annual solar radiation is set equal to 1,750 kWh/m² in Zone I, 1,575 kWh/m² in Zone II, 1,225 kWh/m² in Zone III, and 1,050 kWh/m² in Zone IV, which correspond approximately to 1,850 kWh/kW_p, 1,500 kWh/kW_p, 1,200 kWh/kW_p and 900 kWh/kW_p, respectively. Assuming to install solar panels on all the station and train roofs of the four Zones and also on the available spaces at the trackside land, the total electricity produced is estimated to be around 239.6 TWh annually [18].

A more recent case study has involved the Beijing-Shanghai high-speed railway (BS-HSR) which connects the two megacities in China with a total of 24 stations located in 7 different provinces along the railway [23]. The PV panels are supposed to be installed both on the rooftops of the railway stations and the open spaces along rail lines, as depicted in the sketch of *Figure 22*.

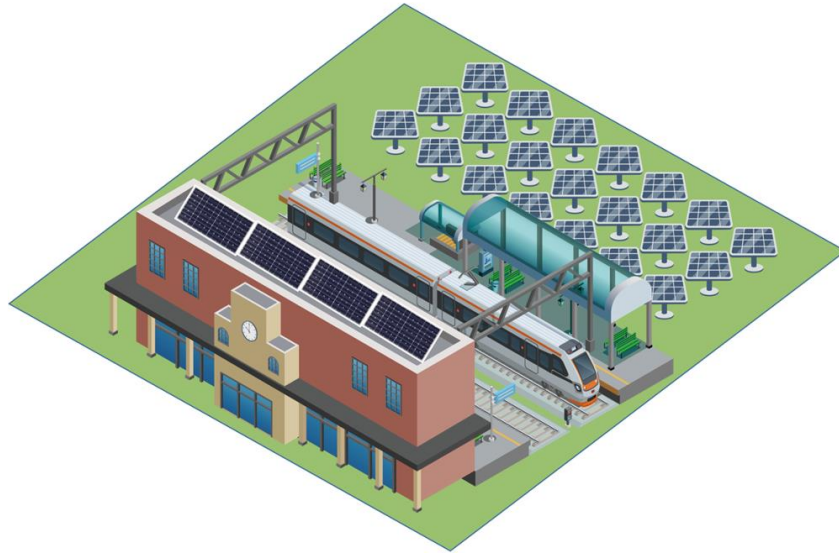


Figure 22 - Concept of the integration of PV and rail transportation systems [5].

The simulation pointed out a total annual power generation of 331 GWh from station PV systems and 6.2 TWh from the areas along the Beijing-Shanghai high-speed railway. *Figure 23* shows that the modules on station roofs can cover the energy consumption of the local section of railway only in two provinces, Beijing and Shanghai, whereas the modules along the rail line can theoretically achieve self-sufficiency in all the regions. Combining the two PV systems, a very large amount of power generated far exceed the electricity consumption of the railway operation, so much that up to 5.37 TWh annually of electricity could be used to supply the surrounding users, being these areas densely populated [23].

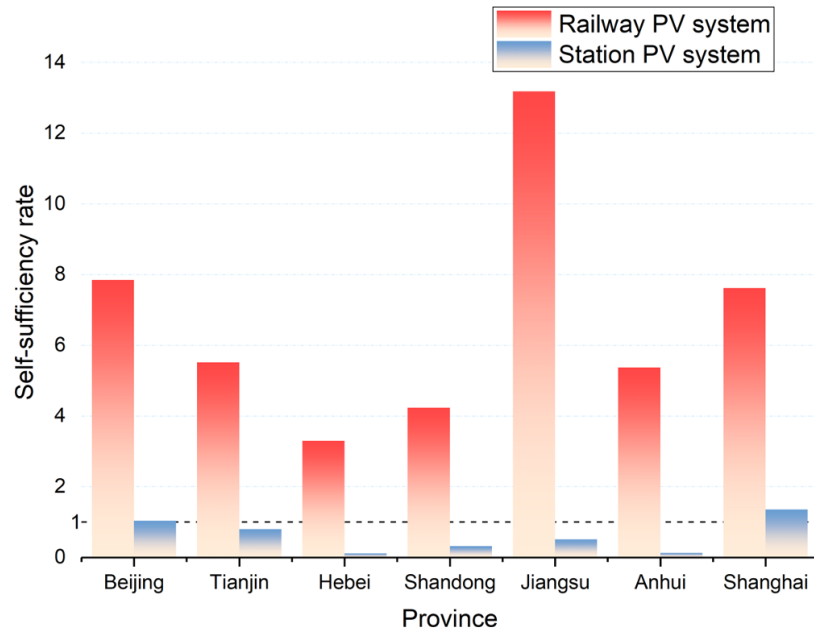


Figure 23 - Self-sufficiency rates in each province [5].

2.1.2. PV and highways

Since there is abundant space alongside highways, including the medians, the slopes and the covered land, it is convenient to place photovoltaic systems here. On one hand, solar panels can feed the energy request of highways related to lightings, video surveillance systems and services, on the other hand they will play a fundamental role in the next future due to the upcoming penetration of e-mobility. In this regard, in 2022 the European Parliament voted to support the ban on the sales of diesel and petrol cars starting in 2035 and, in parallel, the share of EVs in total sales needs to reach around 60% by 2030 to reach net zero CO₂ in 2050 [24]. The mass adoption of EVs will require the deployment of charging infrastructures, which could be easily fed by photovoltaic especially in remote area crossed by highways.

Also in this case, many of the modelling studies on road-photovoltaic integrations are focused on China's highways, where sales of EVs reach 3.3 million compared with 2.3 million in Europe [25]. It is forecasted that the total mileage of highways in China will have a 74.6% increase compared to that in 2018, and it is reported that the total annually electricity consumption of infrastructures, lightings, ventilations in the tunnel and ancillary facilities alongside highways will be around 82.6 TWh by 2030 [18]. A perspective of solar energy applied to road transportation has supposed to place PV modules on the land around the ways, on the building rooftops of the service areas, supplying their own electricity consumption, and on the medians on both ends of the tunnels where panels could feed the lighting facilities. With reference to the previous division of the country in

four Zones based on their average annual radiation, the total annual PV generation potential of China's highways is estimated to be 1022.8 TWh [18].

As for tunnels, a sort of photovoltaic corridor at the entrance and exit has been tested. In addition to the local production of electricity for lighting, it has been demonstrated that the solar photovoltaic corridors can be used as a brightness buffer to meet the dark and bright adaptations of the human eyes due to changes in light intensity improving safety and visual comfort of the entrance and exit of the tunnel [26].



Figure 24 - Example of photovoltaic power generation corridor [6].

The solar photovoltaic technology along highways has been identified as a possible future solution for green energy production in India, which presents a great solar potential whereas the land is becoming a scarce resource. Two areas, namely Ahmedabad-Rajkot national highway road and Ahmedabad-Vadodara national expressway, are taken for modelling. The total length of the Ahmedabad-Rajkot national highway is 205 km, oriented near the east-west direction, and that of the Ahmedabad-Vadodara national express highway is 93 km, oriented near the south-north direction. The panels have been hypothetically disposed over the road, supported by a simple elevated structure. They are tilted at an angle of 23° that is the latitude for the Ahmedabad site [27].

Figure 25 schematizes the layout.

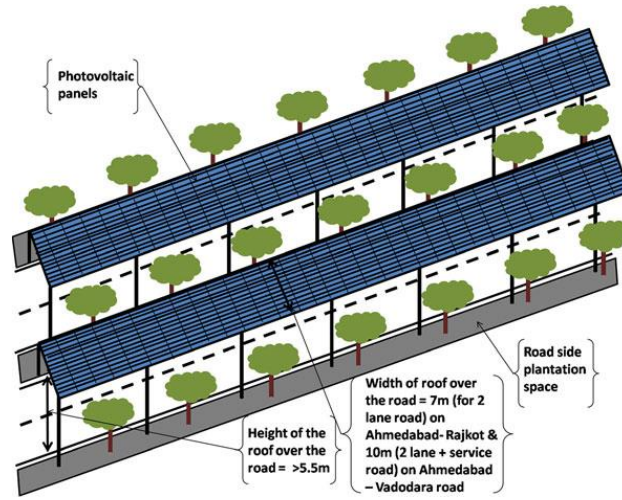


Figure 25 - Schematic layout of the national highway with solar photovoltaic panels [7].

From the simulation, the annual energy generation results approximately 163 GWh along the Ahmedabad-Rajkot and 96 GWh for the Ahmedabad-Vadodara national expressway [27]. Therefore, the national highway space can contribute to the huge amount of energy generation without extra cost for the land. Apart from this, there are various benefits. For example, the shading of panels on the road improves vehicle efficiency, reduces the utilization of energy for air conditioning in vehicles, increases the life of tires and roads and this helps to reduce the fund requirement for road repairs [27].

2.1.3. Photovoltaic and noise barriers

The photovoltaic noise barrier (PVNB) system was developed by combining a PV system with a noise barrier, the common construction located along roadways nearby a densely populated area. On these locations, noise barriers are needed to improve the living environment, since many residents are affected by traffic noises [28], [29]. Such applications of PV are of increasing interest as part of planning of urban transportation infrastructure. PVNB is not a new technology: the first PVNB system was built in Switzerland in 1989 and it still delivers 1000 kWh/kW_p per year to the local grid [30]. After the success of that project, many PVNB types of systems have been installed in Germany, Switzerland, Austria, Netherlands and Australia [28], [31]. However, the majority of the PVNB systems have been installed in Europe [31]. In 1996, a competition for noise barrier designers, PV suppliers and PV installers was hold in Germany and Switzerland, resulting in the construction of three 10 kW_p PVNB plants in Germany and three 10 kW_p PVNB plants in

Switzerland [30]. All the plants are a unique combination of noise protection and PV technology. As can be seen in *Figure 26*, there are several proven experimental methods to combine PV with noise barriers.

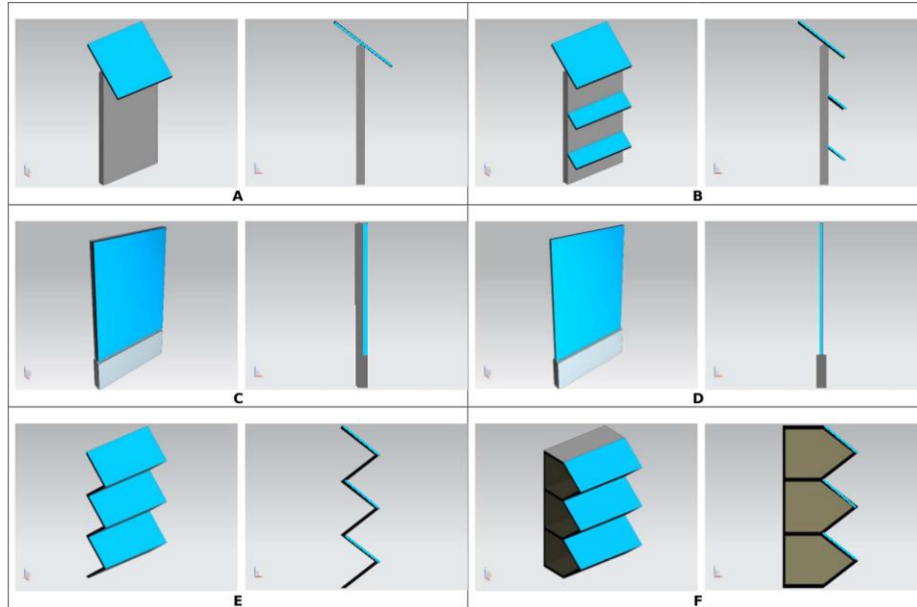


Figure 26 - Types of PVNB shown in perspective and side view: a) PV modules can be mounted on the top of the barrier, b) as shingles down the side of the barrier in addition to the top, c) covering the entire vertical surface, d) a bifacial surface, e) in a horizontal zigzag configuration, and f) cassettes [31].

For instance, the Zürich Wallisellen plant uses zigzag technology and 45 mini-inverters. This PVNB is based on a combination of sound reflection and sound absorption, and it is the first PVNB application along a railway line. Possible electromagnetic interference between the railway and the inverter was studied and proved to be no issue. Another installation is located in Aubrugg, on a north–south motorway near Zürich and it is the world’s first PVNB bifacial plant in which modules act as sound reflecting elements [30].



Figure 27 - a) Zürich Wallisellen plant with zigzag technology, b) Zürich Aubrugg plant with bifacial technology [30].

Over the next decade, thanks to the decline of photovoltaic modules costs, which reach 0.27 \$/Wp in 2021 (Figure 28), the deployment of PVNB on mass scale has been considered.

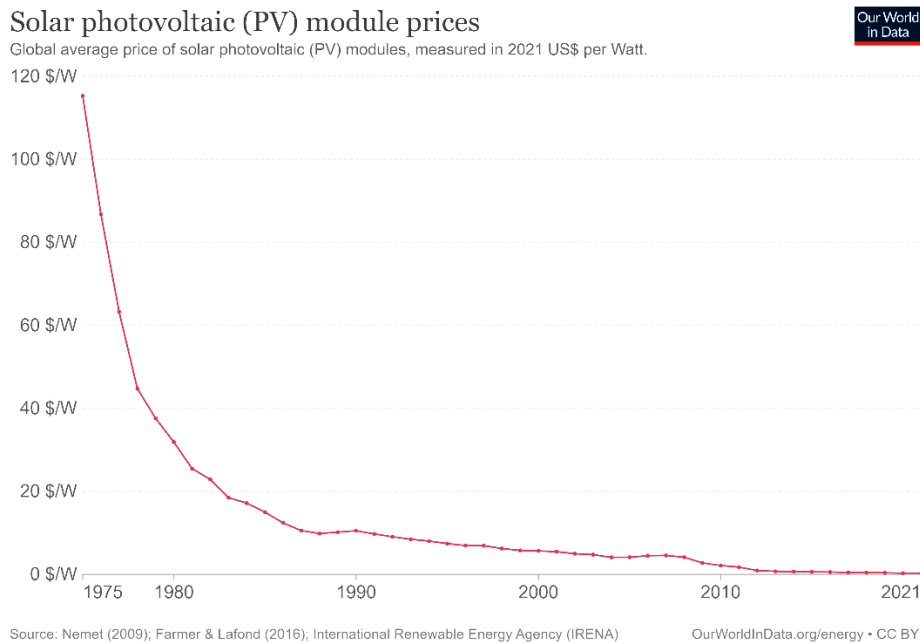


Figure 28 – Historical series of solar PV module prices in US\$/Wp [3].

In this direction, a case study has been carried out for the state of California. Indeed, the U.S. is an ideal candidate country for the employment of PVNB technology because noise abatement mandates fall well short of World Health Organizations [31]. For the simulation, it is assumed that the PV modules run the entire length of the noise barrier and are mounted vertically on the side of the noise barrier. Because of this, thin film PV technology was selected because they possess superior temperature coefficients: this is an advantage because in this case on the backside of the

panels there is no space for ventilation. The panels face the road, and they are mounted on the side of the road which is more favourable in terms of capturing the solar incident irradiation, even if soiling due to vehicular traffic could reduce the power generation [31]. Finally, the estimated total annual energy potential from photovoltaic modules mounted on all existing noise barriers in California is 157.8 GWh. Based on road miles, the results are then extrapolated for the entire U.S. reaching the annual energy potential of 815 GWh. This energy is sufficient to power more than 50,000 homes in the U.S. and result in an annual electricity cost saving of more than \$ 66 million [31]. Moreover, the installed capacity is comparable to the installed capacities of the solar farms in U.S. [31].

A similar approach has been adopted in the analysis focused on the second ring road in Kunming, a city of China. Here, the problem of noise disturbance is becoming increasingly prominent and noise barriers system is urgently needed. For this simulation, the amorphous silicon double-sided glass panels are supposed to be used because they present the widest range of sunlight incident angles, they have the advantages of scattered light acceptance, good low-light response characteristics, stable operation, good sound insulation effect, easy installation, and low cost. The yearly electricity used for lighting on the second ring road in Kunming is up to 40 GWh and it is predicted that the installation of solar noise barriers will generate more than 16 GWh of electricity a year, which can supply a part of the consumption of streetlights. In addition, it can effectively block the transmission of noise and improve the quality of life of nearby residents [32].

2.2. Agrivoltaic

The main concept of agrivoltaic is to co-develop the same area of land for both conventional agriculture and PV systems. This kind of integration brings benefits also to the agricultural land managers: the cost of electricity is reduced, the growing season could be extended, and the shading by the PV panels reduces plant drought stress maintaining the temperature higher at night and colder during the day. This leads to a reduction of water consumption [33]. Several pilot Agri-PV projects has been implemented across the Netherlands and Germany. Recently, a German company has developed an arc-shaped PV system. The company estimated an additional yield at up to 30% compared to conventional ground-mounted systems and up to 60% compared to other agrivoltaic systems [34]. A 45 MW pilot PV project is also currently being planned (*Figure 29.a*).

Meanwhile, a French solar company has realized a new photovoltaic canopy for applications in agrivoltaic projects. The system has a rotating canopy that can host bifacial solar modules at a

height of more than 5.5 m to allow the passage of agricultural machineries. This lighter architecture reduces the carbon footprint of the structure, thanks to the less tons of steel used. In addition, the more aerial structure improves integration into the landscape (*Figure 29.b*). In 2022, the company will start a major program of agrivoltaic demonstrators, with 11 pilot sites of 6 hectares and 3 MWp of photovoltaic capacity each, spread throughout France, but the final goal is to deploy 1 GW by 2025 [35]. A similar PV integration has been tested in France with viticulture. It comes up a water demand reduction between 12 and 34% [36].



Figure 29 - a) Arc-shaped PV system [34], b) Solar canopy for agrivoltaics [35].

An early example of agrivoltaic is the so greenhouse integrated with photovoltaic modules. Among the biggest installations under construction, there are El Coronil IV and El Coronil V, the first two agro-energy greenhouses built in Andalucia. At El Coronil IV, the PV installation can reach an estimated output of 1,787,134 kWh annually, saving more than 700 tons of CO₂ emission. At El Coronil V, the estimated output is 1,250,994 kWh per year, saving more than 490 tons of CO₂ emission [37].



Figure 30 - El Coronil solar-agro energy greenhouse [37].

2.3. Floating PV

A particular attention goes to the floating photovoltaic systems: they are a slightly costly option as compared to the land-based PV installations, but they could bring additional benefits. To prove it, an interesting feasibility study proposes the installation of floating solar PV in the Rajghat dam, in the region of Uttar Pradesh, India. This reservoir serves multipurpose, mainly irrigation and hydroelectric power generation. The floating solar power plant can run with existing hydro power plant which represents an effective integration to meet the seasonal demand variation: the hydro power plant will operate at its peak during monsoon season when solar power generation is minimal and the solar power generation operates at its peak during summer season where water availability in Rajghat dam reduces significantly. It results that annual energy generation is 4,246,105 MWh for 10% PV coverage surface area and 10,623,501 MWh for a coverage area of 25% [38]. Further, it has been noted that the floating solar capacity installation is larger than the existing hydro power generation; the surplus power can be used through pumped hydro storage system for the successful integration of solar PV with the grid. Moreover, covering 25% of the surface area, 9.084 million cubic meters of water annually are saved from evaporation losses, contributing to limitation of water scarcity in agriculture and potable water scarcity [38].

The combination of floating photovoltaic and dams has been considered also for the hydropower plants of High Dam and Aswan Reservoir, in Egypt. Their total installed capacity is 2.65 GW. In this study, it is supposed to cover 50,000 m² of the total High Dam reservoir area with the floating PV panels and to install a floating PV system of 5 MW of capacity on the Aswan Reservoir (*Figure 31*). The results of the simulation show that FPV plants leads to an annual increase of the power generation of the hybrid hydro PV system up to 11.9 GWh for High Dam and 11.3 GWh for Aswan Reservoir, reducing carbon dioxide emissions by 44,270.61 tons [39].

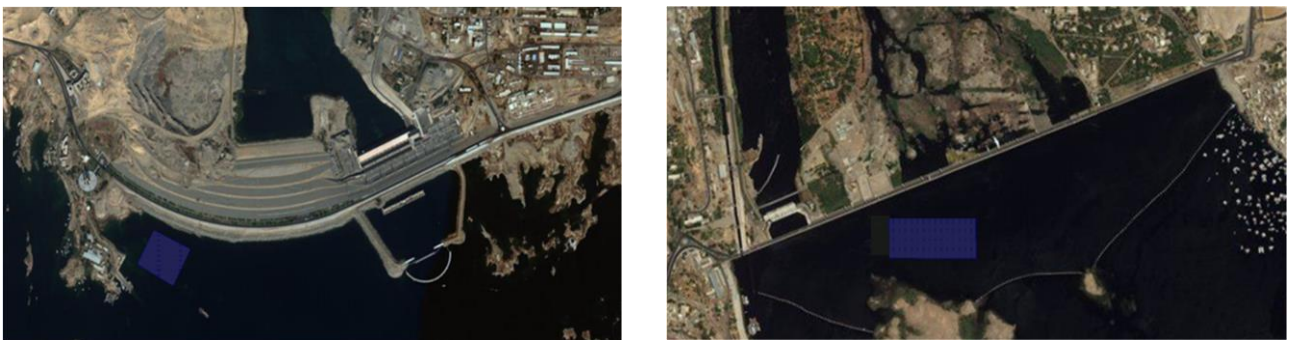


Figure 31 - a) Location of FPV system on the High Dam, b) Location of FPV system on the Aswan Reservoir [39].

In Swiss Alps, a floating PV system has been located at Lac des Toules. This solar park made up of 1440 panels is placed on a dam reservoir and it produces 818,000 kWh yearly. Each panel has an inclination equal to 37° to ensure the disposal of snowfall and maintain the optimal performance [40].



Figure 32 - solar floating plant in Switzerland [40].

Another proven integration of floating photovoltaic is in China, where a 70 MWp floating solar plant on a former coal mining area has been completed. The floating solar plant covers an area of 1.4 km² and is expected to generate up to 77,693 MWh in its first year, which is the electricity consumption of 20,910 households. This installation also preserves water bodies from algae proliferation and oxidation [41].



Figure 33 - Floating solar plant in a former coal mining area in China [41].

3. CableSmart: general system

In this study, a photovoltaic plant is assumed to be integrated into an innovative transport infrastructure derived from traditional cableways. Traditional cable systems have been employed mainly in the mountain tourism transport sector with the aim to move skiers, overcoming notable differences in height and natural obstacles as rivers and woods. This technology, in its traditional form, has not found common application in the urban transport field because of its limits.

The proposed system maintains the strengths of a traditional cableway and meantime overcomes its limits thanks to the synergies with a wheel-based system. It is a hybrid system named CableSmart that gives the possibility to enlarge the utilization of cable transport systems from a context strictly related to the mountain to urban mobility in a sustainable way [42]. The structure and operation of the system is described in the following section.

3.1. Traditional cableway

As already mentioned, the traditional cable-based technology is particularly effective in overcoming the differences in height and anthropic and natural obstacles as rivers and woods. Moreover, traditional cableways are one of the most environmentally friendly means of transportation with a low energy consumption and long service life. In general, all the cable car infrastructures have low land impact and present lower emission compared with the other public transportation systems: in average, the traditional cableway produces 20 gCO₂/(passenger*km) that is 80 % less than a bus [43].

Despite these merits, there are some constraints that limit their installation in urban areas:

- the system can travel only in linear direction without the possibility to perform curvilinear paths;
- the stations are noisy and bulky, and hence complex to integrate in urban areas;
- high maintenance costs;
- the absence of power supply on board implicates the absence of air-conditioning, heating and illumination.

Therefore, the proposed hybrid cable car - self-propelled system called CableSmart, has been designed to overcome these limits combining the advantages of traditional cable-based systems with those of automatic electric self-propelled systems [43].

3.2. Hybrid cable-self-propelled system

CableSmart allows the transmission of motion to the vehicles can be driven in two alternative ways:

- 1) through a hauling cable, as a traditional cableway
- 2) through motorised wheels, making the vehicles self-movable as a suspended monorail.

The sketch in *Figure 34* is reported as an example.



Figure 34 - Sketch of hybrid cable system [44].

The red line is the cable segment in which the system works as a traditional cable car. It allows to overcome notable differences in height and it can provide only a linear displacement. The blue line represents the segment where the motion is given to vehicles through motorized wheels, that move in a tread similar to a monorail, and it is suitable to define curvilinear paths also. Thanks to the hybrid system developed, tunnel and curvilinear trajectories can be covered by the vehicles which are also able to completely stop at the station [45]. In this way, it is possible the easy embarkment and dis-embarkment of people with reduced mobility. Moreover, the passage from one operational modality to another takes place inside the station in a completely automatic manner: in this way, the passengers have not to get off the vehicles. This solution makes the cable public transport suitable also in urban areas.

The vehicles are similar to the traditional cable car, and they can host up to 8-10 passengers, but unlike the latter, they are equipped with electricity power sources [45]. Being an electricity power source available, ancillary services as illumination, heating and air-conditioning are provided, improving the comfort of the transport vehicle with respect to the traditional one [44]. Also a smart system can be included to regulate and optimize the passengers boarding and give them the

possibility to personalize the itinerary: before boarding the cabin, it is possible to select the destination in order to not deboard the vehicle along the itinerary. This leads also to automatically adjusts the departures depending on the number of passengers recorded at boarding. Since the cabins operate only when people are boarding, up to 50% of empty vehicles runs are avoided. This results in less wear on all equipment, reducing significantly the maintenance cost of the whole infrastructure [46].

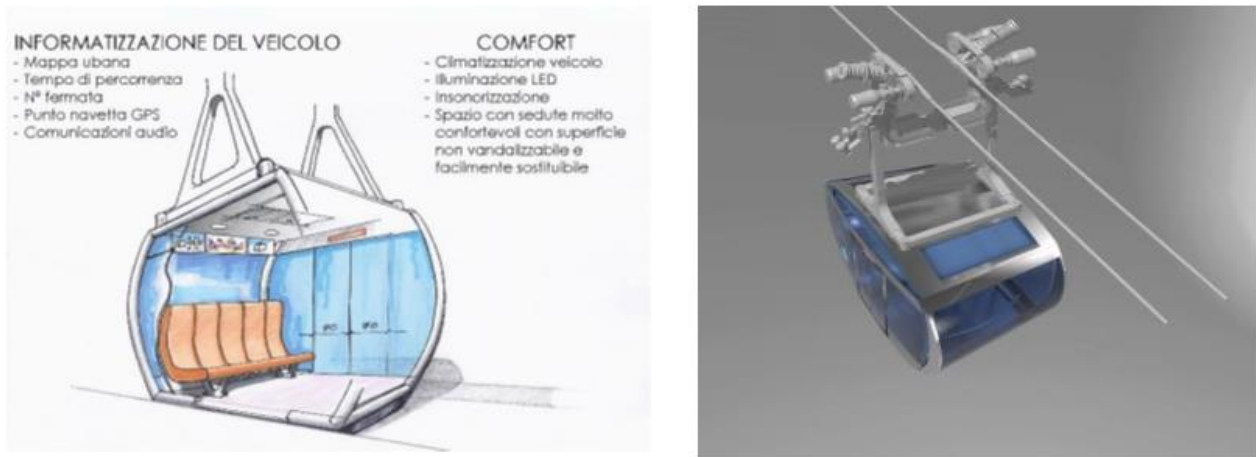


Figure 35 - Sketch of the cabin [40].

Furthermore, terminal and intermediate stations are allowed along the trajectory. The stations become less noisy and bulky, so much that intermediate stations have dimension comparable with the one of a bus station. In this way, it is possible to define a transportation net able to intersect more pathways in one station [43].

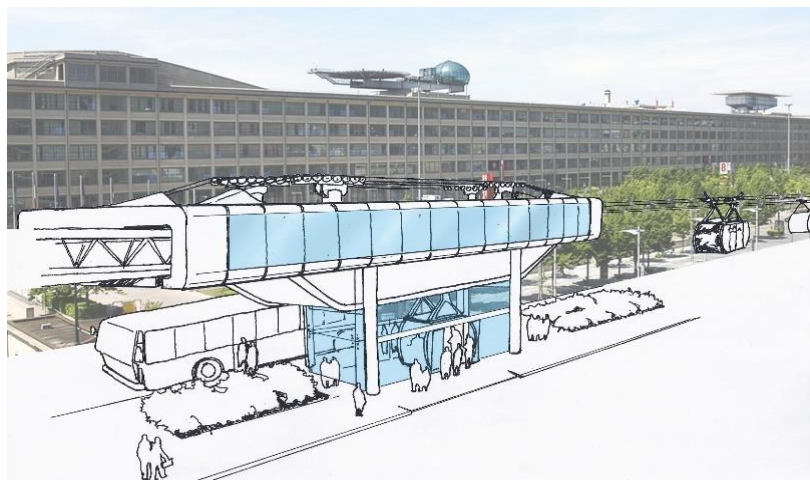


Figure 36 - Sketch of a station of the hybrid system similar to a bus station [39].

From the environmental point of view, the total emissions of the system CableSmart result to be extremely low. It has been estimated that the hybrid system produces around 16 gCO₂/(passenger*km) [43], [47].

Advantages and disadvantages of traditional cable car-based systems and hybrid systems as CableSmart are summed up and listed in *Table 5*.

TRADITIONAL CABLEWAYS	HYBRID CABLE-SELF-PROPELLED SYSTEMS
✓ Low-carbon emissions	✓ Extremely low-carbon emissions
✓ Low land impact	✓ Low land impact
✓ Low installation costs	✓ Low installation costs
✗ High maintenance costs	✓ Low maintenance costs
✓ Overcome high difference in height	✓ Overcome high difference in height
✓ Overcome anthropic and natural obstacles	✓ Overcome anthropic and natural obstacles
✗ Only linear paths	✓ Both linear and curvilinear paths
✗ Noisy and bulky stations	✓ Silent and smaller stations
✗ Not possible to integrate in urban areas	✓ Possible to integrate in urban areas
✗ Electricity power source not available on board	✓ Electricity power source available on board
✗ Vehicles don't stop at stations	✓ Vehicles stop at stations
✗ No possibility of route customization	✓ Possibility of route customization

Table 5 - Comparison between traditional cableways and hybrid cable-self-propelled systems.

The main difference between the traditional system and CableSmart is the presence of the “rail” infrastructure, that gives the possibility of making the vehicles self-movable by equipping them with electrical motors [45]. Indeed, CableSmart presents motorised wheels installed on board, near the grip with the cable. They are fed by a battery located in the bottom part of the cabin and it is useful also for ancillary services, as illumination, climate control system, video surveillance and smart control systems [44].

Figure 37 shows the render of the hybrid system concerning the rail path.

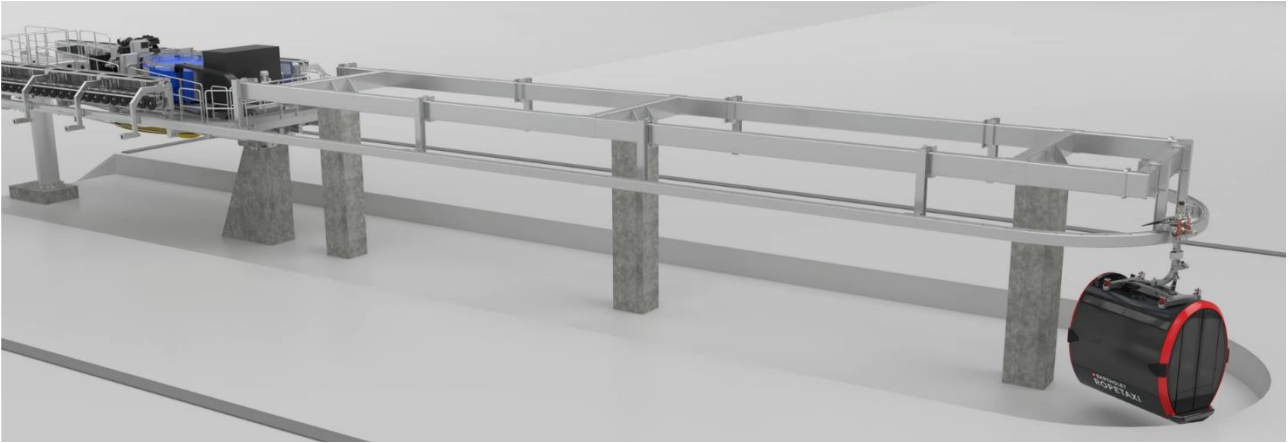


Figure 37 - Render of the suspended monorail [43].

Hence, in addition to structural benefits linked to urban mobility, further benefits of CableSmart have been observed. As already mentioned, from the environmental point of view, the energetic impact of such a hybrid system is very low and can be further reduced integrating the structure with photovoltaic panels. The modules could be installed on the station roofs and on the rail frame along the line, as shown in *Figure 38*. From the economics point of view, the system is more reliable and present lower maintenance costs with respect to the traditional cableway [43].

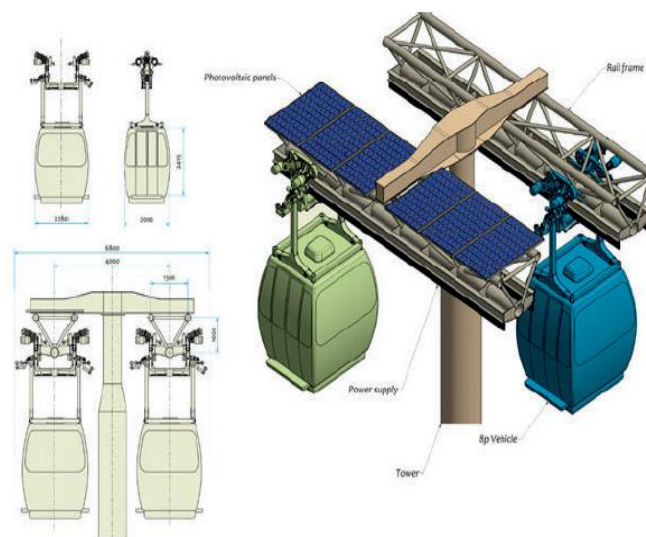


Figure 38 - Installation of the solar panels on the system components [45].

4. The study procedure

This study will focus on the analysis of the transport system previously described. The goal of the thesis is to conduct a feasibility study on the integration of photovoltaic panels with this cable-based system to feed part of its energy request, demonstrating that, from the point of view of the energetic impact, an already innovative system as CableSmart can be further improved, in the perspective of a more sustainable future.

The case study under investigation concerns the future construction of a cableway path located near La Thuile, in the Italian region Aosta Valley. The input parameters that characterize the model of the cableway are:

- 1) the *length* of the line
- 2) the *difference in height* of the line
- 3) the *maximum capacity* of the cableway, here meant as the number of passengers which can be transported per hour per direction
- 4) the *number of rollers* per direction presented along the line
- 5) the *mass* of an empty cabin and its kinematic characteristics
- 6) the *number* and the *length* of terminus and intermediate stations.

All the calculations and analyses are done on hourly basis with time horizon of one year.

At first, the energy load profile of the cableway is calculated under all the hypotheses of the case, explained in *Chapter 5* and results are reported in *Chapter 8.1*.

Then, the production profile of the photovoltaic plant installed in the considered geographical location is obtained. As a first approximation, it has been done by means of the software PVGIS.

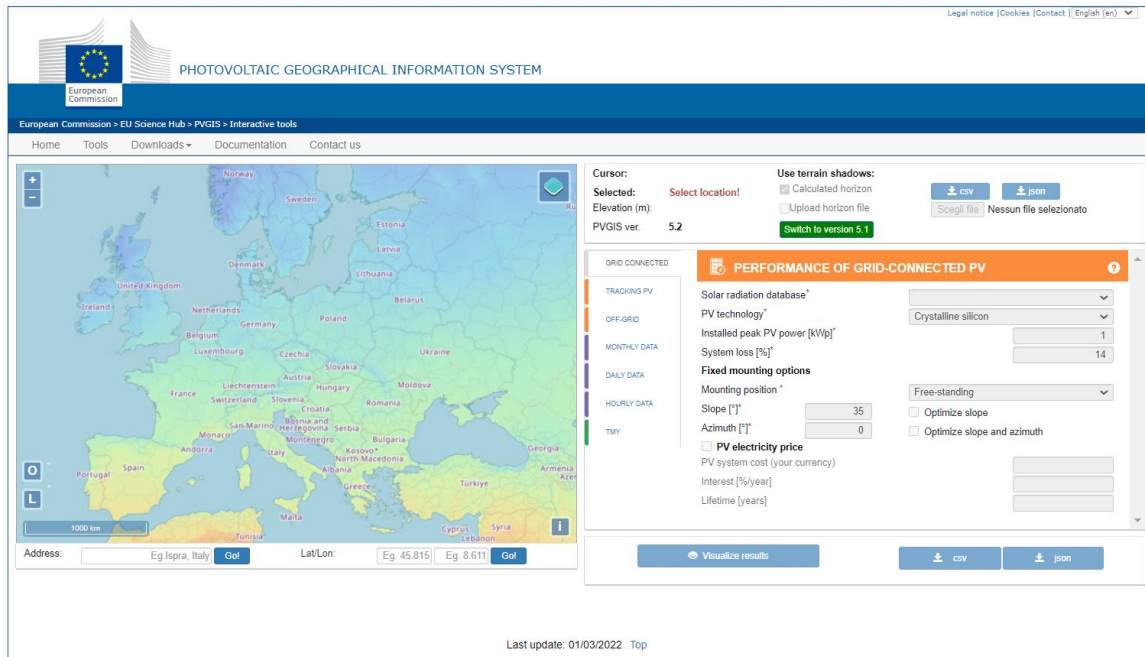


Figure 39 - PVGIS software.

But the values obtained seem to be not suitable with the adopted model: indeed, supposing to install a plant of 1 kW_p, the maximum hourly power produced, results equal to 0.5 kW. This is not realistic, and it is since PVGIS provides data derived by an average of the past years, whereas in this analysis the necessary data are punctual. For this reason, it has been chosen to take the hourly electricity produced by 1 kW_p of an existing solar plant in La Thuile which is monitored by the software *Solarlog*.



Figure 40 - Solarlog software.

These data, together with the nominal power of the PV plant installed and its yearly specific energy, are used to determine the photovoltaic energy produced by the PV system. Indeed, all these information allow to obtain the correct shape of the solar production. The curve is proportionally scaled depending on the annual specific production of the considered PV plant layout and the nominal power installed. Hence, the final hourly energy produced by the photovoltaic system considered is:

$$\text{PV plant energy production} \left[\frac{kWh}{kW_p} \right] = \frac{\text{reference energy production} \left[\frac{kWh}{kW_p} \right]}{\text{reference specific energy} \left[\frac{kWh}{kW_p} \right]} * \frac{\text{PV plant specific energy} \left[\frac{kWh}{kW_p} \right]}{\text{reference specific energy} \left[\frac{kWh}{kW_p} \right]} * \text{PV plant nominal power} \left[kW_p \right]$$

where:

- the *reference energy production* is the hourly energy production by 1 kW_p given by the PV plant monitored by *Solarlog*
- the *reference specific energy* is the annual specific energy given by the PV plant monitored by *Solarlog*
- the *PV plant nominal power* and the *PV plant specific energy* refer to photovoltaic installation of the case study

The *PV plant nominal power* installed is obtained by sizing the system and the *PV plant specific energy* is given by PVGIS.

Once all the necessary information about load and production sides are known, the energy simulation of the system is done on a dedicated Excel model. Basically, two different scenarios are analysed and compared:

- 1) the first scenario, that is the basic scenario of the study, which considers:
 - the installation of *photovoltaic solar panels* on the *avalanche barriers* erected on the mountain close to the transport system
 - the connection with the electric grid in order to buy electricity from the net or sell electricity to the net, according to the necessity
- 2) the second scenario considers:
 - PV panels integrated not only on the *avalanche barriers* erected close to the cableway, but also on *roofs* and *walls* of the stations and the vehicles of the cableway
 - the connection with the electric grid in order to buy electricity from the net or sell electricity to the net, according to the necessity

Then, the *sensitivity analysis* is done changing, one at a time, the key parameters that characterize the transport system and the PV plant. In particular, by changing:

- the *distance* between two subsequent lines of avalanche barriers
- the *tilt angle* of panels integrated with the avalanche barriers
- the *length* of the line
- the *number of rollers* per direction presented along the line

A further subcase of the basic scenario is simulated by considering the possibility to also install a storage system, as a series of *batteries*. The energy simulations have been carried out and the results of the cases with and without the accumulation system are compared.

All the calculations and analyses are done on hourly basis with time horizon of one year.

Numerically, the hourly energy E corresponds to the mean power P_m because the considered interval of time Δt is equal to 1 hour.

$$E(t) = \int_{t_{in}}^{t_{fin}} P_m(t) dt$$

$$E = P_m \Delta t$$

For that reason, all the reported graphs will present energy on the vertical axis.

The economic analysis of all the presented scenarios is then reported.

Finally, it is proposed the comparison between the first scenario of the case study with the CableSmart transport system and the same scenario, with unchanged parameters, applied to a traditional cableway.

All the steps of the energy load and production profile definitions, the energy simulation and the economic analysis are explained in detail in the following sections. Therefore, the case study is presented and results are shown.

5. Energy load profile

The first step of the analysis is to calculate the energy consumption of the cableway, focusing at first on the energy requested by a single vehicle to move along a generic trajectory. The final energy consumption is derived by sum of different energy requirements:

1. Energy for the acceleration phase
2. Energy to overcome the difference in height of the line
3. Energy to compensate the energy dissipated along the line due to frictions

This is done with hourly granularity for one day of each month of the year, introducing the input parameters that affects the energy load of the vehicle and beforementioned in *Chapter 4*:

- the length of the line l
- the difference in height of the line h
- the maximum capacity of the structure q_{MAX}

The last will affect the energy consumption of the vehicle hour by hour and month by month.

5.1. Acceleration phase

The acceleration phase considers the energy that an electric motor must supply to accelerate a cabin at rest to the cruising velocity:

$$E_{ACC,1} = \frac{\frac{1}{2} M_{TOT} v^2}{\eta_{MOT}}$$

where:

- M_{TOT} is the total mass of the cabin, that is the sum of the mass of the empty cabin and the mass of passengers
- v is the cruising velocity, that is the velocity during the regime phase
- η_{MOT} is the efficiency of the electric motor

Since the system is symmetrical in the acceleration and deceleration phases, the kinematic formula is also valid in the deceleration phase of the cabin, in which the energy is lost:

$$E_{DEC,1} = \frac{1}{2} M_{TOT} v^2$$

Under the hypothesis that it is possible to store energy lost during the deceleration phase and to use it during the acceleration phase, the energy required to accelerate the vehicle is:

$$E_{ACC} = E_{ACC,1} - E_{DEC,1} (\eta_{BATT} * \eta_{REC})$$

where:

- η_{BATT} is the efficiency of the battery system
- η_{REC} is the efficiency of the energy recovery system

In the path from valley to mount, the acceleration phase occurs not only at the valley station, but also at the departures of all the intermediate stations presented along the line. Hence, the final energy acceleration necessary to accelerate a cabin is:

$$E_{ACC} = E_{ACC}(1 + N_{IS})$$

where:

- N_{IS} is the number of intermediate stations along the line

If an entire cycle is considered, the acceleration energy becomes equal to:

$$E_{ACC,cycle} = [E_{ACC}(1 + N_{IS})] * 2$$

5.2. Elevation

An amount of energy must be supplied to the vehicle to overcome the difference in height, so to move it from valley to mount. This energy has been calculated as follow:

$$E_g = E_{g,VM} = M_{TOT} g h$$

where:

- h is the difference in height between valley and mount
- g is the gravity acceleration

Supposing that in the path from mount to valley the cabin is empty, the potential energy is considered equal to:

$$E_{g,MV} = M_0 g h$$

where:

- M_0 is the mass of the empty cabin

In this way, the energy necessary to overcome the difference in height for one cycle is:

$$E_{g,cycle} = E_g - E_{g,MV}$$

5.3. Frictions

A surplus of energy must be fed in order to face the dissipations along the entire trajectory. In this analysis, the *rolling friction* between the rollers and the rope of the cableway and the *viscous friction* of the air with the cabin are considered.

Firstly, the *rolling resistance* has been obtained by the following formula:

$$R_R = c M_{TOT} g$$

where:

- c is the *rolling coefficient* between the rollers and the rope of cableway
- g is the gravity acceleration

Then, the computation of the power dissipated due to this phenomenon is split into two separated phases of the motion: during the regime phase, in which the velocity has been considered constant and equal to the cruising velocity v , and during the acceleration and deceleration phases, in which the velocity has been considered equal to the mean value between 0 and the regime velocity v . This leads to the following dissipated powers:

$$P_{R,REG} = R_R v$$

$$P_{R,ACC/DEC} = R_R \frac{v + 0}{2}$$

Knowing the length of each phase, it is possible to calculate the energy dissipated as:

$$E_{R,REG} = P_{R,REG} t_{REG}$$

$$E_{R,ACC/DEC} = P_{R,ACC/DEC} t_{ACC/DEC}$$

where:

- t_{REG} is the time taken to cover the length in regime phase
- $t_{ACC/DEC}$ is the time for covering the length in acceleration and deceleration phases considering the acceleration a of the cabin

In particular:

$$t_{REG} = \frac{L_{REG}}{v}$$

where:

- L_{REG} is the length of the line in which the vehicle travels at regime velocity

L_{REG} is calculated as:

$$L_{REG} = l - N_{IS} * L_{IS} - L_{TS}$$

where:

- l is the total length of the line
- L_{IS} is the length of the intermediate stations
- L_{TS} is length of the terminus stations

And with

$$t_{ACC} = \frac{v - 0}{a}$$

$$t_{DEC} = \frac{0 - v}{-a}$$

Clearly, these two quantities of time are equal.

In addition to t_{ACC} , t_{DEC} and t_{REG} , also the stopping time t_{STOP} is known, that is the stopping time of the cabin at each station. So, the following kinematic parameters are computed:

$$T_c = [t_{REG} + (t_{ACC} + t_{STOP} + t_{DEC}) * (1 + N_{IS})] * 2$$

$$f = \frac{1}{T_c} * 3600$$

where:

- T_c is the cycle time expressed in *seconds*
- f is the frequency expressed in *cycles/hour*

Finally, the energy dissipated by one vehicle due to rolling frictions is:

$$E_{R,roll} = E_{R,REG} + E_{R,ACC/DEC}(1 + N_{IS})$$

$E_{R,roll}$ refers to only one single roller, and so, knowing the total number of rollers per direction of the line n_{roll} , the total energy dissipation is:

$$E_R = n_{roll} * E_{R,roll}$$

If an entire cycle is considered, the energy dissipated becomes equal to:

$$E_{R,cycle} = n_{roll} * E_{R,roll} * 2$$

In the same way, the *aerodynamic resistance* due to *viscous friction* with the air has been defined in the two phases of motion:

$$R_{AER,REG} = \frac{1}{2} \rho C_f A_{\perp} v^2$$

$$R_{AER,ACC/DEC} = \frac{1}{2} \rho C_f A_{\perp} \left(\frac{v + 0}{2} \right)^2$$

where:

- ρ is the air density
- C_f is the *shape coefficient* related to shape of the vehicle and in this study is adopted the shape coefficient of a square surface which is very high
- A_{\perp} is the surface of the frontal face of the cabin, so the face perpendicular to the direction of movement of the vehicle

By following the same procedure used for the *rolling frictions*, it has been obtained the power dissipated due to the *aerodynamic resistance*:

$$P_{AER,REG} = R_{AER,REG} v$$

$$P_{AER,ACC/DEC} = R_{AER,ACC/DEC} \frac{v + 0}{2}$$

Knowing the length of each phase, it is possible to calculate the energy dissipated as:

$$E_{AER,REG} = P_{AER,REG} t_{REG}$$

$$E_{AER,ACC/DEC} = P_{AER,ACC/DEC} t_{ACC}$$

and, finally:

$$E_{AER} = E_{AER,REG} + E_{AER,ACC/DEC} (1 + N_{IS})$$

If the cycle is considered, the energy becomes:

$$E_{AER,cycle} = [E_{AER,REG} + E_{AER,ACC/DEC} (1 + N_{IS})] * 2$$

5.4. The capacity and the final energy load

As mentioned, the capacity is a crucial parameter in the determination of the energy load and such a load is a function of the hour and of the season. The maximum capacity q_{MAX} is predefined for the transport system under investigation. Two other parameters are introduced in order to simulate as faithful as possible the real monthly and hourly capacity that the system must face:

- the *filling factor* μ_h , which takes into account the different capacity from hour to hour of operation of the cableway during the day
- the *capacity factor* μ_m , which takes into account the different capacity from month to month of operation of the cableway during the year

Since the cabins of CableSmart operate only when people are boarding, the previous considerations allow to calculate the number of vehicles involved each hour to satisfy the estimated mobility request:

$$n_V = \frac{\mu_h \mu_m q_{MAX}}{n_p}$$

where:

- n_p is the number of passengers per cabin

This directly affects the total mass M_{TOT} involved in the computation of the energy requested to accelerate the cabin, to overcome the difference in height and to compensate the dissipation of energy due to rolling frictions.

Indeed, it results that in one hour the cableway move from valley to mount a mass of:

$$M_{TOT} = n_V [M_0 + n_p M_p]$$

where:

- M_p is the average mass of one person

The previous formulation for M_{TOT} is used to calculate the beforementioned contributions to the load energy request. Therefore, the hourly energy load is obtained as:

$$E_{load} = E_{ACC} + E_g + E_R + E_{AER}$$

If the cycle is considered:

$$E_{load,cycle} = E_{ACC,cycle} + E_{g,cycle} + E_{R,cycle} + E_{AER,cycle}$$

Finally, the yearly load can be calculated:

$$E_{load,year} = \sum_{m=1}^{m=12} \sum_{h=opening}^{h=closure} E_{load}$$

where:

- m represents all the months of operation of the system
- h all the hours of operation of the system

6. Energy Simulation

At this point, the integration of solar panels is introduced. It is necessary to know the production profile of the photovoltaic installed. As seen before, the hourly energy produced by 1 kW_p is given by the available data of an existing PV plant in La Thuile. This allows to obtain the correct shape of the solar production of another PV system installed in the same place. Indeed, this curve is proportionally scaled depending on the annual specific production of the considered PV plant layout and the nominal power installed. Hence, the final hourly energy produced by the photovoltaic system considered is:

$$\frac{PV \text{ plant energy production}}{[kWh]} = \frac{\text{reference energy production}}{\left[\frac{kWh}{kW_p}\right]} * \frac{PV \text{ plant specific energy } \left[\frac{kWh}{kW_p}\right]}{\text{reference specific energy } \left[\frac{kWh}{kW_p}\right]} * \frac{PV \text{ plant nominal power}}{[kW_p]}$$

where:

- the *reference energy production* is the hourly energy production by 1 kW_p given by the PV plant monitored by *Solarlog*
- the *reference specific energy* is the annual specific energy given by the PV plant monitored by *Solarlog*
- the *PV plant nominal power* and the *PV plant specific energy* refer to photovoltaic installation of the case study

The *PV plant nominal power* installed is obtained by sizing the system and the *PV plant specific energy* is given by PVGIS.

Therefore, the energy simulation is implemented on an Excel model. The energy simulation has been carried out on hourly basis with time horizon of one year.

All these steps of the procedure are explained in detail below.

6.1. PV sizing

To correctly size the system is necessary to define the geometrical characteristics of the support structure. Basing on them, the parameters which interest the photovoltaic panels are found: the azimuth angle, the tilt angle and the number of modules that is possible to integrate and, consequently, the nominal power installed in the site.

The three parameters, and so the production profiles, are defined for these scenarios:

- 1) the first scenario with *photovoltaic solar panels* on the *avalanche barriers* erected on the mountain close to the transport structure
- 2) the second scenario with panels integrated not only on the *avalanche barriers* erected close to the cableway, but also on *roofs* and *walls* of the stations and of the vehicles of the cableway

6.1.1. Avalanche barriers

The tilt angle and the azimuth angle of the solar panels integrated with the avalanche barriers depend on the geometrical parameters of the barriers themselves. Hence, the avalanche barriers are dimensioned according with the rules reported in “*Costruzione di opera di premunizione contro le valanghe nella zona di distacco*” [48] to know the area available to install photovoltaic modules. The idea is to put in pose the panels on the struts of the barriers shown in *Figure 41*.

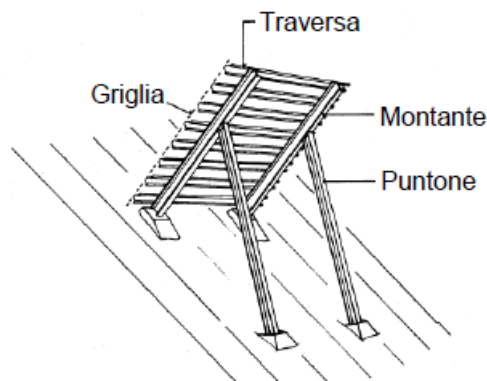


Figure 41 - Sketch of the avalanche barrier [48].

The geometrical parameters of the avalanche barriers are shown in *Figure 42*, where:

- D_k is the *useful* height of the structure grill
- H_k is the height of the structure measured vertically
- B_k is the *real* height of the structure grill
- L_s is the length of the strut
- ψ is the slope angle of the mountain
- α is the slope angle of the strut with respect to the slope of the mountain

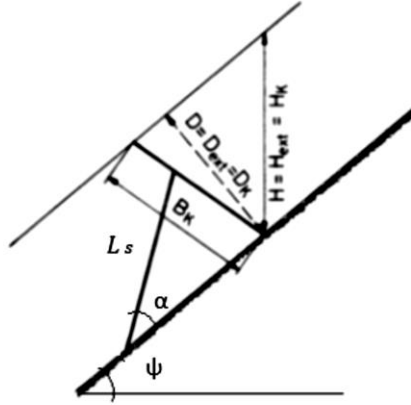


Figure 42 - Geometrical parameters of an avalanche barriers [48].

The azimuth angle γ is set equal to the one of the avalanche barriers and so equal to that of the side of the mountain. Concerning the tilt angle, some hypothesis and computations have been done.

The H_k of the structure must be chosen so that it exceeds the maximum height of the snow mantle reached in that location in the recent years, called the extreme height H_{estr} .

$$H_k \geq H_{estr}$$

Immediately, D_k can be calculated in order to select the suitable model of avalanche barrier.

$$D_k = H_k \cos \psi$$

In this analysis, being the angle between D_k and B_k very very small, the two quantities are considered approximately equal:

$$B_k \cong D_k$$

It means that the grid of the barrier is erected in order to be as perpendicular as possible to the terrain, where in this case the terrain is the sloped side of the mountain.

Knowing the length of the strut L_s and supposing that it is fixed at the structure grill at the point in which the height of the grill is equal to 70% B_k , it results that:

$$\alpha = \sin^{-1} \left(\frac{0.7B_k}{L_s} \right) = \sin^{-1} \left(\frac{0.7D_k}{L_s} \right)$$

In this way, the tilt angle β of the photovoltaic panels can be set equal to:

$$\beta = \alpha + \psi$$

The solar panels are supposed to be integrated along the length of the strut L_s . The number of modules of PV installed per each avalanche barrier results equal to:

$$N_p = \frac{L_s}{u}$$

where:

- u is the width of the type of PV panel installed

The dimensions of the module are known from its datasheet.

Then, the orographic situation has been studied to calculate the number of avalanche barriers that can be erected in the side of the mountain considered in the case study. The correlation useful to compute the optimal distance L between two subsequent and parallel lines of avalanche barriers can be found in literature [48]:

$$L = f_L H_k$$

where:

- f_L is the *distance coefficient*

f_L is function of the slope of the mountain, the *slip coefficient*, the *friction angle* ϕ between the terrain and the snow, and of H_k . The values of these parameters and the corresponding value of L are tabulated in *Costruzione delle opera di premunizione contro le valanghe nella zona di distacco* [48].

The layout of the PV system is simulated by means of the software Helioscope setting the number of panels installed per each barrier N_p , the distance between the avalanche barriers L , the azimuth and the tilt angle of the solar panels. The software returns the nominal power installed in the configuration. Azimuth and tilt angles are then inserted on PVGIS to obtain the yearly specific energy. It is pointed out that there is a very short portion of B_k over the length L_s which could be responsible of shadow effect on the neighbouring solar panels. Because of this, the specific energy from PVGIS has been further reduced by 0.5%.

6.1.2. Roofs and walls

In the second scenario, the integration of photovoltaic also in the transport system is considered. The PV panels installed are the same model adopted in the first scenario.

Starting from the flat roofs of the stations, the azimuth angle of panels is set equal to 180° (if North is considered 0°) so that the plant is South facing, and the tilt angle is set as the optimal one by PVGIS. The distance between two adjacent and parallel rows of panels is investigated to avoid the shading effect. The distance has been defined so that the shadow of one row of panels does not affect the subsequent row during the best hour of the worst day of the year.

The length of the shadow is computed on a dedicate Excel program, in which the input data are:

- the latitude of the place in which the PV plant is installed
- the length of the side of the module responsible for the shadow effect
- the azimuth and tilt angle of the panels
- the solar declination

This information is necessary to compute the maximum solar height δ as:

$$\delta = 90^\circ - \text{latitude} - \text{solar declination}$$

In this case, the length of the side of the module responsible for the shadow effect is u because it is supposed to install panels in *landscape* orientation. Therefore, the length of the shadow x_{shad} is defined as:

$$x_{shad} = \frac{u \sin \beta \cos \gamma}{\tan \delta}$$

Knowing the dimensions of the roofs of all the stations, the number of panels installed is calculated considering a distance of x_{shad} between two subsequent rows of solar panels. Therefore, the nominal power installed is computed. Azimuth and tilt angle are provided to PVGIS to return the annual specific energy. Because of the shadow effect, a decrement by 10% of the annual specific production has been applied for these installations.

For the roofs of the cabins, the azimuth angle of panels is supposed to be 180° and so South facing and tilt angle is null. The shadow of the vertical support of the vehicle affects the performance of the solar system. Moreover, there are parts of the line that are shaded. For these reasons, it is supposed an overall decrement of the specific production, obtained by PVGIS, by 20%. Knowing the dimensions of the roofs of the vehicles, the number of panels per cabin and the nominal power installed per cabin is calculated. The total energy produced by solar panels depends on the number of vehicles involved in the line, which varies hourly and monthly as already explained in *Chapter 5.4*. Hence, in the energy simulation, the hourly operating number of PV panels will be correlated with the hourly operating number of vehicles.

Concerning the four vertical walls of stations and cabins, the tilt angle is always set equal to 90° . Clearly, the power production of each wall of panels is different depending on the orientation of the wall: panels installed on the wall oriented towards South will produce more than panels on the wall

oriented towards North. The angles to enter in PVGIS to return the specific energies are reported in *Table 6*.

Wall orientation	Azimuth angle	Tilt angle
North	0°	90°
South	180°	90°
East	90°	90°
West	270°	90°

Table 6 - Azimuth and tilt angles depending on the orientation.

The arithmetic mean of these four values of specific energy is computed. The obtained specific energy is further reduced by 10% for the walls of the cabins because of the shaded parts of the line. Knowing the dimensions of the walls of stations and cabins, the number of panels and the nominal power installed is calculated. As already seen for the cabin roofs, also for the walls the energy produced by PV is strictly related with the number of vehicles involved in the line.

6.2. Electric grid

In the basic scenario and the second scenario, the energy simulation logic is set so that the energy produced by the PV plant is first used to satisfy the load. In case the electricity produced by solar panels, exceeds the energy requested by the load, the surplus of electricity is sold to the electric grid.

$$E_{PV}(t) > E_{load}(t) \rightarrow E_{grid,sold}(t) = E_{PV}(t) - E_{load}(t)$$

Vice versa, if the electricity produced is not sufficient to satisfy the load, the deficit is covered by the grid, so electricity is bought.

$$E_{PV}(t) < E_{load}(t) \rightarrow E_{grid,bought}(t) = E_{load}(t) - E_{PV}(t)$$

6.3. Storage system

Slightly different is the case in which an accumulation system is supposed to be installed, indeed the energy stored or released by the batteries will be taken into account. The simulation logic is changed.

If the energy produced exceed the load request, a storage system is charged, so in this case, batteries are charged until they reach their maximum capacity C_{MAX} .

$$E_{PV}(t) > E_{load}(t) \left\{ \begin{array}{ll} E_{BATT}(t) = E_{PV}(t) - E_{load}(t) & \text{if } SoC(t-1) * C_{MAX} + E_{PV}(t) - E_{load}(t) \leq C_{MAX} \\ E_{BATT}(t) = C_{MAX} - SoC(t-1) * C_{MAX} & \text{if } SoC(t-1) * C_{MAX} + E_{PV}(t) - E_{load}(t) > C_{MAX} \end{array} \right.$$

where:

- $E_{BATT}(t)$ is the surplus of energy injected into the battery on hourly basis
- C_{MAX} is the maximum capacity of the battery
- $SoC(t-1)$ is the *State of Charge* of the battery of the past hour

The actual *SoC* of the battery is calculated:

$$SoC(t) = SoC(t-1) + \frac{E_{BATT}(t)}{C_{MAX}}$$

When batteries are just fully charged, the surplus of photovoltaic electricity is sold to the grid. So, if:

$$E_{PV}(t) > E_{load}(t)$$

and

$$SoC(t-1) * C_{MAX} + E_{PV}(t) - E_{load}(t) > C_{MAX}$$

and

$$SoC(t) = 100\%$$

hence

$$E_{grid,sold}(t) = E_{PV}(t) - E_{load}(t) - E_{BATT}(t)$$

The energy into the batteries is used when the load request of energy exceeds the production of the PV plant.

$$E_{PV}(t) < E_{load}(t) \left\{ \begin{array}{ll} E_{BATT}(t) = E_{load}(t) - E_{PV}(t) & \text{if } SoC(t-1) * C_{MAX} + E_{PV}(t) - E_{load}(t) \geq 0 \\ E_{BATT}(t) = SoC(t-1) * C_{MAX} & \text{if } SoC(t-1) * C_{MAX} + E_{PV}(t) - E_{load}(t) < 0 \end{array} \right.$$

where:

- $E_{BATT}(t)$ is the energy released by the battery on hourly basis
- C_{MAX} is the maximum capacity of the battery
- $SoC(t-1)$ is the *State of Charge* of the battery of the past hour

The actual *SoC* of the battery is calculated:

$$SoC(t) = SoC(t - 1) - \frac{E_{BATT}(t)}{C_{MAX}}$$

When batteries are fully discharged, the load is satisfied by the electric grid. So, if:

$$E_{PV}(t) < E_{load}(t)$$

and

$$SOC(t) = 0\%$$

and

$$SOC(t - 1) * C_{MAX} + E_{PV}(t) - E_{load} < 0$$

hence

$$E_{grid,bought}(t) = E_{load}(t) - E_{PV}(t) - SoC(t - 1)$$

The maximum capacity C_{MAX} of the batteries is defined by sizing the storage system. The effect of the size of batteries on the energy performance of the system is studied by means of a *sensitivity analysis*.

The *sensitivity analysis* considers mainly two energetic indicators: the *self-sufficiency* and *self-consumption*, both expressed in percentage. *Self-sufficiency* represents the fraction of energy request that is directly fed by the photovoltaic installation, whereas the *self-consumption* represents the fraction of the total energy produced by the solar panels that is used to directly feed the load. In absence of a storage system, *self-sufficiency* and *self-consumption* are defined as:

$$Self - sufficiency = \frac{Energy\ from\ PV\ to\ load}{Energy\ load}$$

$$Self - consumption = \frac{Energy\ from\ PV\ to\ load}{PV\ production}$$

If storage is present, the energetic indicators become:

$$Self - sufficiency = \frac{Energy\ from\ PV\ to\ load + Energy\ from\ storage\ to\ load}{Energy\ load}$$

$$Self - consumption = \frac{Energy\ from\ PV\ to\ load + Energy\ from\ storage\ to\ load}{PV\ production}$$

7. Economic Analysis

Finally, the economic feasibility study of the photovoltaic installations is carried out for the first and second scenario. The economic analysis has been done also in the case in which the accumulation system is added to the basic scenario. The considered period has been set equal to N years that is the lifetime of the photovoltaic plant.

7.1. Fundamental quantities

7.1.1. Initial investment

The *Capital Expenditure* (CAPEX) is the initial investment to face for the installation of the entire photovoltaic plant and, if present, the storage system. The CAPEX is considered for the year zero of construction of the plant. And further cost is eventually added in correspondence to the year of substitution of panels or batteries.

7.1.2. Costs

The *Operating & Maintenance Costs* $C_{O\&M}$ include all the costs to ensure the correct operation of the plant and these costs are present every year of life of the PV system. Yearly, their values correspond to 0.5 % of the PV cost considered in the CAPEX.

$$C_{O\&M} = 0.5\% \text{ PV cost}$$

Together with the *Operating & Maintenance Costs*, also the *Insurance Costs* C_I are annually considered as:

$$C_I = 2\% \text{ PV cost}$$

7.1.3. Incomes

The sources of income are essentially two: the incomes derived from the amount of electricity produced by photovoltaic and sold to the grid and the incomes derived from the electricity produced by photovoltaic and directly consumed by the load. The last are savings due to the failure to

purchase of electricity from the grid. If a storage is present, the photovoltaic energy stored and send to the load at a later time is included into the savings. The actual price of electricity bought and sold to the net are adopted.

7.2. The procedure

Firstly, all the above-mentioned quantities have been calculated for N years of life of the plant. An *inflation* i has been considered for the first n years, for which all the quantities have been calculated following the general formula:

$$X(n, i) = X(n) * (1 + i)^n$$

where:

- $X(n)$ is the quantity at year n calculated without inflation
- $X(n, i)$ is the quantity at year n calculated with the contribution of inflation.

Then, the *cashflow analysis* is done in order to understand the annual trend of costs and savings in the considered configuration of the system.

Finally, the *cumulated cashflow* has been computed to obtain the *Payback Time*. The *cumulated cashflow* demonstrates if the investment is convenient or not and it correspond to the profit earned at year N , whereas the *Payback Time (PBT)* is the period of time necessary to recover the initial investment.

8. CASE STUDY

The study is applied to a future planning of a cableway situated in La Thuile, a municipality in the Italian region Aosta Valley. The layout of the path of the cableway is shown in *Figure 43*.

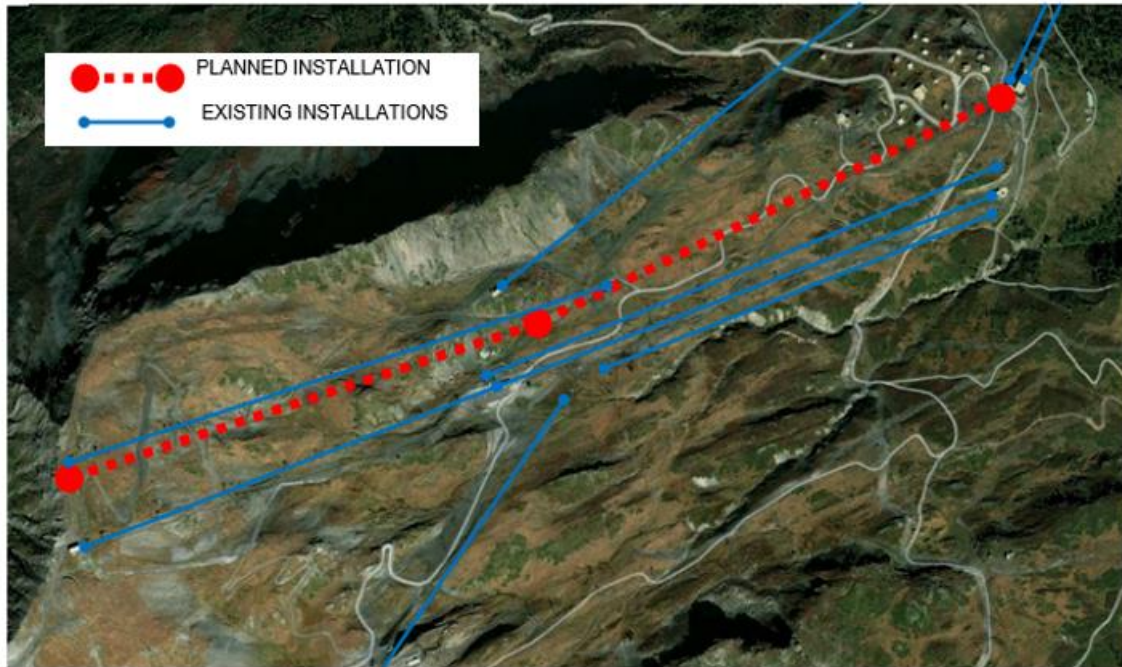


Figure 43 - Layout of the planned cableway.

The planned installation consists in a new cable line between Les Suches and Mont Chaz Dura, at an altitude between 2180 m and 2575 m above the sea level. As seen in *Figure 43*, the project also involves the construction of an intermediate station in addition to the two terminus stations.

The implemented model has been applied to this trajectory of cableway in the direction from the valley station to the mountain station to analyse the effectiveness of the integration of photovoltaic panels with this kind of transport system, following the procedure explained in the previous chapters. Notice that the slope of the mountain is towards South-East and so exposed to the Sun. This allows to assume appropriate the construction of avalanche barriers on it.

The useful parameters of the Les Suches-Chaz Dura line are summarized in *Table 7*.

<i>Length of the line</i>	<i>l</i>	[m]	1929
<i>Difference in height</i>	<i>h</i>	[m]	393
<i>Maximum capacity</i>	<i>q_{MAX}</i>	[p/h]	2500
<i>Cruising velocity</i>	<i>v</i>	[m/s]	4,5
<i>Maximum acceleration</i>	<i>a</i>	[m/s ²]	1
<i>Maximum deceleration</i>	<i>-a</i>	[m/s ²]	-1
<i>Number of intermediate stations</i>	<i>N_{IS}</i>		1
<i>Number of terminus stations</i>	<i>N_{TS}</i>		2
<i>Length of the intermediate stations</i>	<i>L_{IS}</i>	[m]	36
<i>Length of the terminus stations</i>	<i>L_{TS}</i>	[m]	25
<i>Total number of rollers</i>	<i>n_{roll}</i>		138

Table 7 - Parameters of the line.

In Table 8 the parameters of the cabins are reported.

<i>Area of ceilings and floors</i>	<i>A</i>	[m ²]	4,76
<i>Area of the faces parallel to the direction of movement</i>	<i>A</i>	[m ²]	3,68
<i>Area of the faces perpendicular to the direction of movement</i>	<i>A_⊥</i>	[m ²]	4,51
<i>Mass of the empty cabin</i>	<i>M₀</i>	[kg]	1000
<i>Number of passengers per cabin</i>	<i>n_p</i>		10

Table 8 - Parameters of the cabins.

8.1. Energy load profile

The energy consumption of the transport system is calculated on hourly basis with time horizon of one year. Since the cabins of CableSmart operate only when people are boarding, the number of vehicles involved each hour is calculated in order to estimate the mobility energy request. To do this, two factors have been introduced:

- the *filling factor* μ_h , which take into account the different capacity from hour to hour of operation of the cableway during the day
- the *capacity factor* μ_m , which take into account the different capacity from month to month of operation of the cableway during the year

The hourly values of the *filling factor* μ_h are reported in literature and shown below:

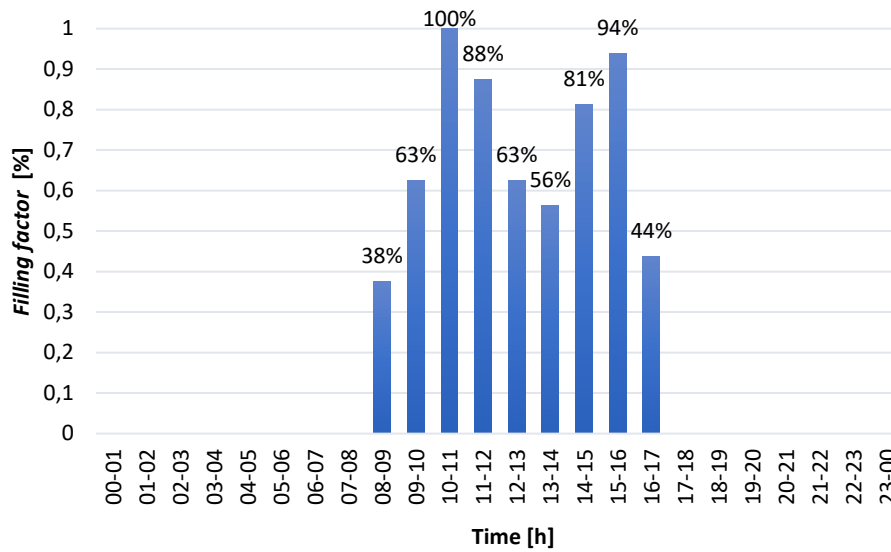


Figure 44 - Filling factor μ_h .

It is clear from *Figure 44*, that the values of μ_h for each hour of operation of the cableway corresponds to the daily trend of the ski tourism with a peak of capacity at time 10:00-11:00 and two other significant high values at 11:00-12:00 and 15:00-16:00. Notice that the hours of operation of the transport system are compatible with the hours of electricity production of a photovoltaic system.

The computation of the *capacity factor* μ_m has been trickier. Firstly, the monthly flow of tourists during the year 2018 in the Mont Blanc tourist area is obtained by the official website of the *Tourism Observatory of the Aosta Valley*. These values are then compared with the percentages of research on the web of the term “*Mont Blanc area*” by means of the tool Google Trends in the same year.

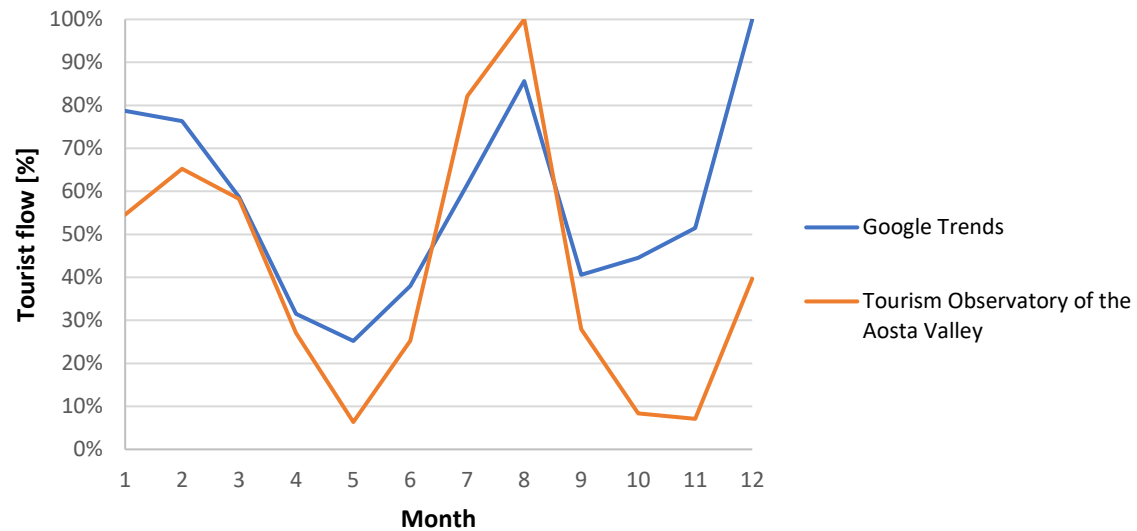


Figure 45 – Tourist flow curves.

Figure 45 evidences that the two curves present the same tendency, so it can be assumed that there is a lack of tourism in the periods from April to June and from September to November, whereas there are peaks of tourism during summer and winter seasons. Looking at the data of the *Tourism Observatory of the Aosta Valley*, in winter the peak of tourist flow is in February. This is possible being February a period of high ski season, whereas in January and December the only period of high season is between December 24th and January 6th.

It is now necessary to understand which part of this tourist flow is ski tourism, and so it requires the utilization of the cableway. For this purpose, the monthly electricity consumption of the existing Courmayeur Mont Blanc cableway during the year 2018, has been obtained by the annual financial statement. By comparing the values of the electricity consumption of the Courmayeur Mont Blanc transport system with the tourist flow given by the *Tourism Observatory of the Aosta Valley*, the percentage of ski tourist flow can be detected.

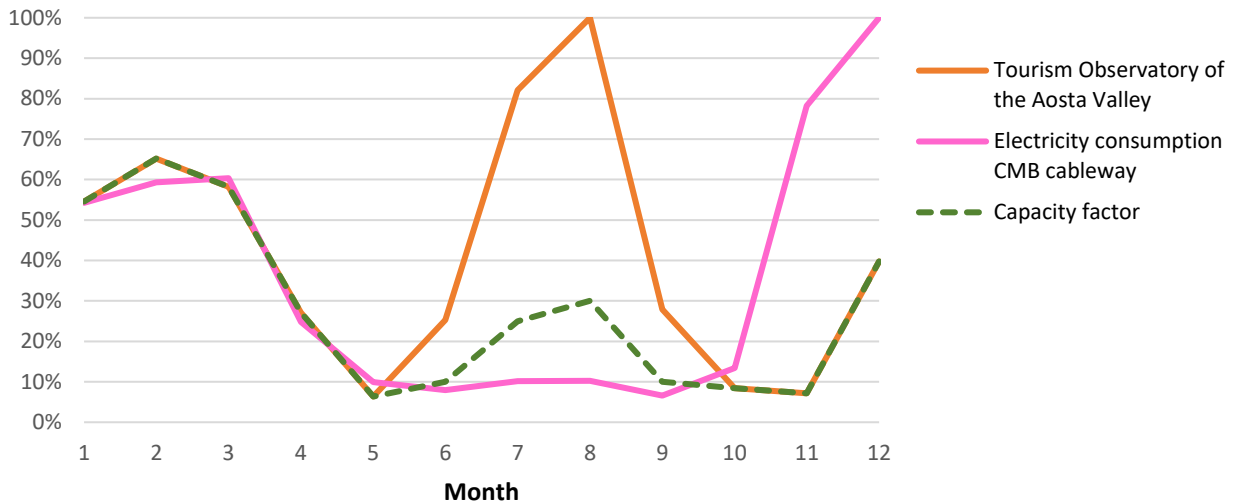


Figure 46 – Comparison between the tourism flow in the Mont Blanc tourist area in 2018, the electricity consumption of the CMB cableway in 2018 and the adopted capacity factor μ_m .

Figure 46 shows that from January to May the electricity consumption of the cableway and the tourist flow are very similar, it means that the percentage of tourist flow in these months can be assumed entirely as ski tourism and so the monthly *capacity factor* μ_m is hypothesized to be equal to the percentage of tourist flow obtained from the *Tourism Observatory of the Aosta Valley*. The same assumption is done for the months from October to December. Notice that November presents a really high consumption of electricity, but the tourist flow is very low. This is probably due to the operations of maintenance effectuated during the month of November, which leads to a higher consumption of electricity without the cableway being in full operation. The big difference between the curves is in the period between June and September. Without regard to the exceptional increment of electricity consumption in December due to the Christmas week, it can be noticed that the average percentage of electricity consumption of the CMB cableway in the ski season from January to March (around 60%) is reduced by about 80% compared to the average percentage of electricity consumption from June to September (around 10%). Since the trend of the end-users of the cableways, and consequently the trend of the *capacity factor* μ_m , follows the trend of the electricity consumption, it turns out that also the end-users of the cableways in the period June-September should be 80% less with respect to the tourists in the period January-March. Put in another way, the tourism flows which uses the transport system in the months June-September should be equal to 20% of the flows in the months January-March. Looking at the values of the *Tourism Observatory of the Aosta Valley*, it appears that the average percentage of tourism flow in the time January-March is almost equal to that in the time June-September: around 60%. So, the *capacity factor* in each month of the time June-September can be assumed equal to 20% of the

tourism flow in the considered month of the period. To be conservative, the *capacity factor* has been incremented and set equal to 30% of the flow tourism of each month of the summer period. This is because the same average percentage of tourism flow in the two periods of time compared, is derived by two different distributions of the tourism: from January to March the percentage of tourism is almost constant, whereas in summer there are two peaks in July and August with respect to June and September.

Finally, the monthly *capacity factor* μ_m adopted in this study, are reported in *Table 9*.

January	55%
February	65%
March	58%
April	27%
May	6%
June	10%
July	25%
August	30%
September	10%
October	8%
November	7%
December	40%

Table 9 - Monthly capacity factor μ_m .

All the parameters necessary to compute the number of vehicles involved each hour of the day for all the month of the year:

$$n_V = \frac{\mu_h \mu_m q_{MAX}}{n_p}$$

It results that in one hour the transport move from valley to mount a mass of:

$$M_{TOT} = n_V [M_0 + n_p M_p]$$

where M_p is the average mass of each person and it is equal to 80 kg, as known in literature [45].

The total mass M_{TOT} is used in the computation of the hourly energy requested to accelerate the cabin, to overcome the difference in height and to compensate the dissipation of energy due to rolling frictions.

All the coefficients necessary to calculate the energy for the acceleration phase, the energy to overcome the difference in height of the line and the energy to compensate the dissipations along the line due to rolling and aerodynamic frictions, are reported in the following tables.

Efficiency of the electric motor	η_{MOT}	0,93
Efficiency of the battery system	η_{BATT}	0,92
Efficiency of the energy recovery system	η_{REC}	0,70

Table 10 - Coefficient for the acceleration phase [45] .

Rolling coefficient	c		0,008
Gravity acceleration	g	[m/s ²]	9,81
Shape coefficient of the vehicle	C_f		1,05
Density of the air	ρ	[kg/m ³]	1,2

Table 11 - Parameters and coefficients for the dissipated energy due to aerodynamic and rolling frictions [45].

This leads to the calculation of the following kinematic parameters of the line:

Time of the acceleration/deceleration phase	$t_{ACC/DEC}$	[s]	4,5
Time of the cruising phase	t_{REG}	[s]	415,11
Length of the cruising phase	L_{REG}	[m]	1868
Stopping time	t_{STOP}	[s]	16
Cycle time	T_c	[s]	930,22
Frequency	f	[cycles/h]	3,87

Table 12 - Kinematic parameters of the line.

Finally, from the energy load on hourly basis, the yearly total energy load of the cableway under investigation has been calculated and the results, in kWh, are summarized in Table 13.

	ACCELERATION	AERODYNAMIC	ROLLING FRICTION	ENERGY TO	TOTAL ENERGY
	PHASE	FRICTION ENERGY	ENERGY	OVERCOME THE	LOAD
				DIFFERENCE IN HEIGHT	
	E_{ACC}	E_{AER}	E_R	E_g	E_{load}
	[kWh]	[kWh]	[kWh]	[kWh]	[kWh]
JANUARY	58,61	8,50	273.031,13	51.750,09	324.848,34
FEBRUARY	52,94	7,68	246.608,76	46.742,02	293.411,40
MARCH	61,86	8,50	288.164,49	54.618,46	342.853,32
APRIL	27,97	8,23	130.281,19	24.693,39	155.010,77
MAY	6,70	8,50	31.212,57	5.916,00	37.143,77
JUNE	10,41	8,23	48.512,20	9.194,96	57.725,80
JULY	26,73	8,50	124.534,98	23.604,26	148.174,48
AUGUST	32,01	8,50	149.126,70	28.265,35	177.432,57
SEPTEMBER	10,41	8,23	48.512,20	9.194,96	57.725,80
OCTOBER	8,73	8,50	40.670,92	7.708,73	48.396,88
NOVEMBER	7,53	8,23	35.087,44	6.650,44	41.753,64
DECEMBER	42,44	8,50	197.679,58	37.468,02	235.198,54
YEAR	346,36	100,10	1.613.422,16	305.806,70	1.919.675,32

Table 13 - Total energy load.

The yearly energy requested by the cableway is around 1.9 GWh. The contribution of each energy requirements to the total energy load is shown below.

E_{ACC}	0,02%
E_{AER}	0,01%
E_R	84,05%
E_g	15,93%

Table 14 - Yearly energy contributions to the total energy load.

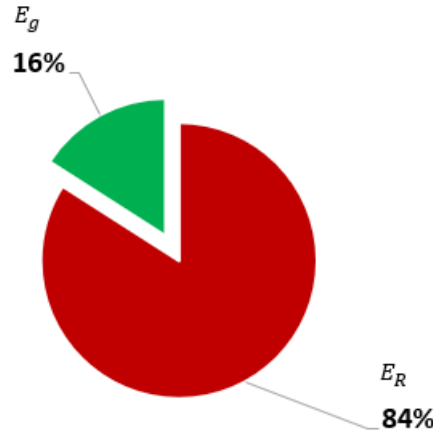


Figure 47 - Yearly energy contributions to the total energy load.

Figure 47 evidences that the major contribution of the energy required by the cableway is due to the compensation of energy dissipated by the rollers along the line: indeed, the rolling friction energy represents around the 84% of the energy request. The remaining 16% of the energy request is needed by the transport system to face the climb from valley to mount. The contributions of the acceleration phase and the aerodynamic friction energy are negligible: they represent 0.02% and 0.01% of the yearly energy load, respectively.

8.2. Energy simulation

8.2.1. First scenario: avalanche barriers integrated PV

First of all, the avalanche barriers are dimensioned according with *Costruzione di opera di premunizione contro le valanghe nella zona di distacco* [48].

The fundamental geometrical parameter which allows the dimensioning of an avalanche barrier is the vertical height of the structure H_k . The H_k of the structure must be chosen so that it exceeds the maximum height of the snow mantle reached in that location in the recent years, called the extreme height H_{estr} .

$$H_k \geq H_{estr}$$

The register on the historic snow in La Thuile has been consulted and it reports 202 cm of snow in the highest average snowfall of recent years [49]. To be conservative, the adopted H_k is set equal to 2.6 m and, following the rules presented in *Chapter 6.1.1.*, the geometrical parameters of the avalanche barriers are calculated and sum up in *Table 15*.

Before calculating the useful height of the structure D_k , it has been extrapolated the slope of the mountain where the avalanche barriers could be erected. This is done by means of the tool GoogleEarth.

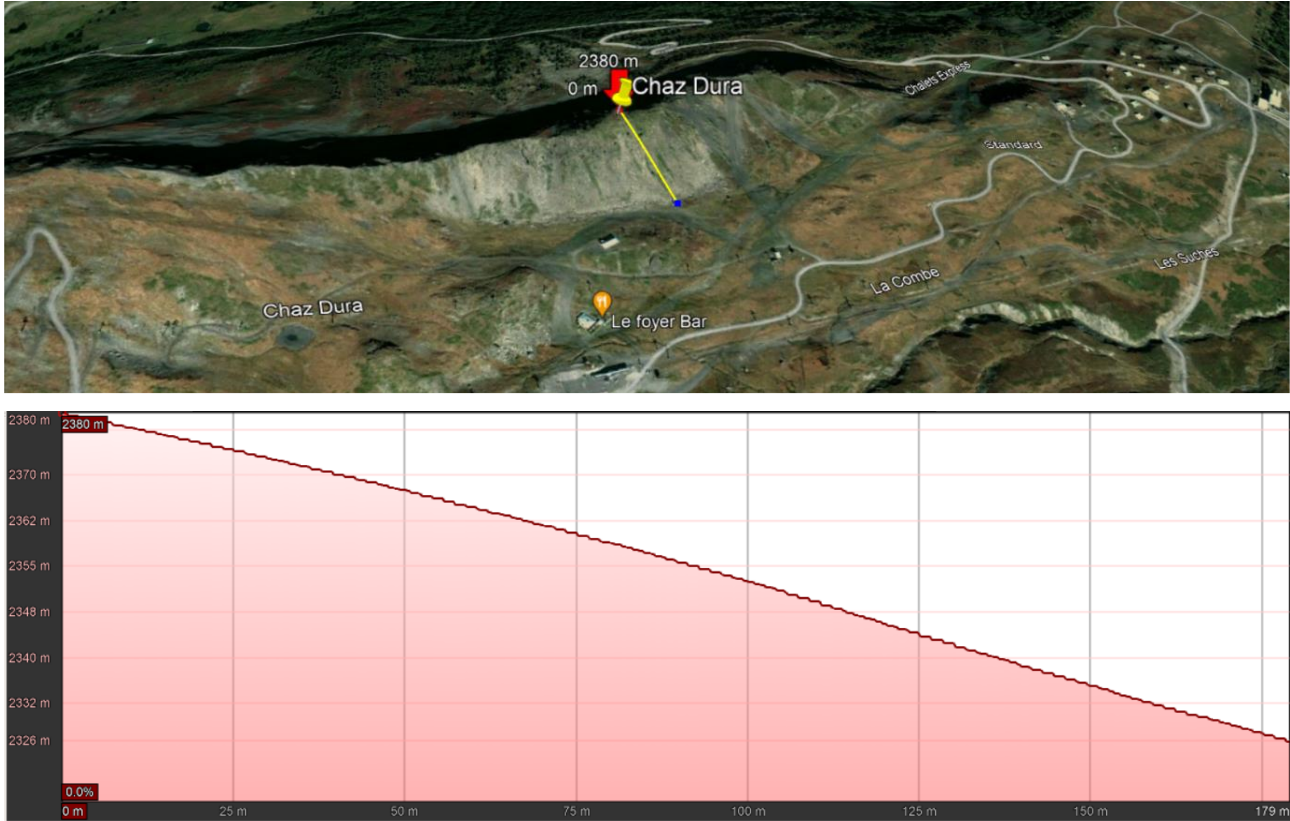


Figure 48 - Elevation profile of the mountain.

From the elevation profile of Figure 48, the slope of the mountain is calculated, and it results:

$$\psi = 16.79^\circ$$

Vertical height of the structure	H_k	[m]	2,6
Useful height of the structure	D_k	[m]	2,5
Real height of the structure	B_k	[m]	2,5
Length of the strut	L_s	[m]	3,0
Strut angle	α	[°]	35,5

Table 15 - Geometrical parameters of the avalanche barriers.

In this way, the tilt angle β of the photovoltaic panels can be set equal to:

$$\beta = \alpha + \psi = 52.3^\circ$$

The type of PV module installed is the one adopted by the software Helioscope, used to illustrate the final layout of the plant. The sketch of this module is taken from the datasheet and shown in *Figure 49*.

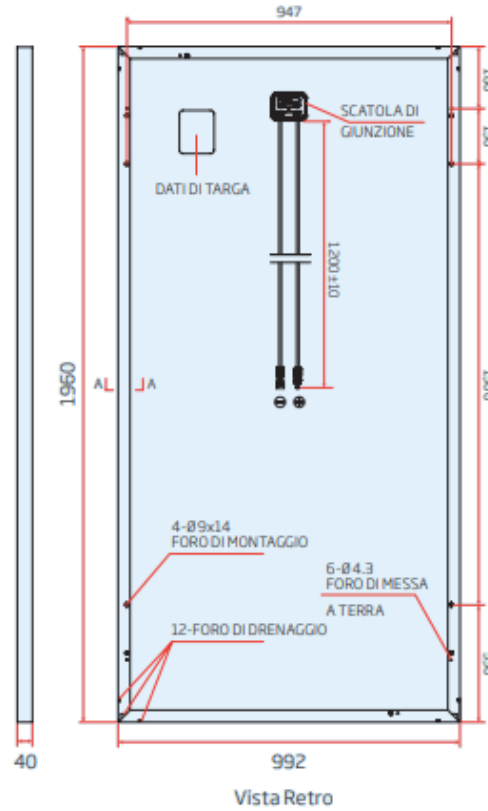


Figure 49 - Sketch of the PV module [50].

The module dimension is $1.960 \times 0.992 \times 0.040$ m and its nominal power is $320 W_p$. The relevant information is the width of the PV panel:

$$u = 0.992 \text{ m}$$

<i>Length of the PV module</i>	<i>l</i>	[m]	1,960
<i>Width of the PV module</i>	<i>u</i>	[m]	0,992
<i>Area of the PV module</i>	<i>A_{panel}</i>	[m ²]	1,944
<i>Nominal power of the module</i>	<i>P_{n,panel}</i>	[W _p]	320

Table 16 - PV module data [50].

The solar panels are supposed to be integrated along the length of the strut L_s . And so, it results that for each avalanche barrier, 3 adjacent solar panels are installed.

$$N_p = 3$$

Then, the distance L between two subsequent and parallel lines of avalanche barriers is found in existing tabulated values. The value is deducted by looking at:

- the minimum slope of the mountain for which the distance L is tabulated in literature
- a *slip coefficient* $N=1.3$ corresponding to a rough surface of the mountainous terrain
- the tangent of the *friction angle* $\tan \varphi = 0.55$ that is the most widely used
- H_k and D_k approximately equal to 2.6 m and 2.5 m, respectively

As a first approximation, it results a distance L equal to about 30 m. But it is still necessary to take into account the particular condition of the case. Indeed, to ensure a sufficient degree of safety, the location and the climate conditions have to be considered opportunely. The distance must be reduced in the case in which the construction is situated in a pre-alpine zone, where abundant snowfalls are probable. Moreover, the slope of the mountain is facing South-East and so more exposed to the Sun. This fact increases the probability of occurrence of an avalanche considerably and leads to a further reduction of the distance between barriers. For these reasons, the distance L is helved. Hence:

$$L = 15 \text{ m}$$

The final layout of the PV plant integrated with the avalanche barriers is simulated on the slope of the mountain by means of the software Helioscope. Looking at the orientation of the side of the mountain, the azimuth angle γ of the solar panels is found:

$$\gamma = 155^\circ$$

The configuration is the one in *Figure 50*.

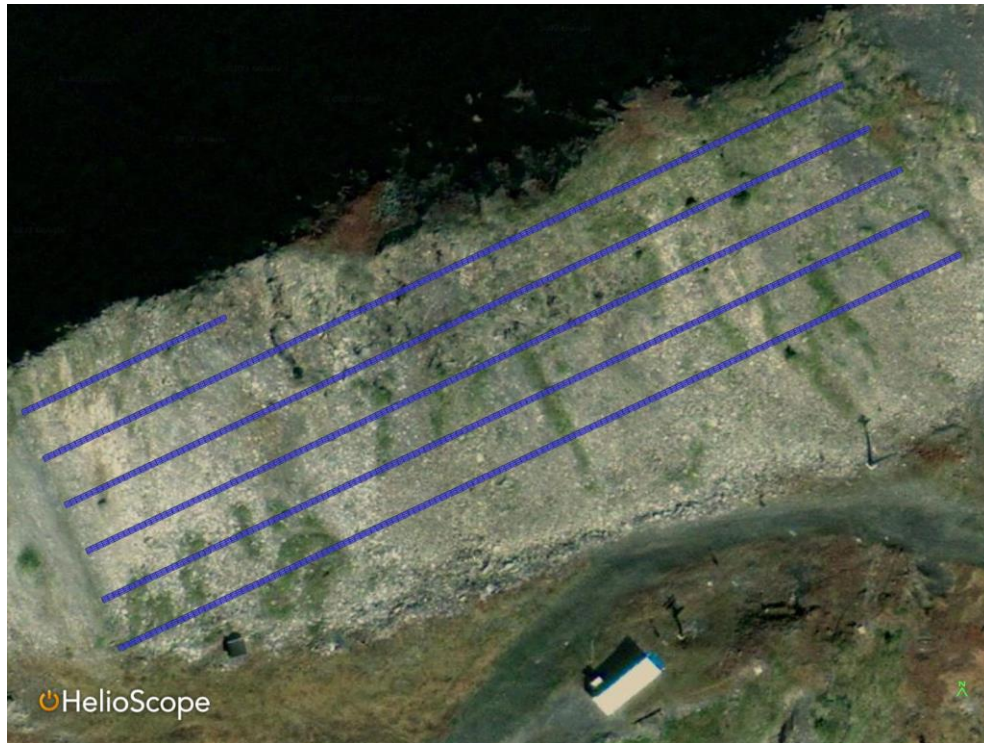


Figure 50 - The layout of the PV system integrated on avalanche barriers from Helioscope.

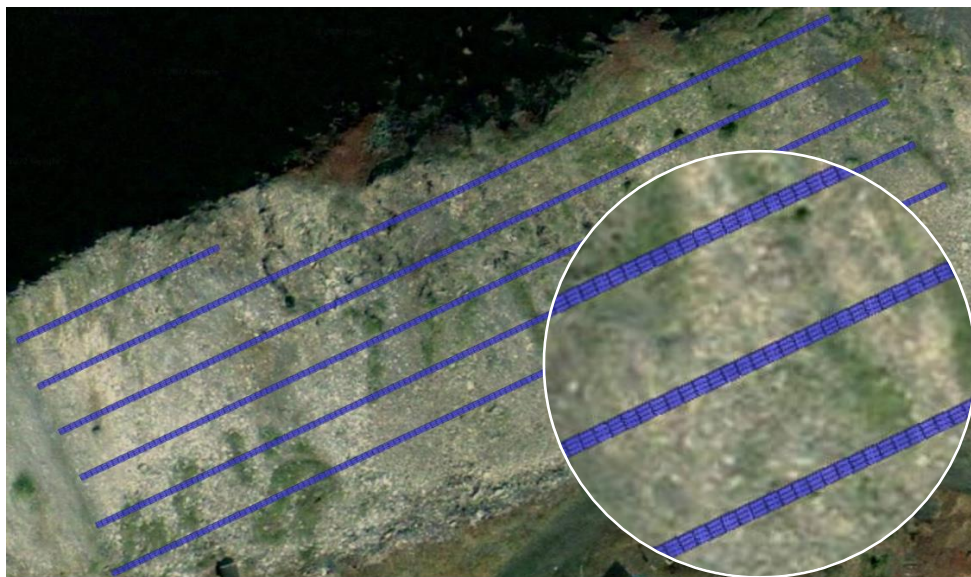


Figure 51 - Detail of the PV layout from Helioscope.

There are six parallel rows of avalanche barriers with photovoltaic modules and in each row there are three panels in *landscape* orientation. From Helioscope, the number of photovoltaic panels integrated into the structure is 2400 resulting in 768 kW_p installed.

By inserting the geographical coordinates, the azimuth and tilt angle of the PV plant on PVGIS, the annual specific energy is obtained, and it results equal to 1018.62 kWh/ kW_p. This value is further reduced by 0.5% because of possible small shadows on the neighbouring panels.

<i>Number of panels installed</i>	N_p		2400
<i>Nominal power installed</i>	P_n	[kW _p]	768
<i>Azimuth angle</i>	γ	[°]	155
<i>Tilt angle</i>	β	[°]	52,3
<i>Annual specific energy of the PV plant</i>	E_{spec}	[kWh/ kW _p]	1013,53

Table 17 - Data of the PV plant integrated with avalanche barriers.

Table 17 reports the data of the PV plant integrated with avalanche barriers. These values are inserted in the Excel model, and the energy production profile is defined with reference to the information obtained by *Solarlog* for the existing photovoltaic installation in La Thuile. Energy and load profiles are known, and the energy simulation of the first scenario is carried out following the logic explained in *Chapter 6*. The results of the energy simulation on monthly basis, are summarized in *Table 18* and shown in *Figure 52*.

	ENERGY LOAD	PV PRODUCTION ENERGY	ENERGY WITHDRAWN FROM THE ELECTRICITY GRID	ENERGY INJECTED INTO THE ELECTRICITY GRID
			$E_{el_{grid},W}$	$E_{el_{grid},I}$
	[kWh]	[kWh]	[kWh]	[kWh]
JANUARY	324.848,34	23.215,23	301.764,24	131,13
FEBRUARY	293.411,40	49.484,40	246.227,47	2.300,46
MARCH	342.853,32	72.870,35	275.053,11	5.070,14
APRIL	155.010,77	74.049,48	100.466,47	19.505,18
MAY	37.143,77	76.739,93	8.426,18	48.022,34
JUNE	57.725,80	86.917,63	9.845,99	39.037,82
JULY	148.174,48	96.862,77	77.993,38	26.681,67
AUGUST	177.432,57	105.423,78	99.056,65	27.047,86
SEPTEMBER	57.725,80	80.154,53	16.413,52	38.842,25
OCTOBER	48.396,88	60.026,57	14.934,97	26.564,65
NOVEMBER	41.753,64	31.779,56	17.748,46	7.774,38
DECEMBER	235.198,54	20.864,43	214.334,12	0,00
YEAR	1.919.675,32	778.388,66	1.382.264,54	240.977,88

Table 18 - Results of the energy simulation of the first scenario.

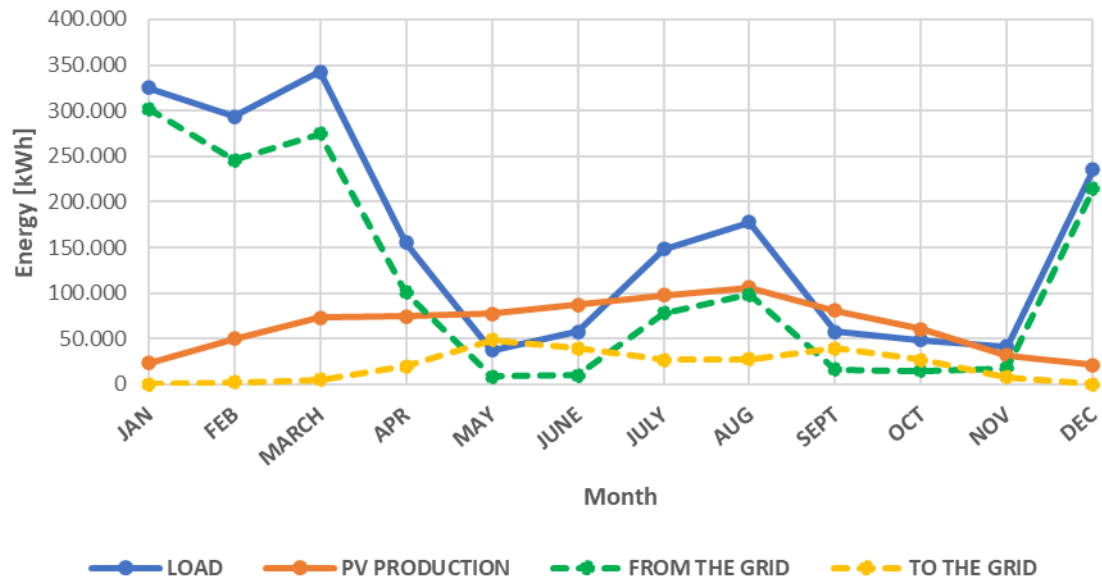


Figure 52 - Results of the energy simulation of the first scenario.

It is clear from *Figure 52* that the period of maximum operation of the transport system, from December to April, corresponds also to the months of the years with lower photovoltaic energy production. In this period the load far exceeds the energy production, and the energy demand is satisfied mainly by the electricity bought from the net up to a maximum of almost 93% of electricity withdrawn from the grid recorded in January. In general, over the entire year, the trend of the electricity bought from the net is essentially the same of the energy load. The PV production exceeds the load energy request in the months with lower tourism flows: from May to June and from September to November. In these periods the electricity is mainly sold to the grid until a maximum of almost 49% recorded in September. In July and August, the energy production of the PV plant is maximum, and it covers 48% and 44% of their monthly load, respectively.

The *self-sufficiency* has been determined for each month and organized in descending order in *Figure 53*. Then, the corresponding values of *self-consumption* are superimposed.

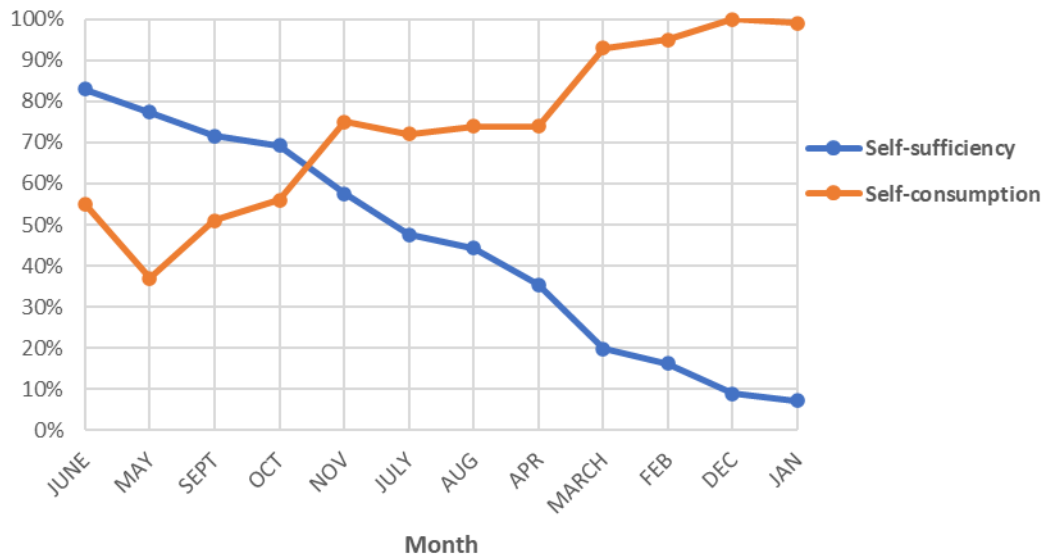


Figure 53 - Self-sufficiency and self-consumption.

Self-sufficiency is higher when the tourism flow goes down, and so the energy load is lower, and in the meantime the energy produced by photovoltaic is quite high: indeed, the highest level of *self-sufficiency* is achieved in June and then in May with values of 83% and 77%, respectively. The lowest *self-sufficiency* is registered in winter season where the situation is inverted than before: it is the period with the greatest energy request of the year, while the production is the lowest one. *Self-sufficiency* reaches 16% in February, 9% in December and 7% in January. As expected, the *self-consumption* presents the opposite trend: in winter season all or almost all the PV electricity is directly used from the load, indeed the curve of the electricity sold to the grid in *Figure 52* is essentially flat and null. In general, the percentages of *self-consumption* are quite high and over 50%, except for the month of May with its 37%. This is because May registers the lowest energy load request of the year and so the photovoltaic energy to feed it, is low with respect to the total amount of energy produced.

The graphical result of the energy simulation of the most representative months of the year are reported below.

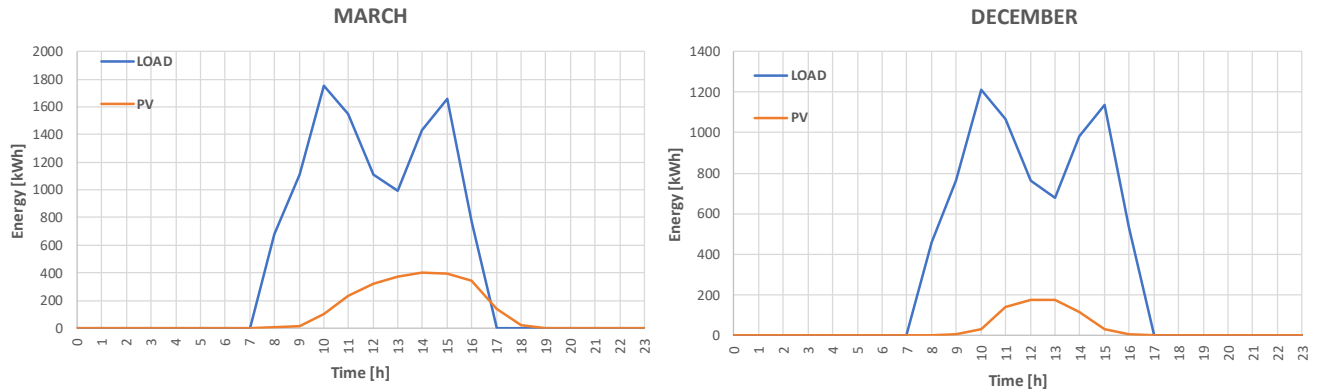


Figure 54 - Energy load and energy production profiles of March and December.

March and December are two representative months of the skiing season. Values and times of energies involved, shown in *Figure 54*, validate the previous mentioned percentages of *self-sufficiency* and *self-consumption*.

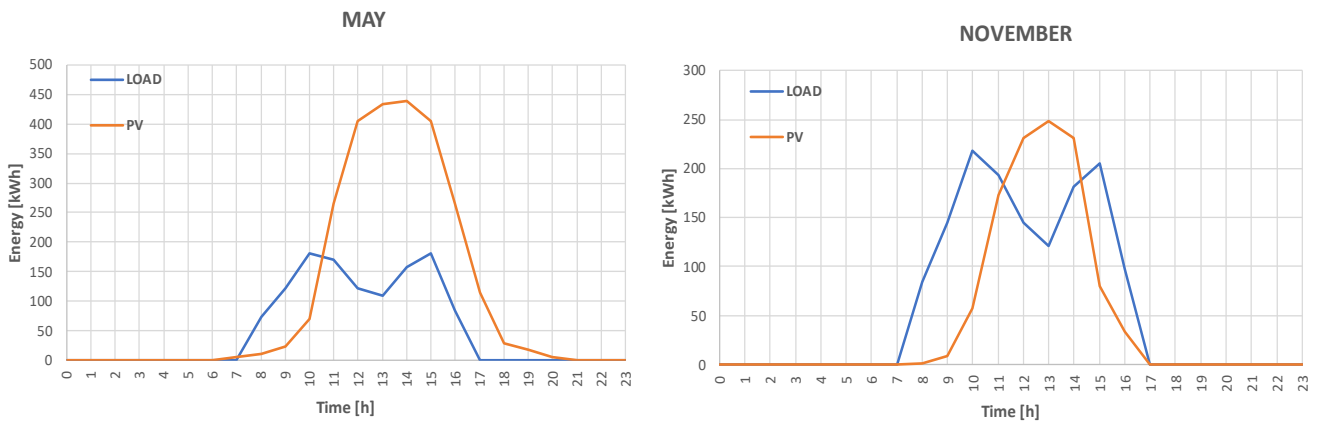


Figure 55 - Energy load and energy production profiles of May and November.

May and November are two representative off-season months. The energy load is more or less the same, but the photovoltaic production in May is more than double that in November. It is the reason why the percentage of *self-sufficiency* is higher in May and the percentage of *self-consumption* is higher in November.

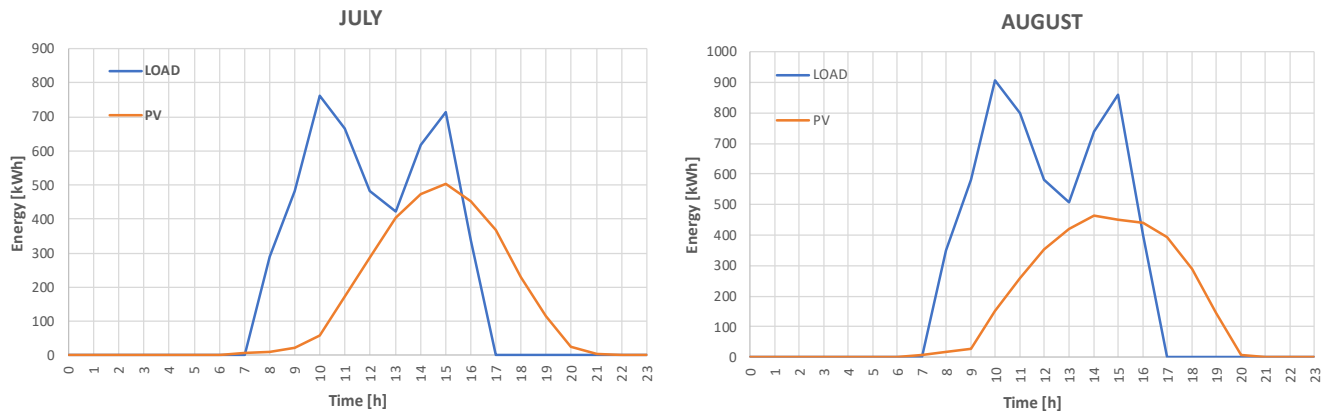


Figure 56 - Energy load and energy production profiles of July and August.

July and August are the intermediate situation in terms of percentages of *self-sufficiency* and *self-consumption*.

The annual energetic situation is shown in Figure 57 and Figure 58.

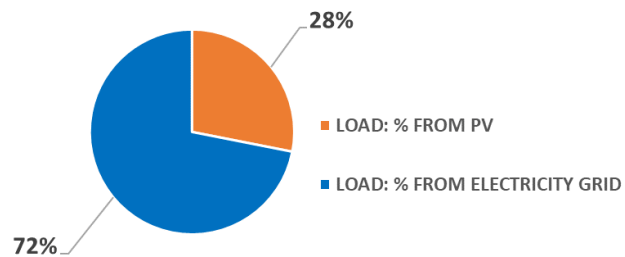


Figure 57- Annual energetic mix from the point of view of the load.

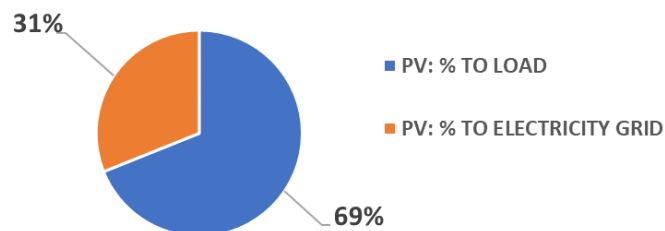


Figure 58 - Annual energetic mix from the point of view of the PV plant.

From the point of view of the load, the yearly energy request is satisfied for 28% by the PV plant integrated with avalanche barriers and the remaining 72% is covered by the electricity grid. Hence,

self-sufficiency on annual basis is 28%. This is a good result if it is considered that solar panels are integrated with an already existing infrastructure with predetermined fixed geometrical parameters that are not the optimal one for the PV system. From the point of view of the photovoltaic system, 69% of the energy produced by solar panels is used to satisfy the load and the remaining 31% is sold to the electricity grid. Hence, *self-consumption* on annual basis is 69%.

8.2.2. Second scenario: cableway integrated PV

The integration of photovoltaic with the transport system is now considered.

At first, the PV plants on the flat roofs of the three stations have been sized. The azimuth angle of panels is set equal to 180° (if North is considered 0°), so that the plant is South facing, and the optimal tilt angle obtained is 35° . Then, the shading effect is studied to determine the distance between two subsequent parallel rows of panels: the spacing is found so that the shadow of one row of panels does not affect the subsequent row during the best hour of the worst day of the year. Data in *Table 19* are obtained by means of a dedicated Excel model realized to calculate the length of the panel shadow, supposing to install panels in *landscape* orientation.

<i>Azimuth angle</i>	γ	[°]	180°
<i>Tilt angle</i>	β	[°]	35°
<i>Sloped side</i>	u	[m]	0,992
<i>Latitude</i>		[°]	45,70
<i>Solar declination</i>		[°]	-23,43
<i>Maximum solar altitude</i>	δ	[°]	21,5
<i>Panel shadow length</i>	x_{shad}	[m]	1,49

Table 19 - Data for the calculation of the shadow effect on PV plant installed on the station roofs.

Knowing the dimension of the roofs of all the stations, the number of panels installed is calculated considering a distance of x_{shad} between two subsequent rows of solar panels. As a consequence, the nominal power installed is computed. The detailed parameter of the valley, the mountain and the intermediate stations are reported in *Table 20*.

	Area of the roof	Number of panels	Nominal power
	$A_{r,st}$	N_p	P_n
	[m ²]		[kWp]
Mountain station	1555	300	96
Intermediate station	1855	360	115,2
Valley station	1050	192	61,44

Table 20 - Data of PV plants installed on station roofs.

Geographical coordinates, azimuth and tilt angle are provided to PVGIS to return the annual specific energy. Because of the possible shadow effect, for these installations has been applied a decrement by 10% of the given annual specific production. Results given by the photovoltaic installed in all the stations are summed and reported in Table 21.

Total number of panels	N_p		852
Nominal power	P_n	[kWp]	272,64
Specific energy	E_{sp}	[kWh/kWp]	990

Table 21 - Data of total PV plant installed on station roofs.

Then, the PV panels on the vehicle roofs are sized and the obtained data for a single cabin are reported below. It is pointed out that the shadow of the vertical support of the vehicles affects the performance of the solar system. Moreover, there are parts of the line that are shaded. For these reasons, the specific production obtained by PVGIS is reduced by 20%.

Azimuth angle	γ	[°]	180°
Tilt angle	β	[°]	0°
Area of the cabin roof	$A_{r,cab}$	[m ²]	4,76
Total number of panels per cabin	N_p		2
Nominal power per cabin	P_n	[kWp]	0,64
Specific energy	E_{sp}	[kWh/kWp]	800

Table 22 - Data of PV installed on one cabin roof.

The total energy produced by solar panels depends on the number of vehicles involved in the line, which varies hourly and monthly, as explained in Chapter 5.4. Hence, in the energy simulation, the

hourly operating number of PV panels will be correlated with the hourly operating number of vehicles.

Finally, the PV panels on the walls of vehicles and stations are sized. The values to enter in PVGIS and the resulting specific energies for each orientation of the walls are in *Table 23*. In the energy simulation, it is used their arithmetic mean for the walls of the stations. For the walls of the cabin the arithmetic mean of the specific energy is further reduced by 10% because of the shaded sections of the line.

Wall orientation	Azimuth angle	Tilt angle	Specific energy
	[°]	[°]	[kWh/kWp]
North	0°	90°	212,12
South	180°	90°	693,25
East	90°	90°	497,41
West	270°	90°	488,79
AVERAGE			472,89

Table 23 - Data of PV plant installed on walls.

All the data of stations and of a single cabin are sum up below.

<i>Area of walls of the mountain station</i>	$A_{w,ms}$	[m ²]	962
<i>Area of walls of the intermediate station</i>	$A_{w,ls}$	[m ²]	480
<i>Area of walls of the valley station</i>	$A_{w,vs}$	[m ²]	690

Table 24 - Dimensions of the walls of the stations.

<i>Total area of the walls of stations</i>	$A_{w,st}$	[m ²]	2132
<i>Total number of panels</i>	N_p		1096
<i>Nominal power</i>	P_n	[kWp]	350,72
<i>Specific energy</i>	E_{sp}	[kWh/kWp]	472,89

Table 25 - Data of total PV installed on station walls.

<i>Area of the cabin walls</i>	$A_{w,cab}$	[m ²]	16,38
<i>Total number of panels per cabin</i>	N_p		8
<i>Nominal power per cabin</i>	P_n	[kWp]	2,56
<i>Specific energy</i>	E_{sp}	[kWh/kWp]	425,60

Table 26 - Data of PV installed on walls of each cabin.

As already seen for the cabin roofs, the total energy produced by solar panels will depend on the number of vehicles involved in the line.

All the given values are added to data of the PV plant on the avalanche barriers, the energy simulation is carried out. The results of the energy simulation on monthly basis, are summarized below.

	ENERGY LOAD	PV PRODUCTION ENERGY	ENERGY WITHDRAWN FROM THE ELECTRICITY GRID	ENERGY INJECTED INTO THE ELECTRICITY GRID
			$E_{elgrid,W}$	$E_{elgrid,I}$
	[kWh]	[kWh]	[kWh]	[kWh]
JANUARY	324.848,34	40.996,25	284.056,64	204,55
FEBRUARY	293.411,40	86.770,25	210.229,48	3.588,33
MARCH	342.853,32	128.281,62	222.480,25	7.908,56
APRIL	155.010,77	121.041,32	73.247,93	39.278,48
MAY	37.143,77	121.390,53	6.547,00	90.793,76
JUNE	57.725,80	138.562,57	4.618,68	85.455,45
JULY	148.174,48	157.850,78	54.972,01	64.648,31
AUGUST	177.432,57	173.292,00	60.888,40	56.747,82
SEPTEMBER	57.725,80	127.526,70	12.417,19	82.218,09
OCTOBER	48.396,88	95.295,43	11.570,22	58.468,76
NOVEMBER	41.753,64	50.446,63	13.913,95	22.606,94
DECEMBER	235.198,54	35.653,53	199.545,01	0,00
YEAR	1.919.675,32	1.277.107,61	1.154.486,76	511.919,05

Table 27 - Results of the energy simulation of the second scenario.

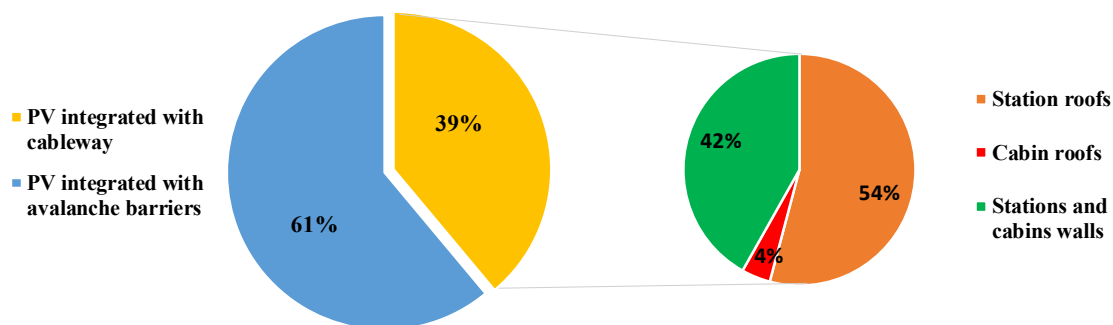


Figure 59 - PV production split.

The new amount of PV production derived 39% from the integration of photovoltaic with the cableway structures. As shown in *Figure 59*, the main contribution is due to solar panels on the roofs of the stations, followed by the electricity from panels covering all the vertical walls.

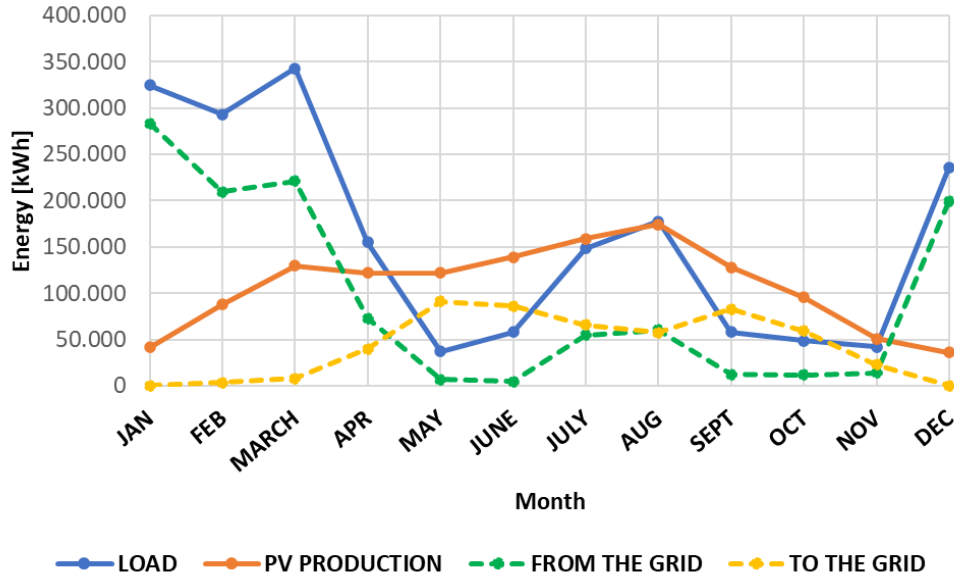


Figure 60 - Results of the energy simulation of the second scenario.

Obviously, the PV production is higher than the production obtained in the first scenario, whereas the trend of the profile is the same (*Figure 60*). Overall, the yearly energy production rises by 64% with respect to the first scenario, leading to a 111% increase of injected electricity. The amount of withdrawn electricity from the net is reduced by 16%. The electricity sold to the grid is more than double: this is mainly due to the periods May-June and September-October, in which the increment of energy production is notable, whereas the load remains very low. In July and August, a greater availability of photovoltaic energy causes a decrement of the withdrawn electricity from the net and an increase of the injected electricity at the same time. The energy exchanged with the net in these two months, in terms of kWh, is almost null. Comparing *Figure 52* and *Figure 60*, it is graphically evident that the addition of solar nominal power installed improves the energy situation also in winter season, especially in February and March, in which the demand of energy from the grid has fallen off.

The *self-sufficiency* has been determined for each month and organized in descending order in *Figure 61*. Then, the corresponding values of *self-consumption* are superimposed.

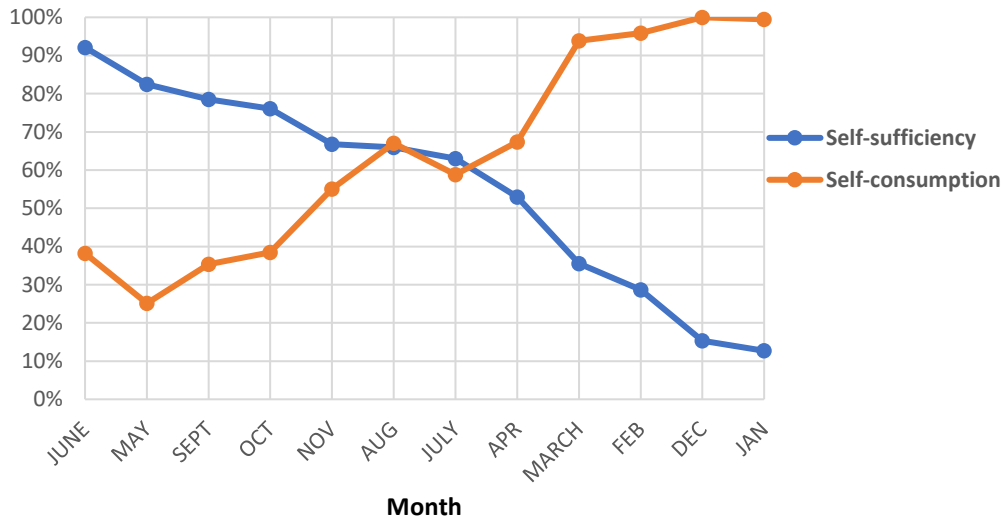


Figure 61 - Self-sufficiency and self-consumption of the second scenario.

As expected, this scenario leads to a notable gain on *self-sufficiency* of the system. Indeed, the *self-sufficiency* registered on yearly basis is around 40%, compared with 28% achieved in the first scenario. It means that 40% of electricity that feeds the load comes from renewable source. The huge amount of electricity sold to the grid implicates lower percentage of *self-consumption* with respect to the first scenario. Anyway, the *self-consumption* on annual basis is slightly decrease to 60%.

The annual energetic situation is shown in Figure 62 and Figure 63.

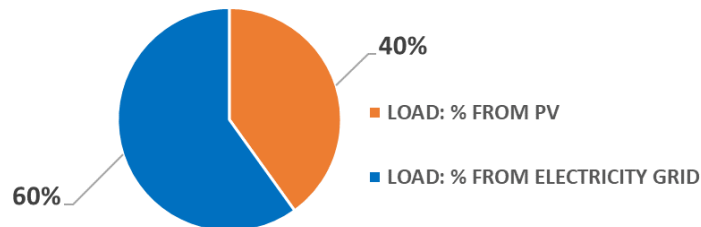


Figure 62 - Energy mix from the point of view of the load.

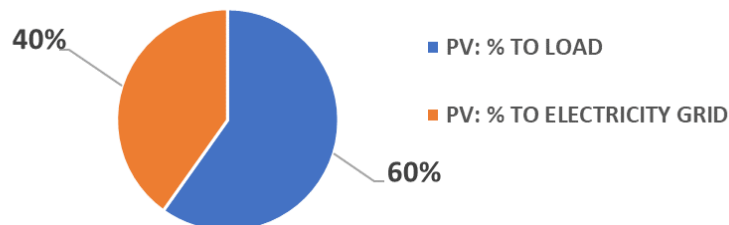


Figure 63 - Energy mix from the point of view of PV.

8.3. Sensitivity analysis

The *sensitivity analysis* on the first scenario is carried out.

The *sensitivity analysis* is done running the energy simulation changing the key parameters that characterize the transport system and the PV plant. In particular:

- a “*energetic*” *sensitivity analysis* is done by changing, one at a time:
 - the distance L between two subsequent lines of avalanche barriers
 - the tilt angle β of the panels integrated with the avalanche barriers
- a “*mechanical*” *sensitivity analysis* is done by changing, one at a time:
 - the length l of the line
 - the number of rollers n_{roll} presented along the entire line

8.3.1. The distance L

At first, the spacing between the avalanche barriers is modified and the assigned values range from 30 meters to 7 meters. The distance selected in the first scenario is included (with 15 meters spacing). All the other parameters of the PV system considered in the first scenario of the case study remain unchanged: the geometrical characteristics of the barriers, azimuth and tilt angle of panels. The reduction of L could accentuate the shadow effect between the lines of avalanche barriers. The length of the shadow is calculated by means of the Excel model adopted in *Chapter 8.2.2.* with the following dataset:

<i>Azimuth angle</i>	γ	[°]	155
<i>Tilt angle</i>	β	[°]	73,21
<i>Sloped side</i>	B_k	[m]	2,5
<i>Latitude</i>		[°]	45,70
<i>Solar declination</i>		[°]	-23,43
<i>Maximum solar altitude</i>	δ	[°]	20,87
<i>Panel shadow length</i>	x_{shad}	[m]	5,69

Table 28 - Parameters for the shadow computation.

Looking at *Figure 42*, the sloped side responsible of the shadow is the real height of the grid of the avalanche barrier B_k , hence, the tilt angle is referred to the incline of this grid. As reported in

Chapter 6.1.1., the avalanche barriers are approximately perpendicular to the sloped terrain. Being ψ the slope of the mountain, the tilt angle results equal to:

$$\beta = 90^\circ + \psi = 73.21^\circ$$

So, the maximum shadow that can be projected is almost 5.7 meters long. Being 7 meters the minimum distance considered between two subsequent lines of avalanche barriers, it is supposed that the shadow effect does not particularly affect the performance of the PV plant and so the specific energy is kept equal to 1013.53 kWh/ kW_p, as in the basic scenario.

<i>Azimuth angle</i>	γ	[°]	155
<i>Tilt angle</i>	β	[°]	52,3
<i>Annual specific energy of the PV plant</i>	E_{spec}	[kWh/ kW _p]	1013,53

Table 29 - PV plant parameters.

The azimuth and tilt angle in Table 29, together with the values of L , are set in the software Helioscope to obtain the corresponding layout and so the new nominal power installed.

L [m]	N_p	P_n [kW_p]
30	1026	328,3
29	1257	402,2
27	1494	478,1
25	1491	477,1
23	1485	475,2
21	1740	556,8
19	1947	623
17	2055	657,6
15	2400	768
13	2853	913
11	3210	1027,2
9	3441	1101
7	4362	1395,8

Table 30 - Nominal power installed as function of the distance between avalanche barriers.

Here some configurations given by Helioscope.



Figure 64 - 30 meters spacing between avalanche barriers.

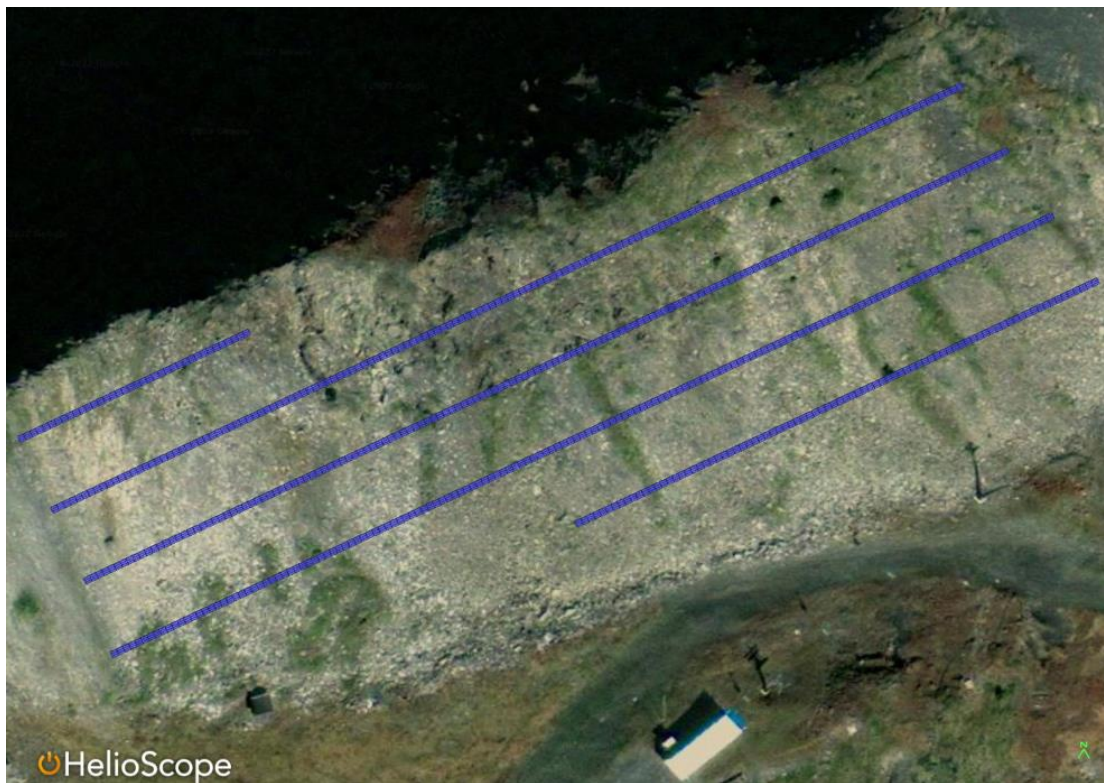


Figure 65 - 21 meters spacing between avalanche barriers.

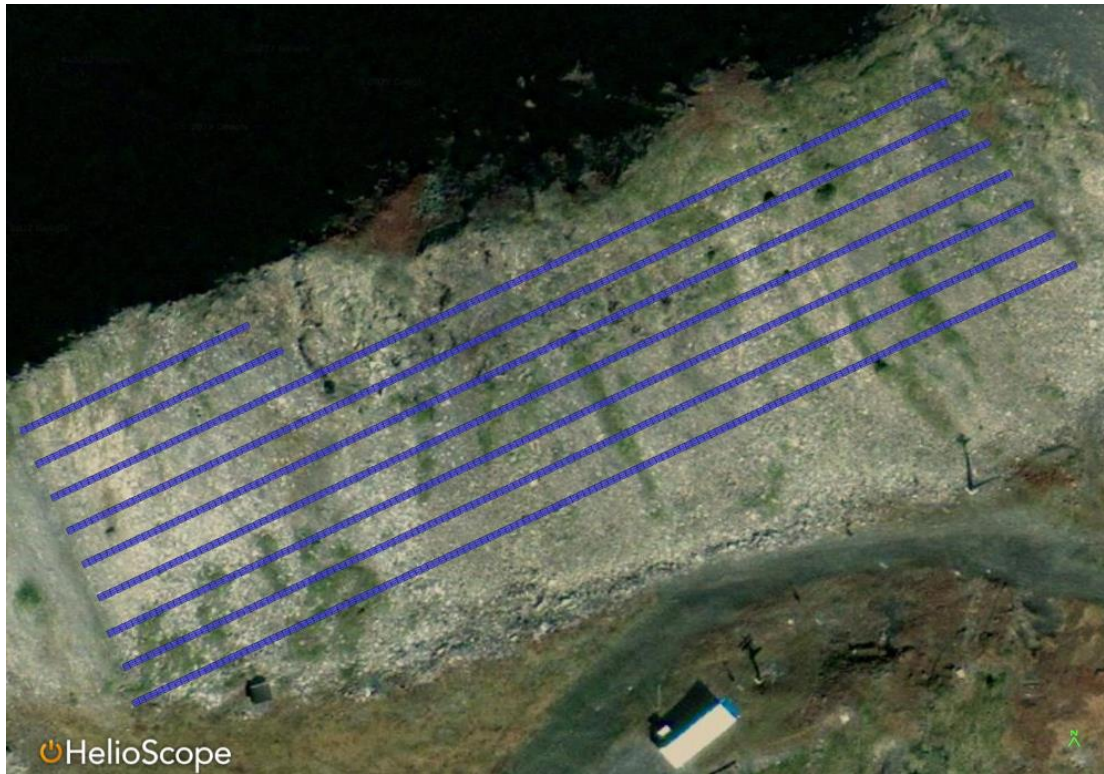


Figure 66 - 9 meters spacing between avalanche barriers.



Figure 67 - 7 meters spacing between avalanche barriers.

For every distance L , the yearly results of the energy simulation are reported in *Table 31*.

AVALANCHE BARRIERS DISTANCE	ENERGY LOAD	PV PRODUCTION ENERGY	ENERGY WITHDRAWN FROM THE ELECTRICITY GRID	ENERGY INJECTED INTO THE ELECTRICITY GRID
L	E_{load}	E_{PV}	$E_{el_{grid},W}$	$E_{el_{grid},I}$
[m]	[kWh]	[kWh]	[kWh]	[kWh]
30	1.919.675,32	332.741,90	1.640.002,27	53.068,85
29	1.919.675,32	407.641,77	1.586.751,31	74.717,76
27	1.919.675,32	484.568,69	1.535.809,60	100.702,97
25	1.919.675,32	483.555,16	1.536.466,30	100.346,14
23	1.919.675,32	481.629,46	1.537.714,68	99.668,81
21	1.919.675,32	564.333,50	1.489.949,09	134.607,27
19	1.919.675,32	631.429,19	1.454.339,90	166.093,77
17	1.919.675,32	666.497,33	1.436.598,69	183.420,70
15	1.919.675,32	778.391,04	1.382.263,42	240.979,13
13	1.919.675,32	925.352,89	1.314.808,04	320.485,61
11	1.919.675,32	1.041.098,02	1.265.074,51	386.497,20
9	1.919.675,32	1.115.896,53	1.234.927,23	431.148,44
7	1.919.675,32	1.414.685,17	1.134.639,46	629.649,32

Table 31 - Energy simulation with different L .

The distance between barriers directly affects the energy production: if space increases, photovoltaic energy decreases. At the minimum distance of 7 meters, the energy production rose 82% with respect to the basic scenario (with 15 meters spacing), whereas it decreases for higher distances until it falls off by 57% at 30 meters distance. Moreover, *Figure 68* evidences that over-production or under-production affects mainly the amount of electricity sold to the grid. In particular, at 7 meters distance, the energy injected into the net is more than double.

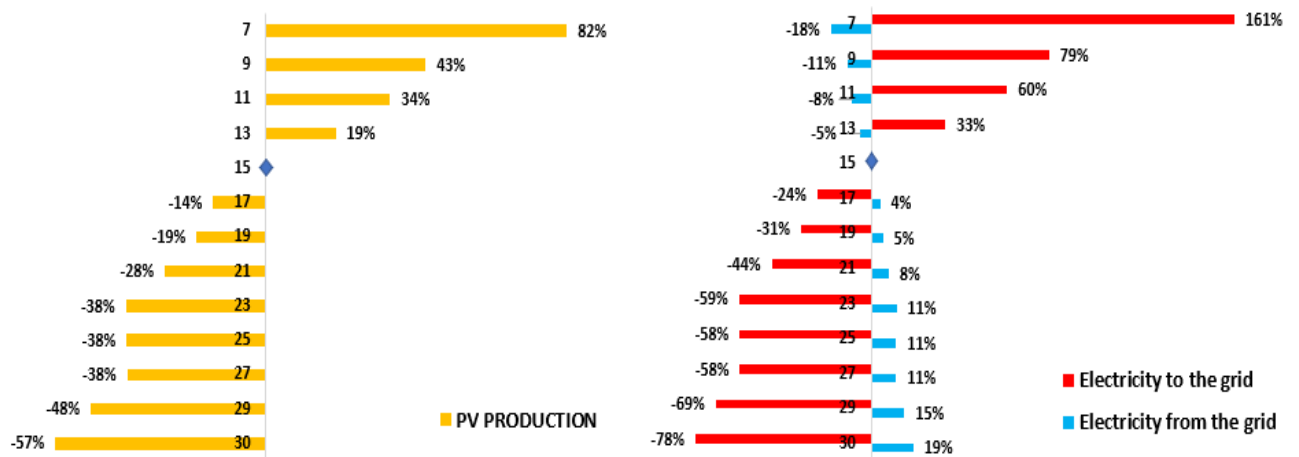


Figure 68 - Energy simulation with respect to the first scenario.

Therefore, *self-sufficiency* and *self-consumption* as function of L are investigated.

The *self-sufficiency* of the system decreases as distance grows. A reduction by a few percent is recorded in the range of L from 7 meters to 17 meters, over this last measure the difference in *self-sufficiency* is not so accentuated.

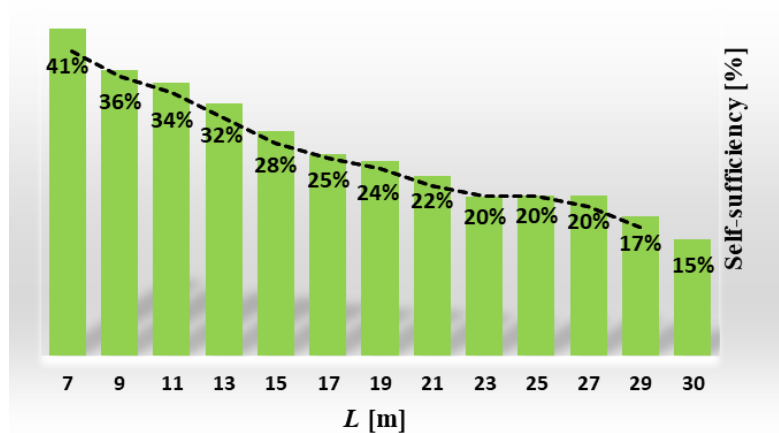


Figure 69 - Self-sufficiency as function of the avalanche barriers distance.

Percentages of *self-consumption* remains quite high with 55% as minimum value. The *self-consumption* increases with space increase. As before, the growing in percentages is notable mainly between lower values of L . A maximum of 84% can be reached with L equal to 30 meters, which corresponds to a very low level of *self-sufficiency* (15%).

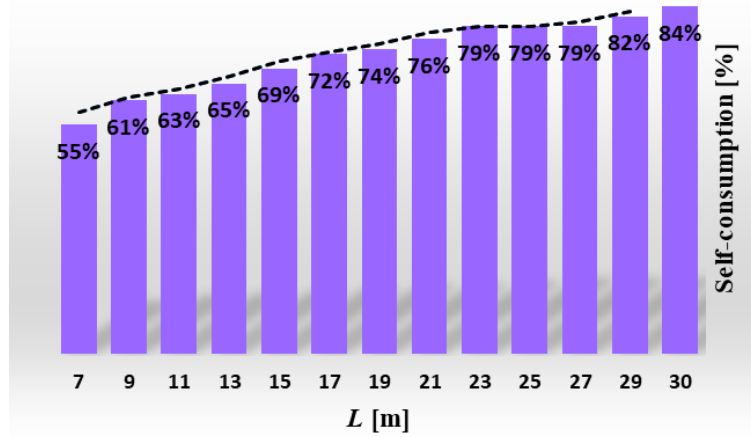


Figure 70 - Self-consumption as function of the avalanche barriers distance.

8.3.2. The tilt angle β

In this analysis it is supposed to change the tilt angle β of the photovoltaic panels integrated with the avalanche barriers. The geographical coordinates of La Thuile, the azimuth of the first scenario and different values assigned to the tilt angle are inserted into PVGIS. The corresponding annual specific energies are obtained and, as in the basic scenario, they have been reduced by 0.5% to take into account the possibility of small portion of panels shaded by the upper part of the barrier grid.

Latitude		[°]	45,7146
Longitude		[°]	6,9521
Azimuth angle	γ	[°]	155

Table 32 - PV plant unchanged parameter for PVGIS.

The tilt angle has been varied by five degrees from 25° to 75°. It is also reported the tilt angle of the basic scenario of the case study.

TILT ANGLE [°]	E_{spec} [kWh/kWp]
25	1076,11
30	1076,11
35	1071,37
40	1060,56
45	1044,48
50	1023,45
52,3	1013,53
55	997,33
60	966,19
65	929,99
70	889,11
75	842,25

Table 33 - Tilt angles and yearly specific energies.

The specific energies in *Table 33* are introduced, one at a time, in the energy simulation. All the other parameter of the PV plant and the cableways are kept equal to the first scenario. The results of all the simulations are in *Table 34*.

TILT ANGLE	ENERGY LOAD	PV PRODUCTION ENERGY	ENERGY WITHDRAWN FROM THE ELECTRICITY GRID	ENERGY INJECTED INTO THE ELECTRICITY GRID
			$E_{el_{grid,W}}$	$E_{el_{grid,I}}$
γ	E_{load}	E_{PV}		
[°]	[kWh]	[kWh]	[kWh]	[kWh]
25	1.919.675,32	826.454,32	1.359.644,18	266.423,18
30	1.919.675,32	826.454,32	1.359.644,18	266.423,18
35	1.919.675,32	822.809,28	1.361.309,06	264.443,02
40	1.919.675,32	814.510,50	1.365.187,38	260.022,57
45	1.919.675,32	802.161,68	1.371.025,48	253.511,84
50	1.919.675,32	786.007,33	1.378.662,69	244.994,71
52,3	1.919.675,32	778.388,66	1.382.264,54	240.977,88
55	1.919.675,32	765.948,13	1.388.145,99	234.418,80
60	1.919.675,32	742.037,57	1.399.450,08	221.812,33
65	1.919.675,32	714.229,79	1.412.713,64	207.268,10
70	1.919.675,32	682.838,09	1.428.409,21	191.571,99
75	1.919.675,32	646.846,16	1.446.447,24	173.618,07

Table 34 - Energy simulation with different tilt angles β .

The variation of the tilt angle directly affects the photovoltaic energy production. The highest values of production are obtained for angles between 25° and 30°, which correspond to the range of optimum tilt angle.

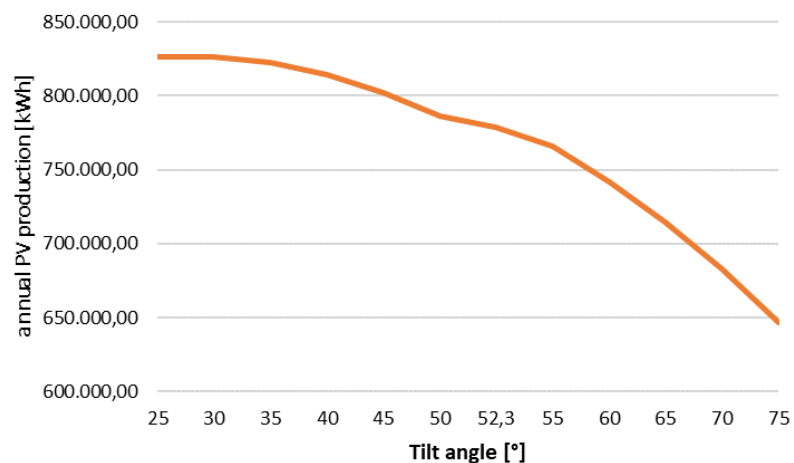


Figure 71 - PV production as function of the tilt angle.

The electricity production is progressively reduced and reaches -5.8% for the angle of 52.3°. After this value, the production decline more severely: indeed, 75° of inclination leads to an energy reduction of 21.7% with respect to the optimal inclination case.

Self-sufficiency and *self-consumption* as function of the tilt angle varies by few percent points.

The maximum *self-sufficiency* reached by the system is 29.2% and it is obtained for inclinations until 40°. It is reduced to 28% for values close to the tilt angle of the basic scenario. Then, it diminishes until 24.7% for 75° of inclination. In an almost specular way, the minimum *self-consumption* of 67.8% is obtained for angles up to 40°. After the tilt angle of the first scenario (52.3°), *self-consumption* increases progressively up to 73%.

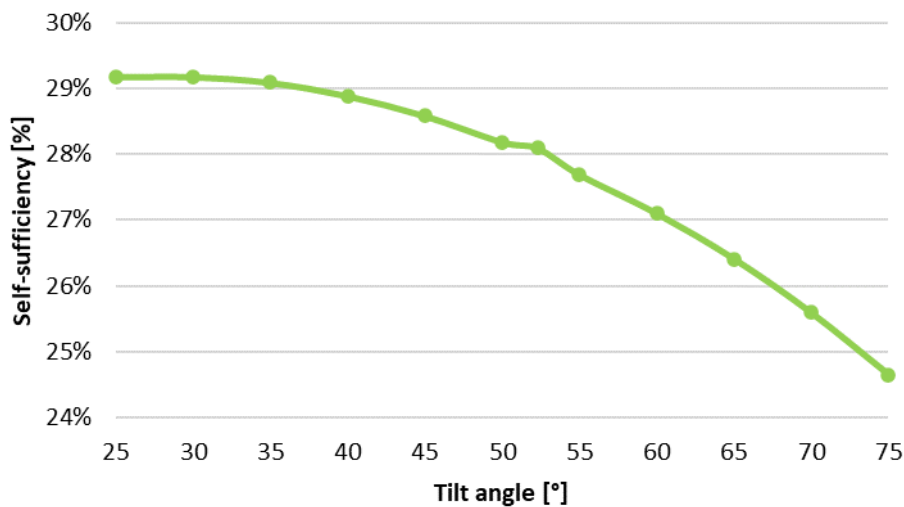


Figure 72 - Self-sufficiency as function of the tilt angle.

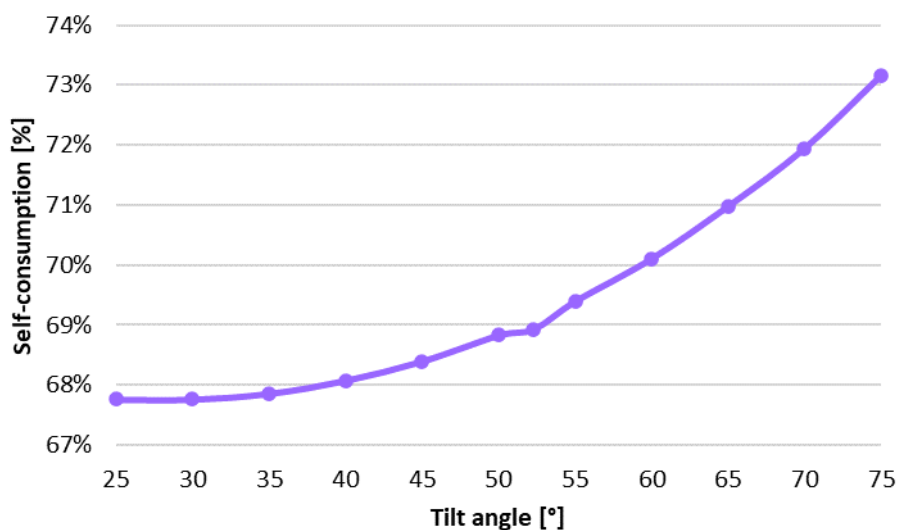


Figure 73 - Self-consumption as function of the tilt angle.

8.3.3. Line length l

In this analysis, the parameter that is made to vary is the total length of the cableway line. All the parameters concerning the PV production side remain unchanged with respect to the first scenario. The values of the length of the line have been changed starting from 1000 meters length, up to 3900 meters, with steps of 300 meters. The line length directly affects the energy load profile, therefore the different contributions obtained in the energy simulation are due to the variation of energy demand, whereas the annual energy production remains always the same of the basic scenario. The selected line lengths are inserted in the Excel model to vary the load demand, the energy simulation has been run and results are reported below.

LINE LENGTH	ENERGY LOAD	PV PRODUCTION ENERGY	ENERGY WITHDRAWN FROM THE ELECTRICITY GRID	ENERGY INJECTED INTO THE ELECTRICITY GRID
l	E_{load}	E_{PV}	$E_{el_{grid},W}$	$E_{el_{grid},I}$
[m]	[kWh]	[kWh]	[kWh]	[kWh]
1000	1.121.559,76	778.391,04	676.691,78	333.523,06
1300	1.379.293,52	778.391,04	896.615,85	295.713,37
1600	1.637.027,29	778.391,04	1.126.042,64	267.406,39
1900	1.894.761,06	778.391,04	1.359.547,93	243.177,91
2200	2.152.494,82	778.391,04	1.595.263,47	221.159,68
2500	2.410.228,59	778.391,04	1.833.438,76	201.601,21
2800	2.667.962,35	778.391,04	2.073.953,74	184.382,42
3100	2.925.696,12	778.391,04	2.316.422,29	169.117,21
3300	3.097.518,63	778.391,04	2.480.388,57	161.260,98
3600	3.355.252,40	778.391,04	2.728.759,56	151.898,20
3900	3.612.986,16	778.391,04	2.978.795,09	144.199,97

Table 35 - Energy simulation with different l .

Figure 74 highlights the linear correlation between the length of the cableway line and the energy requested from the load. Indeed, there is 23% increase of energy demand every step, so every 300 meters.

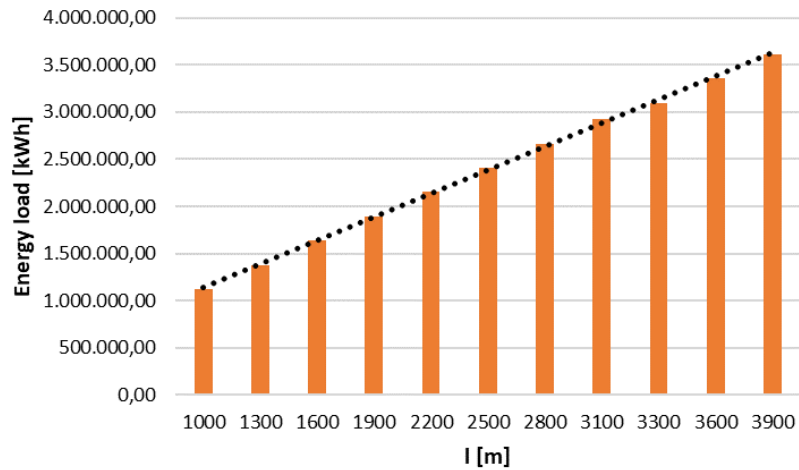


Figure 74 - Energy load as function of the line length.

Also *self-sufficiency* and *self-consumption* vary quite proportional to the line length. The *self-sufficiency* decreases as the length of the line of cableway increases, clearly due to the progressively growth of the energy load. The *self-consumption* is always quite high: the lowest value recorded is 55% for 1000 meters, the maximum percentage is 81% and it is reached at the maximum line length considered.

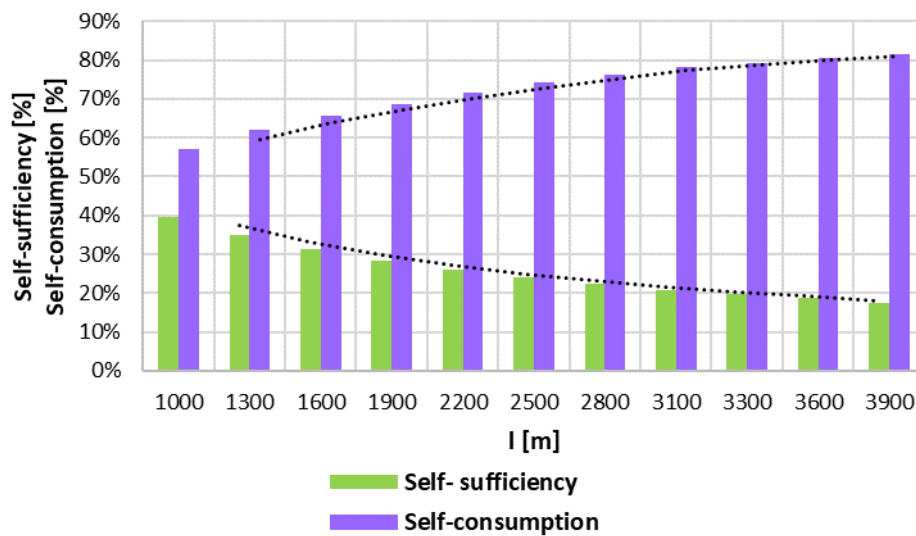


Figure 75 - Self-sufficiency and self-consumption as function of the line length.

8.3.4. Number of rollers n_{roll}

The rollers are important components of the transport system because of their contribution to the energy load, as shown in *Figure 47 (Chapter 8.1.)*. The number of rollers per direction installed along the line has been changed from 80 to 240, with steps of 20. All the other parameters of the cableway are the same of the first scenario. The side of energy production has not been modified. The assigned values are inserted in the Excel model, the energy simulation has been run and results are reported in *Table 36*. The number of rollers affects the energy load profile, therefore the different contributions obtained in the energy simulation are due to the variation of energy demand.

NUMBER OF ROLLERS	ENERGY LOAD	PV PRODUCTION ENERGY	ENERGY WITHDRAWN FROM THE ELECTRICITY GRID	ENERGY INJECTED INTO THE ELECTRICITY GRID
$n_{rollers}$	E_{load}	E_{PV}	$E_{el_{grid},W}$	$E_{el_{grid},I}$
	[kWh]	[kWh]	[kWh]	[kWh]
80	1.241.570,35	778.391,04	777.684,19	314.504,87
100	1.475.399,65	778.391,04	981.244,28	284.235,67
120	1.709.228,95	778.391,04	1.191.160,68	260.322,76
140	1.943.058,25	778.391,04	1.403.582,96	238.915,75
160	2.176.887,55	778.391,04	1.617.764,80	219.268,29
180	2.410.716,85	778.391,04	1.833.896,68	201.570,88
200	2.644.546,15	778.391,04	2.052.034,89	185.879,79
220	2.878.375,44	778.391,04	2.271.547,88	171.563,47
240	3.112.204,74	778.391,04	2.494.548,69	160.734,98

Table 36 - Energy simulation as function of the number of rollers along the line.

The energy requested by the cableway is linearly proportional to the number of rollers involved. In particular, an addition of 20 rollers causes a 19% increase in energy demand. As shown in *Figure 76*, by doubling the number of rollers, from 80 to 160, the load increases by 75%, whereas by tripling rollers, the request of energy rises by 151%.

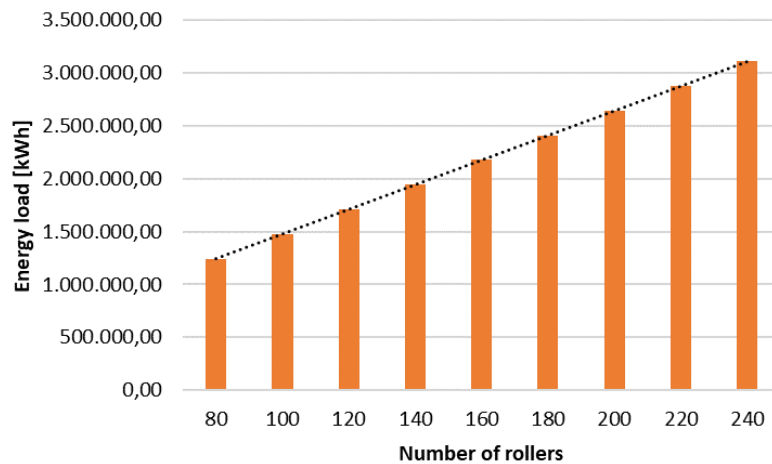


Figure 76 - Energy load as function of the number of rollers.

Self-sufficiency varies in the range between 37% to 20%. Obviously, the maximum value of *self-sufficiency* corresponds to the case with 80 rollers along the line. On the other hand, *self-consumption* varies in the range between 60% to 79%. In this case, the maximum percentage corresponds to 240 rollers.

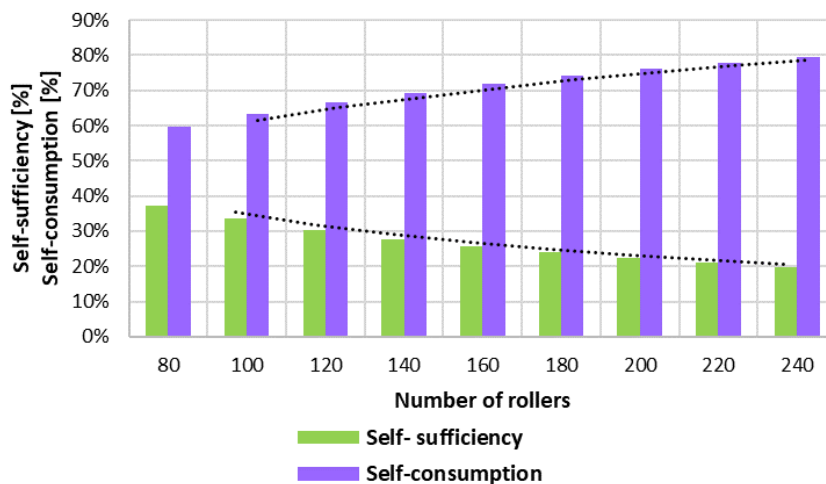


Figure 77 - Self-sufficiency and self-consumption as function of the number of rollers.

Between two following steps, *self-sufficiency* and *self-consumption* are separated by only a few percentage points. Focusing on *self-consumption*, an increment in its percentage is slightly more pronounced between 80 and 160 rollers, whereas for *self-sufficiency* the decline in percentage is more marked from 80 to 120 rollers.

8.4. First scenario with storage

The basic scenario is further improved by adding an accumulation system, in this case batteries. The parameter that characterizes a battery is its maximum capacity C_{MAX} which is taken into account in the next energy simulation following the logic explained in *Chapter 6.3*. At first, some considerations are done in order to select a proper size of the battery.

The initial energy simulation of the first scenario without storage is reported below.

	ENERGY LOAD	PV PRODUCTION ENERGY	ENERGY WITHDRAWN FROM THE ELECTRICITY GRID	ENERGY INJECTED INTO THE ELECTRICITY GRID
			$E_{el_{grid},W}$	$E_{el_{grid},I}$
	[kWh]	[kWh]	[kWh]	[kWh]
JANUARY	324.848,34	23.215,23	301.764,24	131,13
FEBRUARY	293.411,40	49.484,40	246.227,47	2.300,46
MARCH	342.853,32	72.870,35	275.053,11	5.070,14
APRIL	155.010,77	74.049,48	100.466,47	19.505,18
MAY	37.143,77	76.739,93	8.426,18	48.022,34
JUNE	57.725,80	86.917,63	9.845,99	39.037,82
JULY	148.174,48	96.862,77	77.993,38	26.681,67
AUGUST	177.432,57	105.423,78	99.056,65	27.047,86
SEPTEMBER	57.725,80	80.154,53	16.413,52	38.842,25
OCTOBER	48.396,88	60.026,57	14.934,97	26.564,65
NOVEMBER	41.753,64	31.779,56	17.748,46	7.774,38
DECEMBER	235.198,54	20.864,43	214.334,12	0,00
YEAR	1.919.675,32	778.388,66	1.382.264,54	240.977,88

Table 37 - Energy simulation of the first scenario without storage.

The month of January seems to be the worst month of the year from an energetic point of view: the load is very high in respect of a low photovoltaic energy production. Almost all the energy produced directly feeds the load, only a very small fraction is injected into the grid between 17:00

and 18:00. Looking at the model on daily basis, this amount corresponds to 4,23 kWh/daily. The energy profile of a January day is plotted in *Figure 78*.

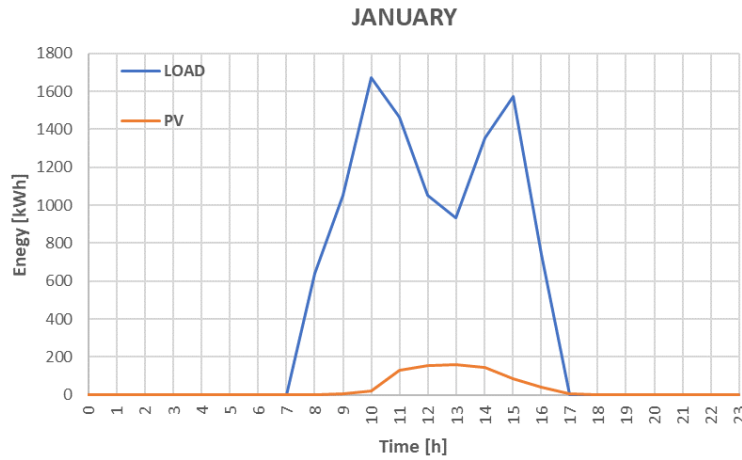


Figure 78 - Energy profile in January in the first scenario.

On the contrary, the month of May presents the lowest energy demand in respect of a quite high production which is largely given to the net and it is not exploited at best: indeed, from 8:00 to 11:00 it is necessary to withdraw energy from the electric grid. Basing on the energy simulation, the electricity sold to the grid during a day of May is almost 1549 kWh/day, whereas near 272 kWh/day are bought.

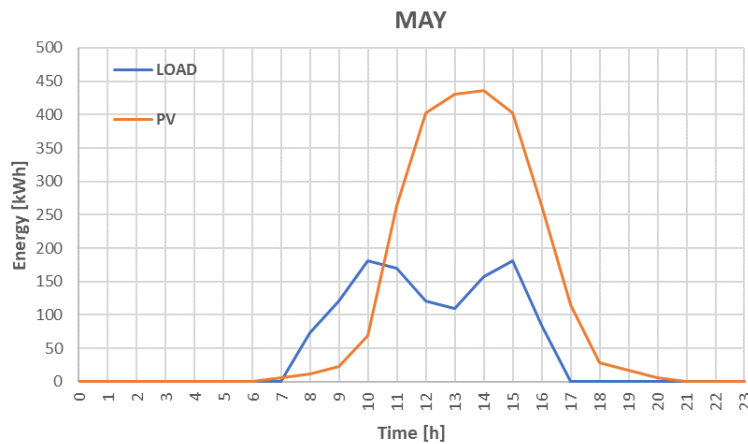


Figure 79 - Energy situation in May in the first scenario.

All the other months of the year present an intermediate situation between January and May.

The energy simulations turn out that batteries are mainly charged during the day. Hence, the stored energy is supposed to be released during the night. For that reason, it has been added a residual load during the night due to illumination and artificial snow systems during the ski season and only the illumination system during the remaining part of the year. It has been calculated cable cars are responsible for 87% of the electricity consumption of a ski area, whereas the remaining part (13%) is consumed by illumination and artificial snow systems which operate when ski slopes are free and temperature lowers enough [51].

For instance, *Figure 80* reports the model of the month of April supposing a battery maximum capacity of 200 kWh.

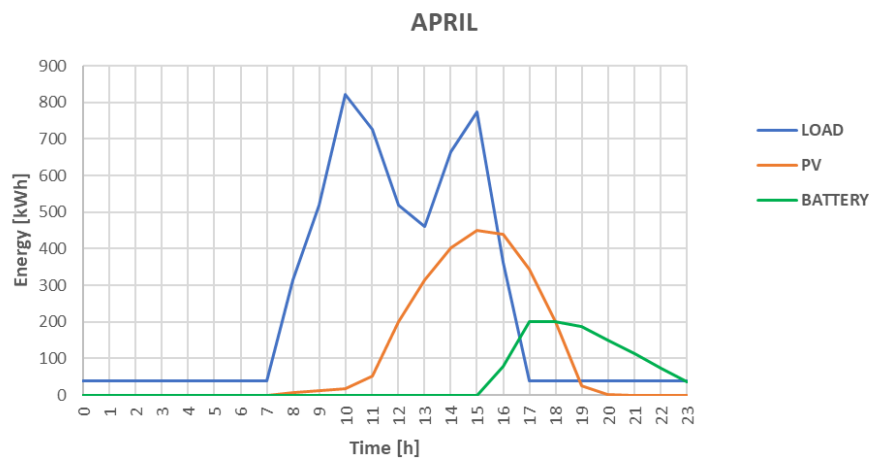


Figure 80 - Energy simulation in April with 200 kWh storage.

Hence, a constant night base load has been added considering that the energy load in *Table 37* corresponds to 87% of the total electricity consumption for the months from January to March and December. The night residual load in April is supposed to be slightly lower because the artificial snow systems operate only half a month: so, the night load has been set equal to 10% of total energy consumption. For all the other months of the year (from May to November), the night base load is due to the illumination system only: because of that the night load has been set equal to 5% of the total load.

	DIURNAL ENERGY LOAD	NIGHT ENERGY LOAD	TOTAL ENERGY LOAD
	$E_{load,diurnal}$	$E_{load,night}$	E_{load}
	[kWh]	[kWh]	[kWh]
JANUARY	324.848,34	48.540,56	373.388,89
FEBRUARY	293.411,40	43.843,08	337.254,48
MARCH	342.853,32	51.230,96	394.084,27
APRIL	155.010,77	17.223,42	172.234,19
MAY	37.143,77	1.954,94	39.098,71
JUNE	57.725,80	3.038,20	60.764,00
JULY	148.174,48	7.798,66	155.973,13
AUGUST	177.432,57	9.338,56	186.771,13
SEPTEMBER	57.725,80	3.038,20	60.764,00
OCTOBER	48.396,88	2.547,20	50.944,09
NOVEMBER	41.753,64	2.197,56	43.951,20
DECEMBER	235.198,54	35.144,61	270.343,15
YEAR	1.919.675,32	225.895,94	2.145.571,26

Table 38 - Total energy load split.

	ENERGY LOAD	PV PRODUCTION ENERGY	ENERGY WITHDRAWN FROM THE ELECTRICITY GRID	ENERGY INJECTED INTO THE ELECTRICITY GRID
			$E_{el_{grid,W}}$	$E_{el_{grid,I}}$
	[kWh]	[kWh]	[kWh]	[kWh]
JANUARY	373.388,89	23.215,23	350.173,66	0,00
FEBRUARY	337.254,48	49.484,40	287.770,09	0,00
MARCH	394.084,27	72.870,35	322.139,52	925,59
APRIL	172.234,19	74.049,48	114.587,16	16.402,45
MAY	39.098,71	76.739,93	9.728,34	47.369,56
JUNE	60.764,00	86.917,63	11.901,70	38.055,33
JULY	155.973,13	96.862,77	83.368,73	24.258,37
AUGUST	186.771,13	105.423,78	106.092,83	24.745,49
SEPTEMBER	60.764,00	80.154,53	18.844,08	38.234,61
OCTOBER	50.944,09	60.026,57	17.142,54	26.225,02
NOVEMBER	43.951,20	31.779,56	19.931,25	7.759,61
DECEMBER	270.343,15	20.864,43	249.478,73	0,00
YEAR	2.145.571,26	778.388,66	1.591.158,62	223.976,02

Table 39 - Energy simulation with night base load addition and without storage.

The annual energetic situation with the new total load and without storage is shown in Figure 81 and Figure 82. The new *self-sufficiency* and *self-consumption* are 26% and 71%.

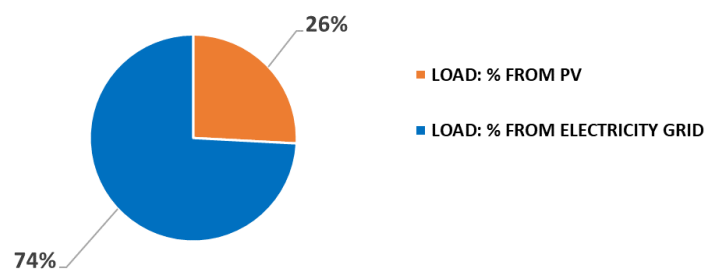


Figure 81 - Annual energetic mix from the point of view of the load (without storage).

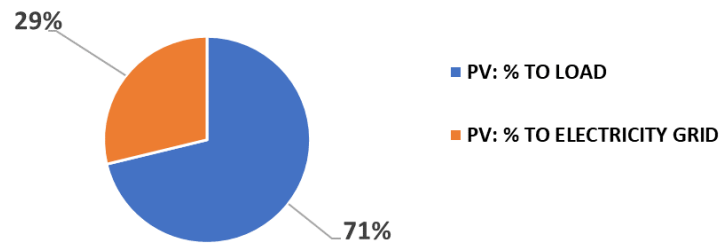


Figure 82 - Annual energetic mix from the point of view of the PV plant (without storage).

The battery has been dimensioned basing on the night energy load reported in *Table 38* so that it is covered by the surplus of energy stored during day.

The month of May presents the lowest base load at night with 1954.94 kWh. Looking at the model on daily basis, this amount corresponds to 63.06 kWh/daily. The highest one is recorded by the month of March with 51,230.96 kWh corresponding to 1652.61 kWh/daily.

Therefore, a *sensitivity analysis* is done with different sizes of storage: the energy simulation has been run varying the maximum capacity C_{MAX} of batteries from 50 kWh to 1700 kWh to be conservative.

Therefore, simulations are run and results are summarized in *Table 40*.

MAXIMUM CAPACITY	ENERGY LOAD	PV PRODUCTION ENERGY	ENERGY WITHDRAWN FROM THE ELECTRICITY GRID	ENERGY INJECTED INTO THE ELECTRICITY GRID
C_{MAX}	E_{load}	E_{PV}	$E_{el_{grid},W}$	$E_{el_{grid},I}$
[kWh]	[kWh]	[kWh]	[kWh]	[kWh]
0	2.145.571,26	778.388,66	1.591.158,62	223.976,02
50	2.145.571,26	778.388,66	1.578.280,87	210.850,44
100	2.145.571,26	778.388,66	1.570.409,39	198.650,44
200	2.145.571,26	778.388,66	1.559.328,42	174.250,44
300	2.145.571,26	778.388,66	1.554.132,59	151.090,83
400	2.145.571,26	778.388,66	1.551.132,59	129.690,83
500	2.145.571,26	778.388,66	1.550.160,13	108.290,83
600	2.145.571,26	778.388,66	1.550.160,13	88.488,38
700	2.145.571,26	778.388,66	1.550.160,13	70.088,38
800	2.145.571,26	778.388,66	1.550.160,13	52.284,52
900	2.145.571,26	778.388,66	1.550.160,13	41.759,50
1000	2.145.571,26	778.388,66	1.550.160,13	32.659,50
1100	2.145.571,26	778.388,66	1.550.160,13	23.559,50
1200	2.145.571,26	778.388,66	1.550.160,13	14.459,50
1300	2.145.571,26	778.388,66	1.550.160,13	7.399,79
1400	2.145.571,26	778.388,66	1.550.160,13	4.299,79
1500	2.145.571,26	778.388,66	1.550.160,13	1.199,79
1600	2.145.571,26	778.388,66	1.550.160,13	377,95
1700	2.145.571,26	778.388,66	1.550.160,13	377,95

Table 40 - Energy simulation as function of the battery capacity.

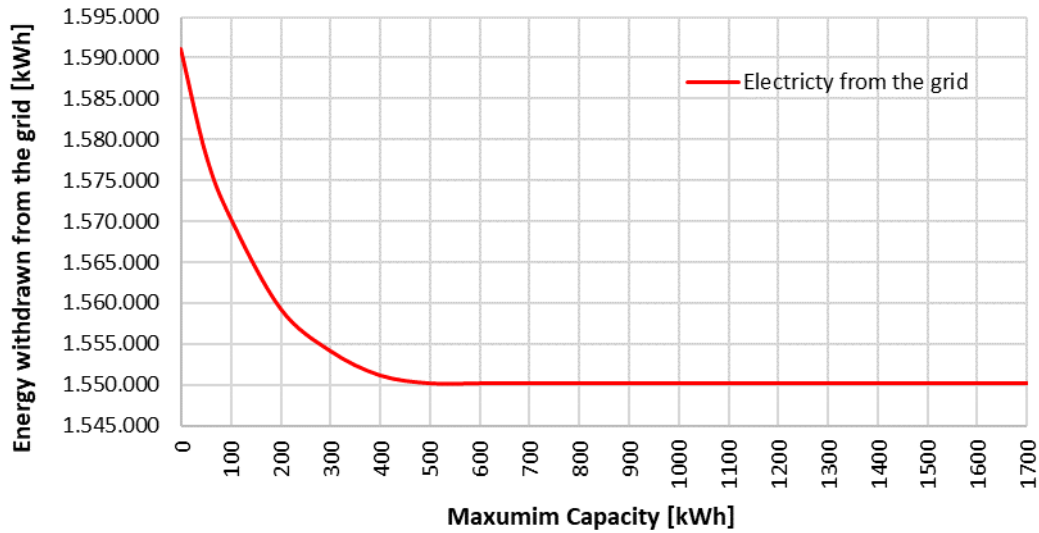


Figure 83 - Electricity withdrawn from the net as function of the battery capacity.

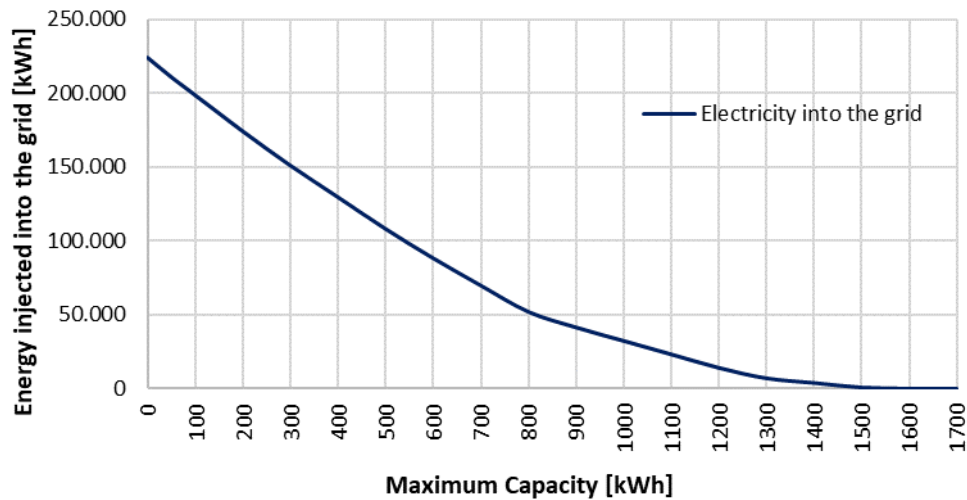


Figure 84 - Electricity injected into the net as function of the battery capacity.

By increasing the size of the battery, the amount of energy exchanged with the electric grid decreases with exponential trend. The electricity bought from the grid decreases until the capacity of 500 kWh. After this capacity, the energy withdrawn is always around 1.55 GWh regardless of the size of batteries, as shown in *Figure 83*. The amount of energy injected into the grid when batteries are fully charged, decreases significantly until the size of 1500 kWh.

Now, *self-sufficiency* and *self-consumption* take into account the energy stored and released by the accumulation system. The *self-sufficiency* increases from 25.8% to 27.8%, the last percentage reached at 500 kWh of capacity. In particular, the percentage variation of *self-sufficiency* is more

relevant up to the capacity of 400 kWh, whereas there is no variation in *self-sufficiency* after 600 kWh. The *self-consumption* increases from 71.2% to 76.5%, the last percentage reached again at 500 kWh of capacity. The percentage variation of *self-consumption* is more accentuated with respect to the percentage variation of *self-sufficiency*. Also in this case, there is no variation in *self-consumption* after 600 kWh. Notice that the highest percentage variation is recorded between 100 and 200 kWh of battery size both for *self-sufficiency* and *self-consumption* (Figure 86).

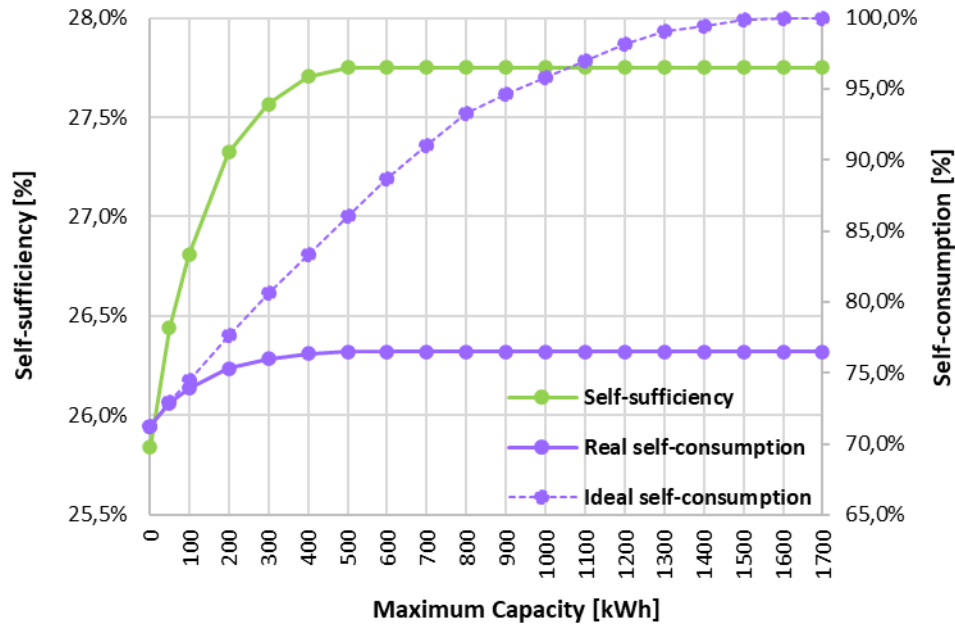


Figure 85 - Self-sufficiency and self-consumption as function of the battery capacity.

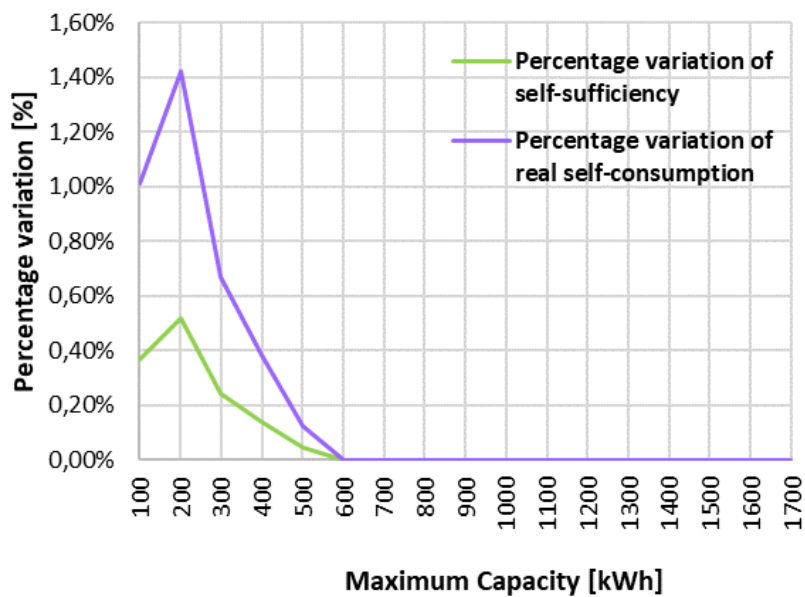


Figure 86 - Percentage variation of self-sufficiency and self-consumption.

Figure 85 reports two different curves for *self-consumption*: the *real* curve takes into account the effective amount of energy provided to the load directly from photovoltaic and from battery, the *ideal* curve shows what the values of *self-consumption* would be if all the energy stored into the accumulation system was used. The *ideal* curve reaches 91% of *self-consumption* at 700 kWh of capacity and continues to grow until it achieves 100% at 1600 kWh. In general, from a maximum capacity of 400 kWh onwards, there is a substantial difference between the two curves: the amount of electricity stored and then lost, is significative. The losses of stored energy are mainly caused by the months of the years with quite high PV production and low energy request: here, batteries are fully charged, but only a fraction of this energy is used.

The yearly maximum *State of Charge* (SoC) reaches 100% for all the battery sizes below 1600 kWh.

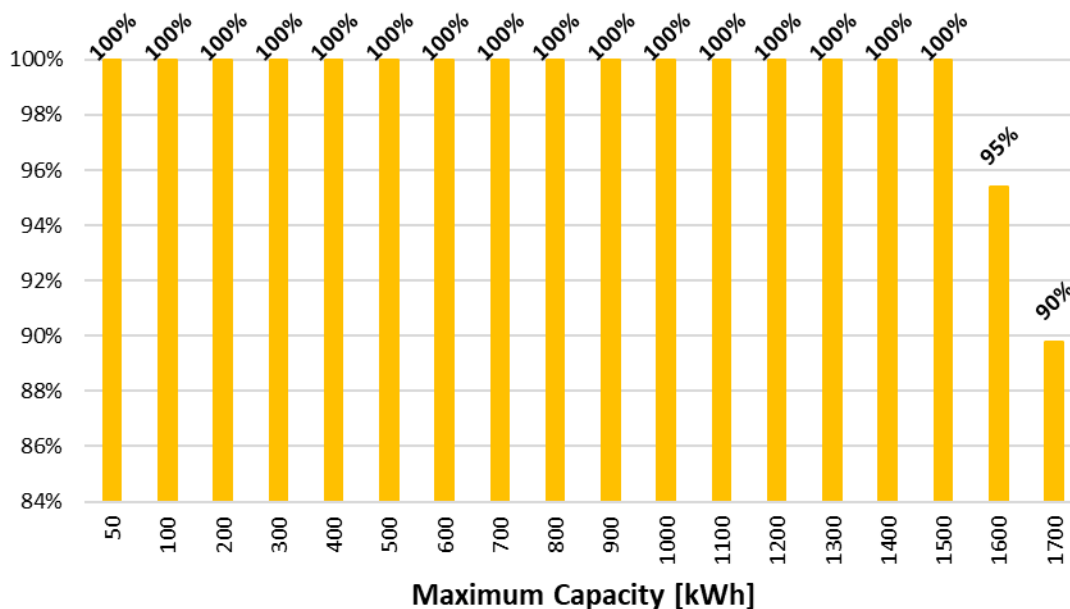


Figure 87 - SoC of batteries.

Looking at the previous graphs, it can be deduced that it has no meaning to adopt batteries with capacity higher than 500 kWh. Indeed, the amount of energy bought from the electric grid (Figure 83), and values of *self-sufficiency* and *self-consumption* (Figure 85 and Figure 86) remain almost unchanged.

The SoC on monthly basis is plotted for batteries up to 600 kWh of capacity:

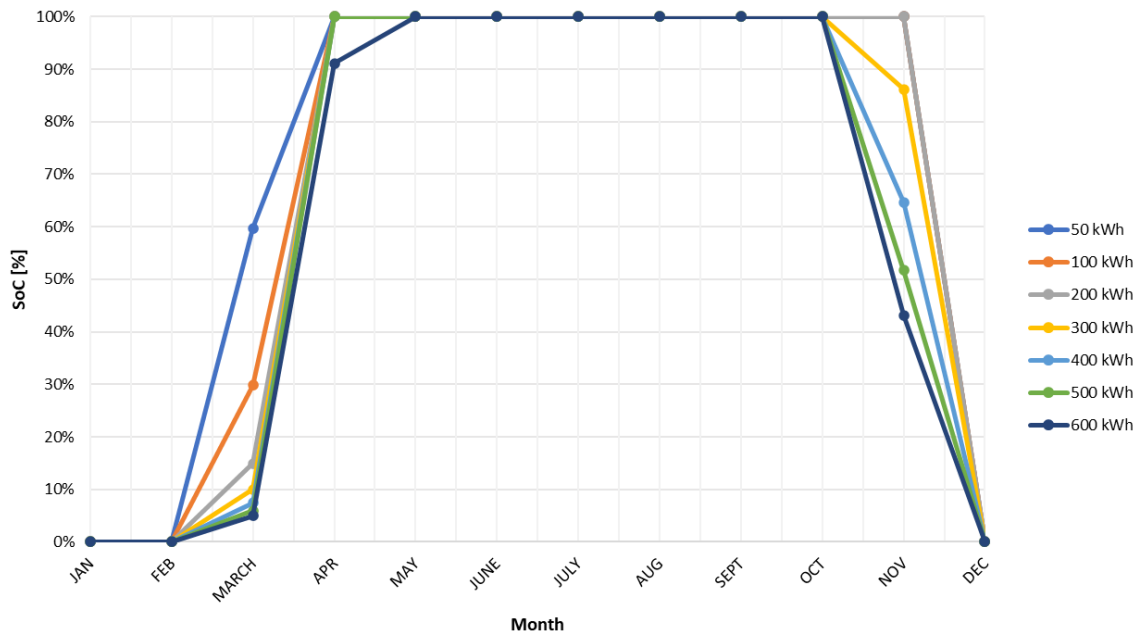


Figure 88 - SoC of batteries on monthly basis.

This analysis has been done only from an energetic point of view. To evaluate the effective convenience or not of the storage system integration, the economic analysis should support this study. The case is presented in the following chapter.

8.5. Economic analysis

8.5.1. First scenario

The input data for the computation of the economic analysis of the first scenario are summarized below.

<i>PV plant cost</i>		[€/kWp]	2000
<i>Lifetime solar panels</i>	<i>N</i>	[y]	20
<i>O&M costs</i>	<i>C_{O&M}</i>	[%]	0,5
<i>Insurance costs</i>	<i>C_I</i>	[%]	2
<i>Inflation</i>	<i>i</i>	[%]	5
<i>Years of inflation</i>		[y]	10

Table 41 - Input data for economic analysis.

Operation and maintenance costs and insurance costs are expressed as percentages of the CAPEX, which is only the investment for the PV plant construction at year zero. The economic analysis is done considering a time of 20 years, as the life span of the panels. Hence, the substitution costs of the PV modules have never been added. Moreover, the inflation is considered for the first 10 years of life of the photovoltaic system.

The sources of income are essentially two: the incomes derived from the amount of electricity sold to the grid and the incomes derived from the electricity produced by photovoltaic and directly consumed by the load. The last are savings due to the failure to purchase of electricity from the grid. *Table 42* reports the prices of electricity adopted.

<i>Price of electricity bought from the grid</i>	[c€/kWh]	19,9
<i>Price of electricity sold to the grid</i>	[c€/kWh]	10

Table 42 - Electricity prices [52], [53].

The price of 19.9 c€/kWh is referred to year 2019, before the COVID pandemic that influenced the electricity price, and it is reported by ARERA [52].

The cashflow and the cumulated cashflow are calculated and the results are in *Table 43*.

YEAR	CAPEX	OPEX: O&M COST	OPEX: INSURANCE COST	SAVINGS	INCOME: ELECTRICITY SOLD TO THE GRID	CASHFLOW	CUMULATED CASHFLOW
N		$C_{O\&M}$	C_I	S	I	CF	CCF
[y]	[€]	[€]	[€]	[€]	[€]	[€]	[€]
0	1.536.000					-1.536.000	-1.536.000
1		8.064	32.256	112.292	25.303	97.275	-1.438.725
2		8.467	33.869	117.907	26.568	102.138	-1.336.587
3		8.891	35.562	123.802	27.896	107.245	-1.229.342
4		9.335	37.340	129.992	29.291	112.608	-1.116.734
5		9.802	39.207	136.492	30.756	118.238	-998.496
6		10.292	41.168	143.316	32.293	124.150	-874.346
7		10.807	43.226	150.482	33.908	130.357	-743.989
8		11.347	45.387	158.006	35.603	136.875	-607.114
9		11.914	47.657	165.906	37.384	143.719	-463.395
10		12.510	50.040	174.202	39.253	150.905	-312.490
11		12.510	50.040	174.202	39.253	150.905	-161.585
12		12.510	50.040	174.202	39.253	150.905	-10.680
13		12.510	50.040	174.202	39.253	150.905	140.225
14		12.510	50.040	174.202	39.253	150.905	291.130
15		12.510	50.040	174.202	39.253	150.905	442.035
16		12.510	50.040	174.202	39.253	150.905	592.940
17		12.510	50.040	174.202	39.253	150.905	743.845
18		12.510	50.040	174.202	39.253	150.905	894.750
19		12.510	50.040	174.202	39.253	150.905	1.045.655
20		12.510	50.040	174.202	39.253	150.905	1.196.559

Table 43 - Cashflow analysis of the basic scenario.

From Table 43, the cumulated cashflow (CCF) and the Payback Time (PBT) are computed.

CCF (N=20 years)	[€]	1.196.559
PBT	[y]	12,07

Table 44 - CCF and PBT of the basic scenario.

The initial expenditure is recovered in almost 12 years. The last year the financial return results equal to 1,196,559 €.

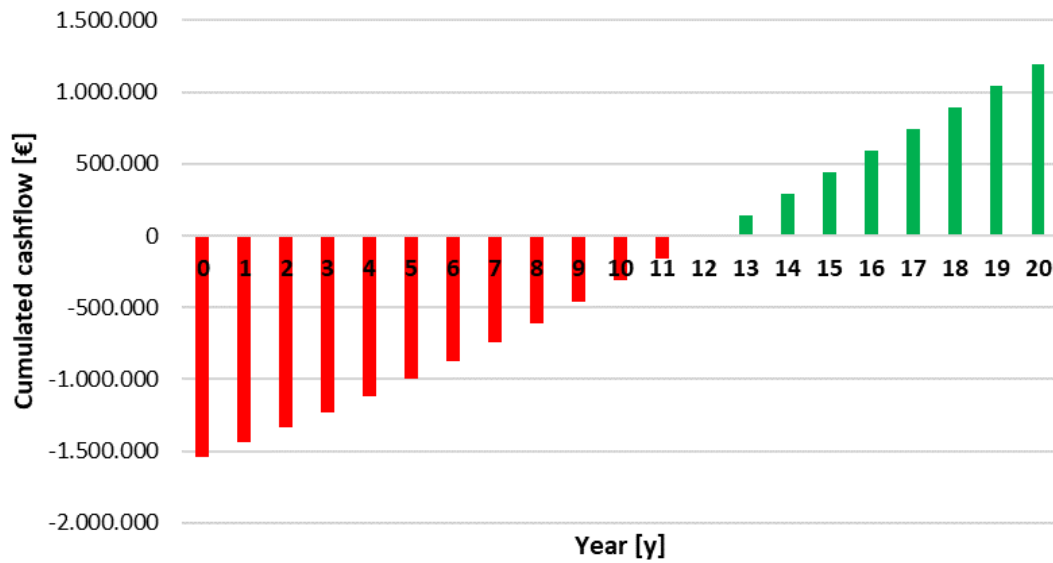


Figure 89 - Cumulated cashflow of the first scenario.

The integration of photovoltaic with avalanche barriers for the model of cableway described in the first scenario seems to be energetically and economically profitable.

8.5.2. Second scenario

The main difference with respect to the previous case is the initial investment because of the higher power installed. The nominal power installed on the avalanche barriers, and on roofs and walls of the three stations are the same reported in *Chapter 8.2.2*.

	Nominal power	
	P_n	
	[kWp]	
PV on avalanche barriers	768	
PV on stations roofs	272,64	
PV on stations walls	350,72	

Table 45 – Nominal power of PV integrated with the avalanche barriers and stations.

As regard the vehicles, the nominal power installed per single cabin is known.

	Nominal power	
	P_n	
	[kWp/cabin]	
PV on cabin roofs		0,64
PV on cabin walls		2,56

Table 46 - Nominal power of PV integrated with each cabin.

From the energy load analysis done in *Chapter 8.1.*, it has been possible to find the maximum number of vehicle rides which are made hourly along the line. It corresponds to 145 rides involved in one hour. Since the *frequency* of each cabin is found equal to 3.87 cycles/hour (*Table 10*), it results that the maximum number of vehicles which travel along the entire line is 38. So, it has been supposed to integrate solar panels on 38 vehicles. The resulting nominal powers installed are in *Table 47*.

	Nominal power	
	P_n	
	[kWp]	
PV on cabin roofs		24,32
PV on cabin walls		97,28

Table 47 - Nominal power of PV integrated with cabins.

The total nominal power installed is 1512.96 kWp. It is almost double compared with the first scenario, and so also the initial investment.

The input data for the computation of the economic analysis of the second scenario are the same of the first scenario (*Table 41* and *Table 42*). The cashflow and the cumulated cashflow are calculated and the results are in *Table 48*.

YEAR	CAPEX	OPEX: O&M COST	OPEX: INSURANCE COST	SAVINGS	INCOME: ELECTRICITY SOLD TO THE GRID	CASHFLOW	CUMULATED CASHFLOW
N		$C_{O\&M}$	C_I	S	I	CF	CCF
[y]	[€]	[€]	[€]	[€]	[€]	[€]	[€]
0	3.025.920					-3.025.920	-3.025.920
1		15.886	63.544	159.886	80.345	160.801	-2.865.119
2		16.680	66.722	167.880	84.362	168.841	-2.696.279
3		17.514	70.058	176.274	88.580	177.283	-2.518.996
4		18.390	73.560	185.088	93.009	186.147	-2.332.850
5		19.310	77.239	194.343	97.660	195.454	-2.137.395
6		20.275	81.100	204.060	102.543	205.227	-1.932.169
7		21.289	85.155	214.263	107.670	215.488	-1.716.681
8		22.353	89.413	224.976	113.053	226.263	-1.490.418
9		23.471	93.884	236.225	118.706	237.576	-1.252.842
10		24.645	98.578	248.036	124.641	249.454	-1.003.388
11		24.645	98.578	248.036	124.641	249.454	-753.934
12		24.645	98.578	248.036	124.641	249.454	-504.479
13		24.645	98.578	248.036	124.641	249.454	-255.025
14		24.645	98.578	248.036	124.641	249.454	-5.570
15		24.645	98.578	248.036	124.641	249.454	243.884
16		24.645	98.578	248.036	124.641	249.454	493.339
17		24.645	98.578	248.036	124.641	249.454	742.793
18		24.645	98.578	248.036	124.641	249.454	992.247
19		24.645	98.578	248.036	124.641	249.454	1.241.702
20		24.645	98.578	248.036	124.641	249.454	1.491.156

Table 48 - Cashflow analysis of the second scenario.

From Table 48, the cumulated cashflow (CCF) and the Payback Time (PBT) are computed.

CCF (N=20 years)	[€]	1.491.156
PBT	[y]	14,02

Table 49 - CCF and PBT of the second scenario.

The initial expenditure is recovered in almost 14 years, two years later with respect to the case in which solar panels are integrated only with avalanche barriers, but the last year the financial return results equal to 1,491,156 €, that is almost 25% more than the CCF of the first scenario.

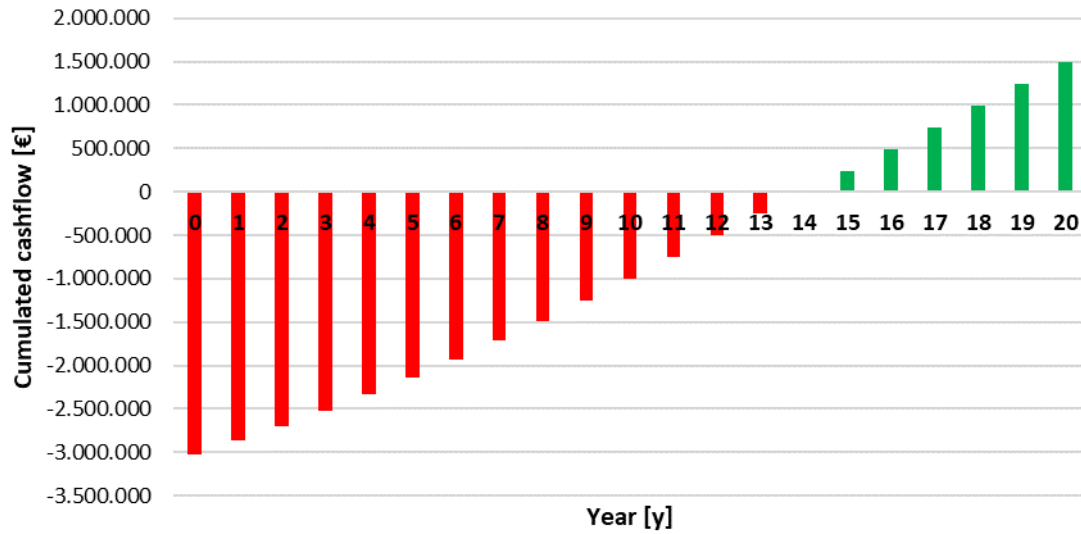


Figure 90 - Cumulated cashflow of the second scenario.

The integration of photovoltaic with avalanche barriers and cableway seems to be energetically and economically profitable.

8.5.3. First scenario with storage

The economic analysis has been carried out also considering the presence of the accumulation systems in addition to the photovoltaic integrated to the avalanche barriers only, as reported in *Chapter 8.4*. The economic data in *Table 41* and *Table 42* are still valid. Information related to the battery costs are added to the analysis and summarized in *Table 50*.

Battery cost		[€/kWh]	1000
Lifetime battery	<i>N</i>	[y]	15

Table 50 - Battery data.

The cost of installation of the storage is added to the initial investment of *Table 43*. Moreover, batteries have a life span shorter with respect to the time considered in the analysis. It means that at year 15, a substitution of the storage system is taken into account as a cost.

The cashflow and cumulated cashflow have been calculated for all the capacities C_{MAX} and the resulting CCF are reported below.

C_{max} [kWh]	CCF (N=20 years) [€]
0	1.246.206
50	1.183.810
100	1.106.796
200	939.153
300	754.325
400	563.085
500	365.925
600	165.925
700	-34.075
800	-234.075
900	-434.075
1000	-634.075
1100	-834.075
1200	-1.034.075
1300	-1.234.075
1400	-1.434.075
1500	-1.634.075
1600	-1.834.075
1700	-2.034.075

Table 51 - CCF as function of the battery capacity.

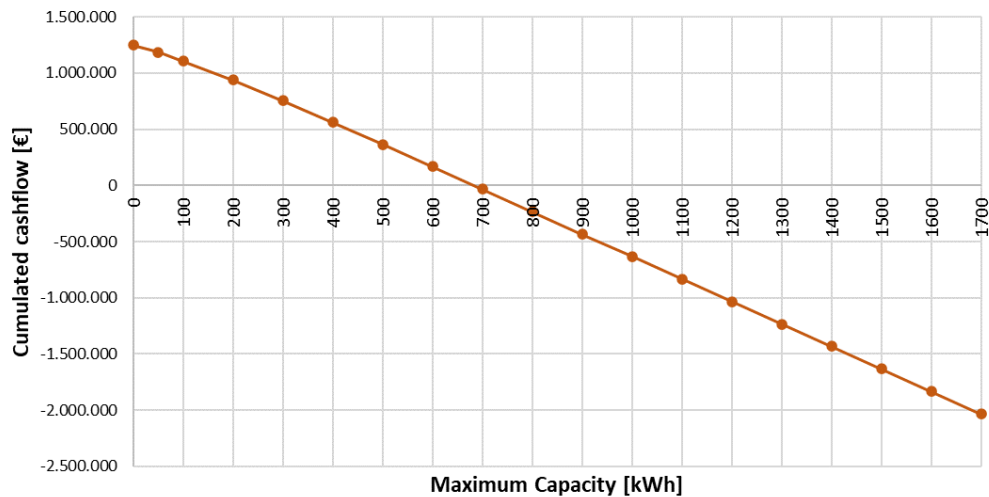


Figure 91 - CCF as function of the battery capacity.

The case is economically profitable for battery capacity lower than 700 kWh. Obviously, by increasing the size of the accumulation system, the CCF progressively decreases. The percentages of reduction of the profits with respect to the CCF of the scenario without storage system (but with night basic load) are in the following table for values of battery capacity lower than 700 kWh.

C_{\max} [kWh]	CCF reduction [%]
50	-5,01%
100	-11,19%
200	-24,64%
300	-39,47%
400	-54,82%
500	-70,64%
600	-86,69%

Table 52 - CCF reduction percentages.

An acceptable compromise should be to opt for a battery capacity of 200 kWh. Looking at the energy analysis in *Chapter 8.4.*, such a choice would lead to a *self-sufficiency* of 27.3% (more than one percentage points higher than the case without storage) and to a *self-consumption* of 75.3% (four percentage points higher than the case without storage). Therefore for 200 kWh, real and ideal curves of *self-consumption* are not so far because most of the energy stored is exploited by the load.

The annual energy mix from the point of view of the load and of the photovoltaic system are reported below.

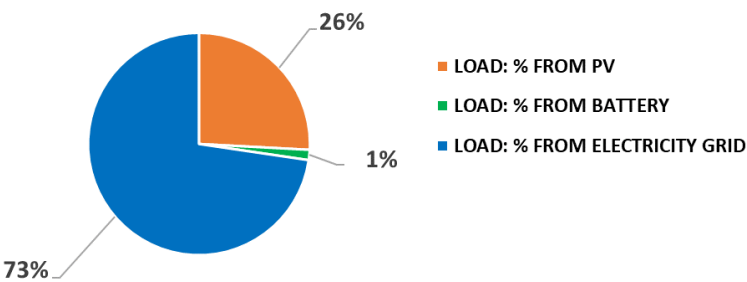


Figure 92 - Energy mix from the point of view of the load.

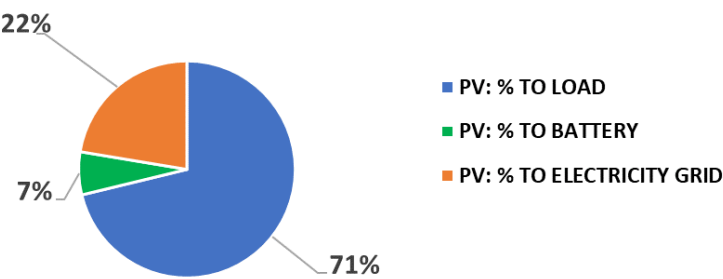


Figure 93 - Energy mix from the point of view of the PV.

By way of example, the economic analysis has been run for 200 kWh of capacity of battery by maintaining data of Table 41 and Table 42 .

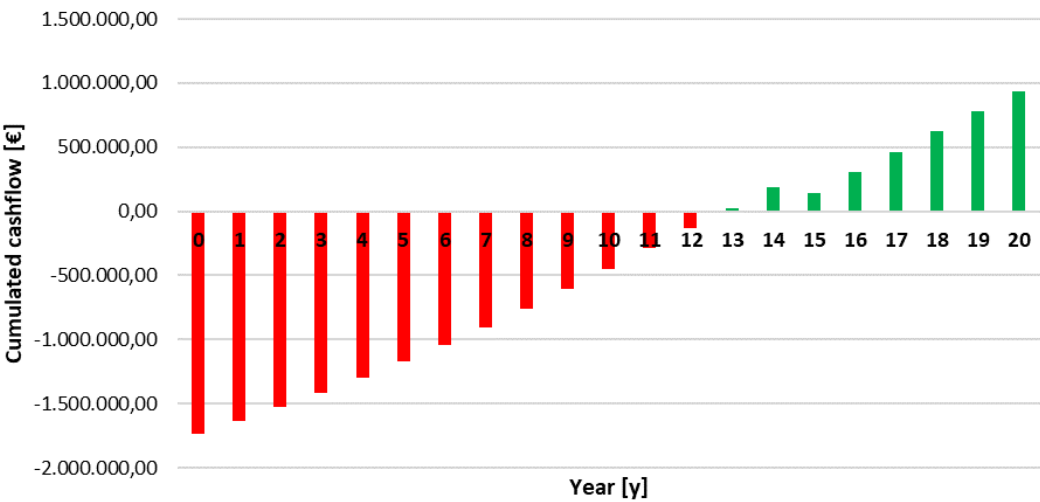


Figure 94 - Cumulated cashflow for basic scenario with battery capacity of 200 kWh.

The initial investment is 1,736,000 € and it is entirely recovered before 13 years, only one year later the case without batteries. At year 15 the gain presents a drop because of the cost of substitution of batteries, nevertheless the cumulated cashflow of that year is still positive. Finally, the CCF results equal to 939,153 € as reported in *Table 51*.

9. CableSmart and traditional cableway

The present thesis fits into the context of sustainability focusing on the theme related to renewable energy systems, in this case adopting the photovoltaic technology. Energy and environmental sustainability are pursued not only by the ways in which power is generated, but also by the way in which power is consumed. The latter can be also embraced into the concept of sustainable mobility, which is included in the present case study. Indeed, the considered ropeway (CableSmart) is more efficient with respect to a traditional cableway due to its operation feature. As already explained in *Chapter 3*, CableSmart is conceived so that the departures of vehicles are adjusted depending on the number of passengers recorded at boarding. This leads to avoid empty vehicles runs and the energy load demand is considerably reduced. The energy load request in *Chapter 8.1* has been calculated basing on this model. Now, it is supposed that the presented transport system operates as a traditional cableway. Practically, it means that the *filling factor* and the *capacity factor* are set always equal to 100% and so the hourly capacity of the ropeway corresponds to the maximum capacity q_{MAX} every hour of every day of the year regardless the season.

The contributions to the final energy load are reported below.

	ACCELERATION PHASE	AERODYNAMIC FRICTION ENERGY	ROLLING FRICTION ENERGY	ENERGY TO OVERCOME THE DIFFERENCE IN HEIGHT	TOTAL ENERGY LOAD
	E_{ACC}	E_{AER}	E_R	E_g	E_{load}
	[kWh]	[kWh]	[kWh]	[kWh]	[kWh]
JANUARY	152,29	8,50	709.376,49	134.454,63	843.991,91
FEBRUARY	137,55	7,68	640.727,15	121.442,90	762.315,27
MARCH	152,29	8,50	709.376,49	134.454,63	843.991,91
APRIL	147,37	8,23	686.493,38	130.117,39	816.766,36
MAY	152,29	8,50	709.376,49	134.454,63	843.991,91
JUNE	147,37	8,23	686.493,38	130.117,39	816.766,36
JULY	152,29	8,50	709.376,49	134.454,63	843.991,91
AUGUST	152,29	8,50	709.376,49	134.454,63	843.991,91
SEPTEMBER	147,37	8,23	686.493,38	130.117,39	816.766,36
OCTOBER	152,29	8,50	709.376,49	134.454,63	843.991,91
NOVEMBER	147,37	8,23	686.493,38	130.117,39	816.766,36
DECEMBER	152,29	8,50	709.376,49	134.454,63	843.991,91
YEAR	1.793,03	100,10	8.352.336,09	1.583.094,88	9.937.324,10

Table 53 – Total energy load for the traditional cableway setup.

It derives that the load obtained for the traditional cableway is five times higher than the load adopting the CableSmart model (*Chapter 8.1, Table 13*). The main contribution to the load is done by the energy provided to overcome the difference in height and to compensate the dissipations due to rolling frictions.

The big difference between traditional and CableSmart cableway has been demonstrated by the computations.

For completeness, the energy simulation has been carried out with the power installed in the first scenario of the case study (*Chapter 8.2.1*) and results are reported below to further highlight the variations with the CableSmart transport system.

	ENERGY LOAD	PV PRODUCTION ENERGY	ENERGY WITHDRAWN FROM THE ELECTRICITY GRID	ENERGY INJECTED INTO THE ELECTRICITY GRID
			$E_{el_{grid,W}}$	$E_{el_{grid,I}}$
	[kWh]	[kWh]	[kWh]	[kWh]
JANUARY	843.991,91	23.215,23	820.907,81	131,13
FEBRUARY	762.315,27	49.484,40	715.131,34	2.300,46
MARCH	843.991,91	72.870,35	776.191,70	5.070,14
APRIL	816.766,36	74.049,48	759.892,12	17.175,23
MAY	843.991,91	76.739,93	772.594,56	5.342,58
JUNE	816.766,36	86.917,63	737.823,43	7.974,70
JULY	843.991,91	96.862,77	770.370,37	23.241,23
AUGUST	843.991,91	105.423,78	764.463,69	25.895,56
SEPTEMBER	816.766,36	80.154,53	749.975,02	13.363,19
OCTOBER	843.991,91	60.026,57	789.634,63	5.669,28
NOVEMBER	816.766,36	31.779,56	785.001,57	14,77
DECEMBER	843.991,91	20.864,43	823.127,48	0,00
YEAR	9.937.324,10	778.388,66	9.265.113,72	106.178,28

Table 54 - Energy simulation results for traditional cableway.

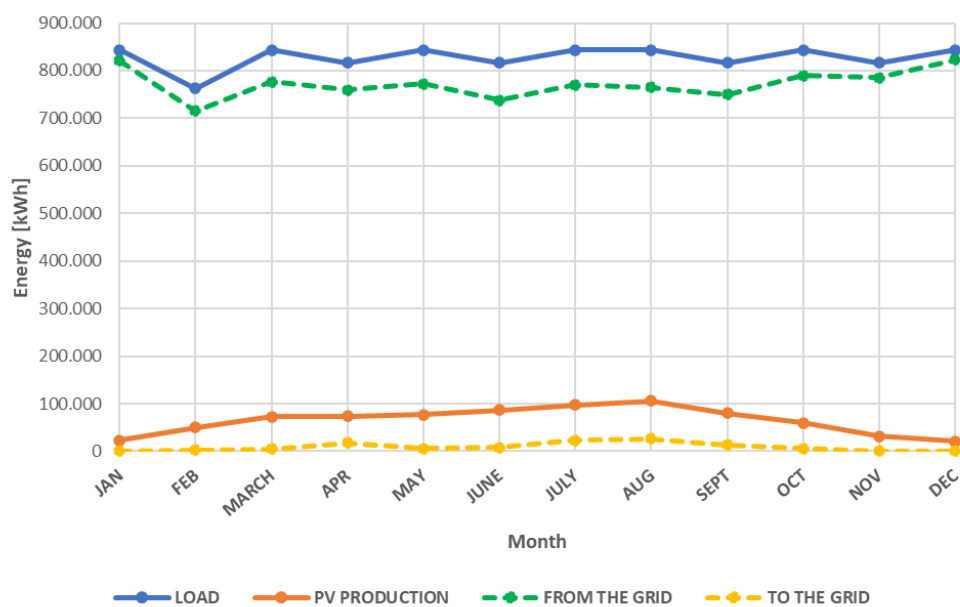


Figure 95 - Energy simulation graph for traditional cableway.

From *Figure 95* is evident that the energy situation is really different: the load is much higher and the contribution of photovoltaics is low. As an example, the daily energy situation of some months representative of the main tourist seasons of the year are shown.

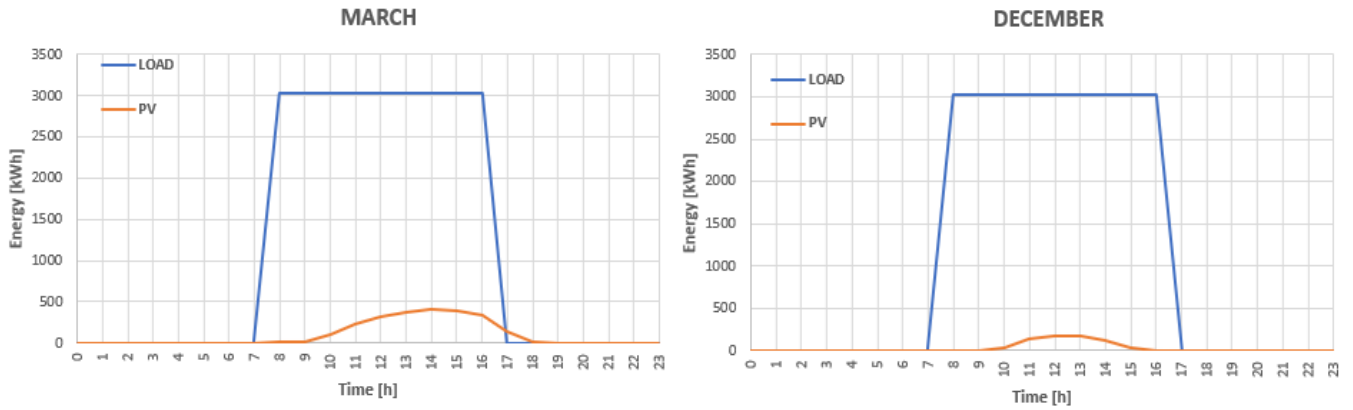


Figure 96 - Energy simulation of March and December.

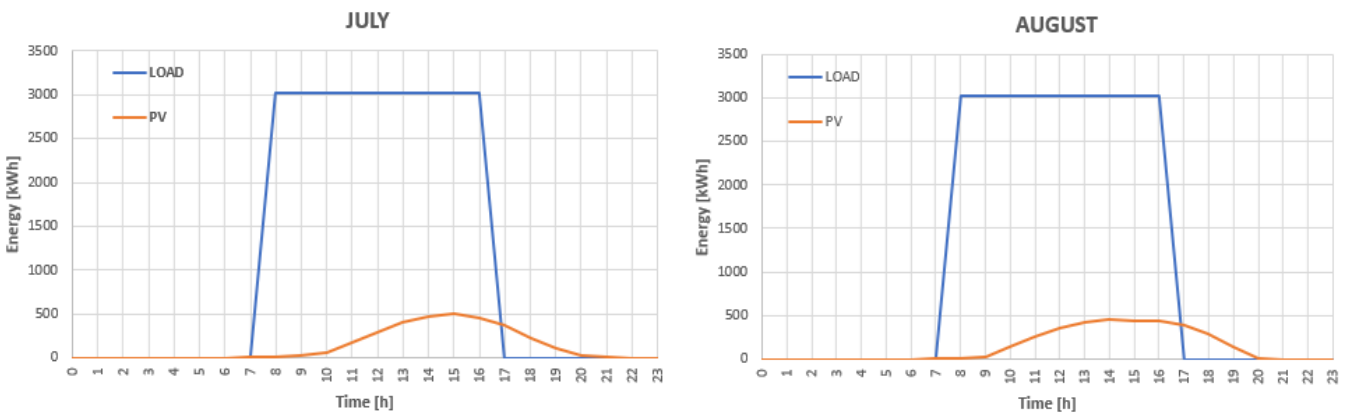


Figure 97 - Energy simulation of July and August.

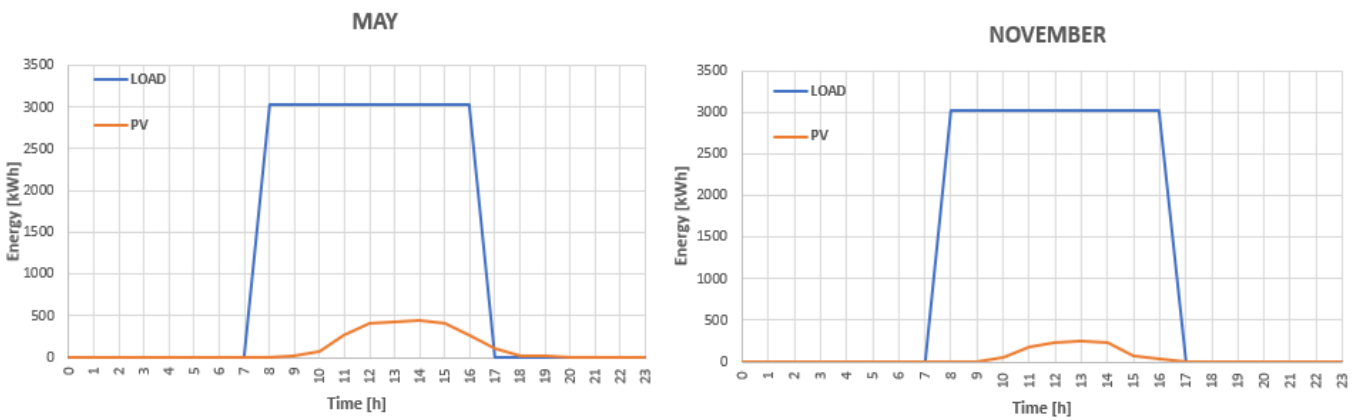


Figure 98 - Energy simulation of May and November.

On yearly basis, the amount of energy generated by solar panels installed on the avalanche barriers and used to directly feed the load rises to 86% compared with 69% of the first scenario with CableSmart. This is because of the increase of the load energy request which leads to a lower amount of electricity sold to the grid. *Self-consumption* of the PV system is equal to 86%. On the contrary, the amount of energy load covered by the photovoltaic panels is around 7% with respect to 28% of the first scenario with CableSmart. Hence, *self-sufficiency* of the case results equal to 7%.

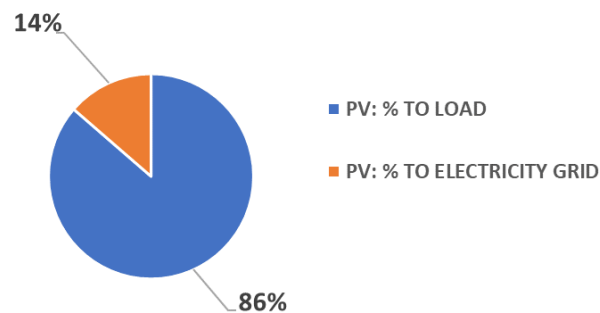


Figure 99 - Energy mix from the point of view of the PV system.

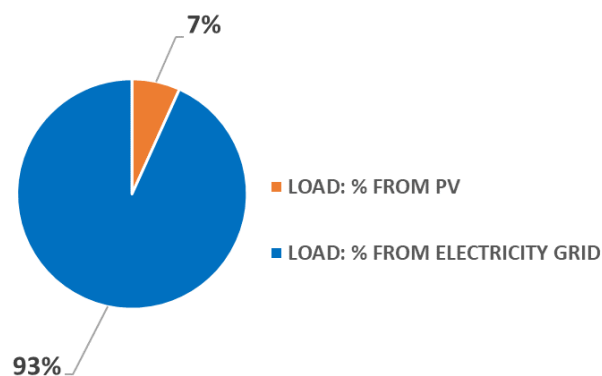


Figure 100 - Energy mix from the point of view of the load.

It has been calculated that to reach the same *self-sufficiency* of the case with the CableSmart transport system, 3200 kWp of photovoltaic power should be installed: it is more than four times the nominal power integrated in this scenario.

10. Conclusion

With the increasing emergence of renewable energy sites, new impacts on the landscape and scenery can be observed. High mountain photovoltaic sites are considered promising: their annual energy production is higher than in low-altitude locations because they receive more direct, diffuse and reflected radiation [54]. In particular, the share of reflected radiation depends on the albedo effect and the highest value of albedo is reached for freshly fallen snow. It has been demonstrated that the albedo effect of the snow has a considerably positive impact on PV energy production [55], [56]. Indeed, good test results have been achieved for high alpine PV systems even up to 30% better performance thanks to stronger sun radiation, also because they are located above the fog line, and lower temperatures as compared to plants in lower regions [57]. The increased performance in high alpine regions could be in vain due to the high installation costs at many locations: because of that, the focus is on solar integration with already existing high alpine infrastructures as dams, railways, ski lifts or avalanche barriers as shown in the figures below [57]. For instance, in 2012 a pilot project with PV installations on avalanche barriers was launched in the ski area of Bellwald, in Switzerland (*Figure 102*) [54].



Figure 101 - Example of PV integrated with avalanche barriers [57].



Figure 102 - Pilot project of PV on avalanche barriers in Bellwald [54].

In this prospective, the present thesis has carried out the analysis of the energy production of a PV system to feed part of the energy request of a cableway located in La Thuile. The basic scenario considers solar panels integrated with avalanche barriers, and to these, other photovoltaic modules were then added on roofs and walls of stations and cabins. The reported results demonstrate the feasibility and effectiveness of that kind of PV integration.

The 768 kW_p plant with panels installed into the avalanche barriers covers 28% of the yearly energy load requested by the transport system. From the point of view of the PV plant, the annual *self-consumption* recorded is equal to 69%, the remaining 31% of energy produced by solar panels is sold to the grid. It has been estimated that the initial expenditure to realize this solution is recovered in almost 12 years and at year 20 the financial return results equal to 1,196,559 €.

In the second scenario, additional photovoltaic modules are installed on roofs and walls of stations and cabins rising the yearly energy production by 64% with respect to the previous case. On annual basis the *self-sufficiency* registered is around 40%, compared with 28% achieved in the first scenario, whereas the *self-consumption* of the PV system is slightly decrease to 60% because of the higher amount of electricity sold to the grid. The economic analysis shows that the initial expenditure is recovered in almost 14 years and at year 20 the financial return results equal to 1,491,156 €, that is almost 25% more than the CCF of the previous case.

Looking at the basic scenario, the performance of the entire system changes depending on the characteristic parameters of the photovoltaic plant and of the cableway.

The *sensitivity analysis* demonstrates that the *self-sufficiency* of the system increases as the distance between the lines of avalanche barriers decreases. It reaches 41% at the minimum distance of 7 meters which corresponds also to a *self-consumption* of 55%, quite high as minimum value. Indeed, *self-consumption* presents the opposite trend: it increases with space increase reaching a maximum of 84% with 30 meters distance.

Also the variation of the tilt angle of panels directly affects the photovoltaic energy production. Tilt angle is supposed to be changed between 25° and 75°. The maximum *self-sufficiency* reached is 29.2% and it is obtained for inclinations lower than 40°. It is reduced to 28% for values close to the tilt angle of the basic scenario. Then, it diminishes until 24.7% for 75° of inclination. In an almost specular way, the minimum *self-consumption* of 67.8% is obtained for angles up to 40°. After the tilt angle of the first scenario (52.3°), *self-consumption* increases progressively up to 73%.

Then, calculations shows that *self-sufficiency* and *self-consumption* vary quite proportional to the cableway line length. The *self-sufficiency* decreases as the length of the line increases, clearly due to the progressively growth of the energy load, whereas the *self-consumption* is always quite high: the lowest value recorded is 55% for 1000 meters length.

The rollers are important components of the transport system because of their contribution to the energy load. So, the number of rollers per direction installed along the line has been changed from 80 to 240, with steps of 20 and results that the energy requested by the cableway is linearly proportional to the number of rollers involved. *Self-sufficiency* varies in the range between 37% to 20%. On the other hand, *self-consumption* varies in the range between 60% to 79%.

Therefore, it has been considered the installation of batteries by taking into account also a night base load to exploit the energy stored during the day. The battery has been dimensioned basing on this night energy request, hence the energy simulation has been run varying the maximum capacity C_{MAX} of batteries from 50 kWh to 1700 kWh to be conservative. By increasing the size of the battery, the electricity bought from the grid decreases until the capacity of 500 kWh. The *self-sufficiency* increases from 25.8% to 27.8%, the last percentage reached at 500 kWh of capacity. The *self-consumption* increases from 71.2% to 76.5%, the last percentage reached again at 500 kWh of capacity. The case is economically profitable for battery capacity lower than 700 kWh. By way of example, the economic analysis has been run for 200 kWh of capacity of battery and it results a PBT lower than 13 years and a financial return at year 20 equal to 939,153 €.

Then, the big difference between traditional and CableSmart cableway has been demonstrated by the computations and it derives that the load obtained for the traditional cableway is five times

higher than the load adopting the CableSmart model. To reach the same *self-sufficiency* of the case with the CableSmart transport system, 3200 kWp of photovoltaic power should be installed: it is more than four times the nominal power integrated in the basic scenario.

This project is perfectly consistent with the actual energy policies: it meets some of the objectives reported in the NRRP (*Chapter 1.2, Figure 15*). Obviously, being the case study focused on the integration of photovoltaic panels, it is totally compliant with all the interventions to launch green transition in Italy regulated by *Mission 2* of the Plan (*Green Revolution and Ecological Transition*). The increase in new renewable energy installations is not the only task encompasses by this study: special investments are considered in *Component 2* of *Mission 2 (ENERGY TRANSITION AND SUSTAINABLE MOBILITY)* for the empowerment of mass transport infrastructures including cableways. Furthermore, the presented innovative cableway system is perfectly in line with *Component 3* of *Mission 1: TOURISME AND CULTURE 4.0*, which provides actions for the improvement of tourism structures following the philosophy of environmental sustainability.

Climate changes have made the start of the ecological transition unavoidable. Reversing the course is possible and necessary for present and future generations.

Bibliography

- [1] *PROPOSTA PER IL PIANO DI TRANSIZIONE ECOLOGICA.*, 2021.
- [2] C. David, *Energy Economics*, 2021.
- [3] “Our World in Data,” [Online]. Available: <https://ourworldindata.org/>.
- [4] “Global Energy Review: CO2 Emissions in 2021,” *IEA (International Energy Agency)*.
- [5] “Le fonti rinnovabili. Risultati, obiettivi, incentivi e progetti di sviluppo nel PNRR,” in *Camera dei deputati, XVIII legislatura, Documentazione e ricerche*, 2021.
- [6] “L'agenda globale per lo sviluppo sostenibile,” Camera dei deputati. Documentazione parlamentare, [Online]. Available: <https://temi.camera.it/leg18/agenda.html>.
- [7] “ECOMONDO. THE GREEN TECHNOLOGY EXPO.,” 20 Aprile 2022. [Online]. Available: <https://www.ecomondo.com/blog/20307263/rigenerazione-ambientale-green-deal-europeo>.
- [8] “THE 17 GOALS,” United Nations-Department of Economic and Social Affairs, Sustainable Development, [Online]. Available: <https://sdgs.un.org/goals>.
- [9] “Clean energy for all Europeans package,” European Commission, [Online]. Available: https://energy.ec.europa.eu/topics/energy-strategy/clean-energy-all-europeans-package_en.
- [10] “I principali contenuti della Direttiva RED II,” Camera dei deputati. Documentazione parlamentare., 27 Gennaio 2022. [Online]. Available: <https://temi.camera.it/leg18/post/i-principali-contenuti-della-direttiva-red-ii.html>.
- [11] “The EU Green Deal – a roadmap to sustainable economies,” [Online]. Available: <https://www.switchtogreen.eu/the-eu-green-deal-promoting-a-green-notable-circular-economy/>.
- [12] *PIANO NAZIONALE DI RIPRESA E RESILIENZA.*, 2021.
- [13] “The National Recovery and Resilience Plan,” Agenzia per la Coesione Territoriale, [Online]. Available: <https://www.agenziacoesione.gov.it/comunicazione/piano-nazionale-di-ripresa-e-resilienza/?lang=en>.
- [14] *Cambiamenti climatici*, Camera dei deputati. Servizi Studi. XVIII Legislatura., 2022.
- [15] “RAPPORTO STATISTICO 2020- ENERGIA DA FONTI RINNOVABILI IN ITALIA,” GSE, 2021.
- [16] Publications Office of the European Union, 2011. [Online]. Available: <https://op.europa.eu/en/publication-detail/-/publication/bfaa7afd-7d56-4a8d-b44d-2d1630448855/language-en>.
- [17] [Online]. Available: <https://www.governo.it/en/approfondimento/nrrp-missions-and-components/19325>.
- [18] L. M. Jia, J. Ma, P. Cheng and Y. K. Liu, “A Perspective on Solar Energy-powered Road and Rail Transportation in China,” *CSEE JOURNAL OF POWER AND ENERGY SYSTEMS*, 2020.

- [19] IEA, September 2022. [Online]. Available: <https://www.iea.org/reports/rail>.
- [20] J. Li, N. Fuwei, M. Jing and J. Limin, "SWOT analysis for orchestrated development of a solar railway system in China," *IET Renewable Power Generation*, vol. 14, pp. 3628-3635, 2020.
- [21] Clean Energy Council, 16 October 2019. [Online]. Available: <https://www.cleanenergycouncil.org.au/news/the-worlds-first-solar-powered-train>.
- [22] S. V. M., V. G.A., S. J. and R. Sheela K, "Rail coaches with rooftop solar photovoltaic systems: A feasibility study," *Energy* 118, pp. 684-691, 2017.
- [23] Z. Chen, M. Jiang, L. Qi, W. Wei, Z. Yu and W. Wei, "Using existing infrastructures of high-speed railways for photovoltaic electricity generation," *Resources, Conservation & Recycling* 178, 2022.
- [24] IEA, September 2022. [Online]. Available: <https://www.iea.org/reports/by-2030-evs-represent-more-than-60-of-vehicles-sold-globally-and-require-an-adequate-surge-in-chargers-installed-in-buildings>.
- [25] "Global Electric Vehicle Outlook 2022: la IEA sul presente e futuro del mercato delle auto elettriche e ibride plug-in nel mondo," MOTUS-E, 10 June 2022. [Online]. Available: <https://www.motus-e.org/news/global-electric-vehicle-outlook-2022-la-iea-sul-presente-e-futuro-del-mercato-delle-auto-elettriche-e-ibride-plug-in-nel-mondo/>.
- [26] X. Jianfu, L. Zhiqiang and J. Haifeng, "Study on Application of Solar Energy in Highway," *E3S Web of Conferences* 261, 2021.
- [27] P. Sharma and T. Harinarayana, "Solar energy generation potential along national highways," *International Journal of Energy and Environmental Engineering*, 2013.
- [28] M. Gu, Y. Liu, J. Yang, L. Peng, C. Zhao, Z. Yang, J. Yang, W. Fang, J. Fang and Z. Zhao, "Estimation of environmental effect of PVNB installed along a metro line in China," *Renewable Energy* 45, pp. 237-244, 2012.
- [29] E. D. Schepper, S. V. Passel, J. Manca and T. Thewys, "Combining photovoltaics and sound barriers: A feasibility study," *Renewable Energy* 46, pp. 297-303, 2012.
- [30] T. Nordmann and L. Clavadetscher, "PV on Noise Barriers," *PROGRESS IN PHOTOVOLTAICS: RESEARCH AND APPLICATIONS*, pp. 485-495, 2004.
- [31] S. R. Wadhawana and J. M. Pearce, "Power and energy potential of mass-scale photovoltaic noise barrier deployment: A case study for the U.S," *Renewable and Sustainable Energy Reviews* 80, pp. 125-132, 2017.
- [32] Y. Wang, "Application of Solar Noise Barrier Power Generation System Envisaged on Urban Elevated Roads," *Journal of Physics: Conference Series*, 2020.
- [33] L. Rodríguez, "RatedPower," 14 September 2021. [Online]. Available: <https://ratedpower.com/blog/benefits-agrivoltaics-examples/>.
- [34] S. ENKHARDT, "Arc-shaped PV system for agrivoltaics from Germany," *pv magazine*, 23 July 2021. [Online]. Available: <https://www.pv-magazine.com/2021/07/23/arc-shaped-pv-system-for-agrivoltaics-from-germany/>.

- [35] G. DEBOUTTE, "New solar canopy for agrivoltaics from France," pv magazine, 4 April 2022. [Online]. Available: <https://www.pv-magazine.com/2022/04/04/new-solar-canopy-for-agrivoltaics-from-france/>.
- [36] C. ROLLET, "A good year for solar: Agrivoltaics in vineyards," pv magazine, 31 March 2020. [Online]. Available: <https://www.pv-magazine.com/2020/03/31/a-good-year-for-solar-agrivoltaics-in-vineyards/>.
- [37] "El Coronil Solar Agro-Energy Greenhouses," WSP, [Online]. Available: <https://www.wsp.com/en-GL/projects/el-coronil-solar-agro-energy-greenhouses>.
- [38] K. K. Agrawal, S. K. Jha, R. KantMittal and S. Vashishtha, "Assessment of floating solar PV (FSPV) potential and water conservation: Case study on Rajghat Dam in Uttar Pradesh, India," *Energy for Sustainable Development* 66, pp. 287-295, 2022.
- [39] N. Ravichandran, H. H. Fayek and E. Rusu, "Emerging Floating Photovoltaic System—Case Studies High Dam and Aswan Reservoir in Egypt," *Processes*, 2021.
- [40] "Impianto fotovoltaico galleggiante: in Svizzera la prima centrale dell'arco alpino," TEKNORING, 7 January 2021. [Online]. Available: <https://www.teknoring.com/news/energie-rinnovabili/impianto-fotovoltaico-galleggiante-svizzera/>.
- [41] D. Gleeson, "Solar power up and floating at former coal mine in Anhui, China," INTERNATIONAL MINING, 21 March 2019. [Online]. Available: <https://im-mining.com/2019/03/21/solar-power-floating-former-coal-mine-anhui-china/>.
- [42] DIMENSIONE INGENIERIE, *Nuovo trasporto alpino*, 2022.
- [43] D. INGENIERIE, *Sistema ibrido fune-automotore, Descrizione del Sistema*, 2021.
- [44] DIMENSIONE INGENIERIE, *Sistema di trasporto pubblico urbano IBRIDO fune-automotore, Descrizione del Progetto*, 2021.
- [45] S. BAZZOLO, S. BLENGINI and B. D. CHIARA, "Energy load analysis of a fully automated hybrid cable-driven public transport system: simulation with a photovoltaic system and storage," *SCIENZA E TECNICA*, pp. 963-989, 2019.
- [46] "BARTHOLET," [Online]. Available: <https://www.bartholet.swiss/en/ropetaxi>.
- [47] M. Affatato, S. Blengini, B. Dalla Chiara and E. Vair, "Automated People Movers with rope traction: engineering and modelling an innovative hybrid solution to optimise energy use.," 2015.
- [48] S. Margreth, *Costruzione di opere di premunizione contro le valanghe nella zona di distacco. Direttiva tecnica: aiuto all'esecuzione.*, 2007.
- [49] [Online]. Available: <https://www.skiinfo.it/valle-daosta/la-thuille/storico-neve>.
- [50] [Online]. Available: https://static.trinasolar.com/sites/default/files/IT_TSM_PD14_datasheet_B_2017_web.pdf.
- [51] D. S. Jacopo, "ARBON FOOTPRINT DELLE STAZIONI SCIISTICHE: METODI DI QUANTIFICAZIONE E IPOTESI DI CONTENIMENTO," Politecnico di Torino, 2020.

- [52] "ARERA-Autorità di Regolazione per Energia Reti e Ambiente," [Online]. Available: <https://www.arera.it/it/dati/eep35.htm>.
- [53] [Online]. Available: <https://www.otovo.it/blog/scambio-sul-posto-cose-come-funziona/#:~:text=Quanto%20paga%20il%20GSE%20a,0%2C15%20%E2%82%AC%20a%20kWh..>
- [54] A. H. Michel, M. Buchecker and N. Backhaus, "Renewable Energy, Authenticity, and Tourism: Social Acceptance of Photovoltaic Installations in a Swiss Alpine Region.," *Mountain Research and Development*, vol. 35, no. 2, pp. 161-170, 2015.
- [55] "Più energia solare in inverno grazie alla neve," WSL Istituto per lo studio della neve e delle valanghe SLF, 07 01 2019. [Online]. Available: <https://www.slf.ch/it/news/2019/01/piu-energia-solare-in-inverno-grazie-alla-neve.html>.
- [56] "Alta montagna e neve per più energia solare," 16 01 2019. [Online]. Available: https://www.tvsvizzera.it/tvs/qui-svizzera/energie-rinnovabili_alta-montagna-e-neve-per-pi%C3%B9-energia-solare/44685664.
- [57] S. Jeanette, "Photovoltaics has a future," Axpo, 25 03 2019. [Online]. Available: <https://www.axpo.com/it/en/home/news-and-media/magazine.detail.html/magazine/renewable-energy/photovoltaics-has-a-future.html>.
- [58] "National energy and climate plans (NECPs)," European Commission, [Online]. Available: https://energy.ec.europa.eu/topics/energy-strategy/national-energy-and-climate-plans-necps_en.
- [59] "Piano Nazionale Integrato per l'Energia e il Clima 2030 (PNIEC)," ENEA, 02 Febbraio 2021. [Online]. Available: <https://www.efficienzaenergetica.enea.it/glossario-efficienza-energetica/lettera-p/piano-nazionale-integrato-per-l-energia-e-il-clima-2030-pniec.html>.